University of Bologna

FACULTY OF INDUSTRIAL CHEMISTRY

Department of Industrial Chemistry and Materials

Evaluation of the Impact of Nitrogen Oxides (NOx) and Conservation Treatments on Stone Building Materials

PhD Thesis in Industrial Chemistry
XX cycle – CHIM/12

Presented by:

Simone Bugani

Coordinator:
Prof. **Luigi Angiolini**

Promoter:
Prof. **Luciano Morselli**

Co-promoters:
Dr. **Mara Camaiti**
Prof. **Koen Janssens**

2005 - 2007

Ad Alba, Renato e Matteo

Contents

Introduction & motivation

Continuous chemical and physical changes, related to the dynamic equilibrium between the environment and Cultural Heritage, affect historical artefacts. In modern times, the conservation of works of art has become a more and more complex issue and it is therefore essential to achieve a greater knowledge of the mechanisms and causes of decay.

In the case of stone artefacts, historical buildings and statues are exposed to the action of physical factors, such as rain and wind, as well as of chemical factors, such as atmospheric pollutants. These have undoubtedly become the major villain in stone decay and weathering, especially in urban areas, where emission sources, like traffic and heating plants, are concentrated. Among the atmospheric pollutants, sulphur oxides (SOx) and nitrogen oxides (NOx), with their remarkable acidic properties, are indeed the most dangerous and harmful for the stone works of art.

The effects of SOx on rock materials have been studied for a long time, both ‘‘in situ’’ and through accelerated ageing systems, considering also the synergic action with others contaminants. However, the use of fuel with a low content of sulphur and the recent introduction of DeSOx systems have caused a great decrease in the emission of SOx, as shown in the time series of the emission in the area of the European Union with fifteen members, EU 15 (Fig. 1).

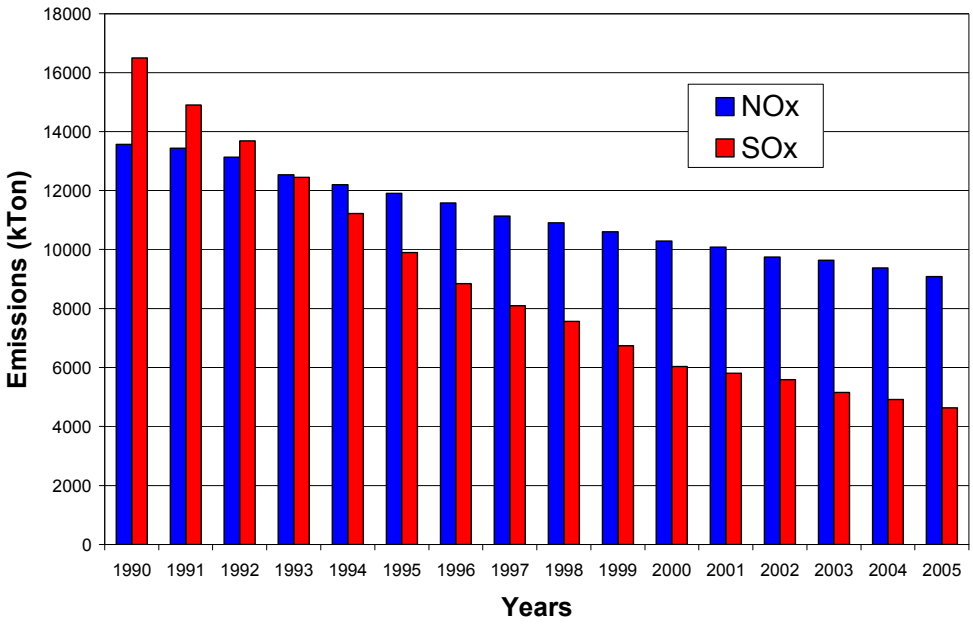

Fig. 0.1 – Time series of emissions of SOx and NOx in the EU 15 area [1]

On the other hand, Figure 1 also shows that the same remarkable decrease has not been observed for NOx emissions, which have only slightly decreased. Nitrogen oxides have been widely studied from the point of view of their action as SOx oxidants, but their direct action on stone materials is still not clear and/or considered a minor factor.

Field research on the impact of atmospheric contaminants on materials is often complicated, due to the synergic effects, i.e. the simultaneous action of two or more compounds, and the great variability of environmental conditions. Therefore, the most effective approach is first to investigate the action of a single pollutant by means of ageing systems which allow to control all the exposure parameters.

Another relevant aspect is the application of conservation treatments, which are used to consolidate and/or protect the objects. Since water is involved in all the weathering processes, the conservation products are applied with the aim of providing the surfaces of the stone with water repellence. However, their capability to keep water out does not assure that they are able to reduce the decay caused by the atmospheric pollutants and their performances in this sense is still not extensively studied and evaluated.

The aims of the present PhD thesis are:

- To investigate the interaction of NOx with stone building materials through an accelerate ageing system which allows to control all the exposure parameters;
- To evaluate the performances of protective treatments used in stone conservation and their efficacy with regard to the action of gaseous atmospheric pollutants, such as NOx;
- To assess the impact of the conservation treatments on the physical, morphological and petrological characteristics of the rock materials;
- To test and apply emerging non-destructive imaging techniques, such as x-ray and neutron tomography;
- To improve the knowledge of the complex processes and mechanisms involved in the stone decay and conservation field.

The intention of the present work is to implement a multidisciplinary approach to unsolved problems in the stone conservation field and to integrate the information obtained with conventional and well established techniques with others of new and innovative application.

Chapter 1

STONE DECAY AND CONSERVATION

1.1 Weathering of the stone materials

All the materials both quarried from the external crust of the Earth and those obtained by means of working and transformation processes can be classified as stone building materials. The natural rocks can be divided in 3 main groups [2]: igneous, formed by solidification of cooled magma, i.e. molten rock, with or without crystallization, either below the surface as intrusive (plutonic) rocks or on the surface as extrusive (volcanic) rocks; sedimentary rocks, formed when particles of sediment are deposited out of air, ice, wind, gravity, or water flows and they undergo to the lithification processes, i.e. rock formation; metamorphic rocks, formed as a result of the transformation of a pre-existing rock type.

Stone building materials can be constituted by several minerals, such as carbonates, silicates and allumino-silicates, and they are generally porous materials. As a consequence of their composition and morphological structure, these materials in nature continually undergo the deterioration caused by physical, chemical and biological processes. The weathering of sculptures and buildings and the transformations of the stone artefacts resulting from their interaction with the environment in which they are placed have been described since the ancient writers, such as Vitruvius [3]. In ancient times some attempts of conservation have been tried, but stone conservation science was born only at the beginning of the 20^{th} Century, in order to understand the nature and the mechanisms of the decay processes and then to find solutions to retard them.

The deterioration of the rocks depends on different factors, both intrinsic, such as mineralogical and chemical composition and properties, and extrinsic, such as topography, climate and pollution. A large number of types of stones has been used for artistic and historic artworks, ranging from porous, friable tuffs and calcarenites, to dense, hard basalts and quartzite. Moreover, also the environmental conditions, to which stones are subjected, are similarly diversified, so all these factors have to be considered during the decay evaluation and study. Nowadays, artworks are exposed not only to daily and seasonal thermo-hygrometric cycles, but also to aggressive compounds that can accelerate the processes of decay. This can be observed especially in urban areas, where there is a high concentration of sources of pollutants, like traffic and heating plants. If stone decay is a natural unstoppable process, as mentioned before, the increased atmospheric pollution has undoubtedly become the primary responsible of

this process. In fact, different decay phenomena, mainly related to the presence of the pollutants, can take place:

- formation of crusts due to the action of SOx and dust [4] (Fig. 1.1),
- corrosion of the material due to the acidic atmospheric pollutants [5],
- formation of efflorescences and subflorescences due to the dissolution/reprecipitation of salts, such as nitrates, sulphates and chlorides [6],
- formation of internal cracks due to frost-thaw cycles of the imbibed water or growth of the salt crystals [7].

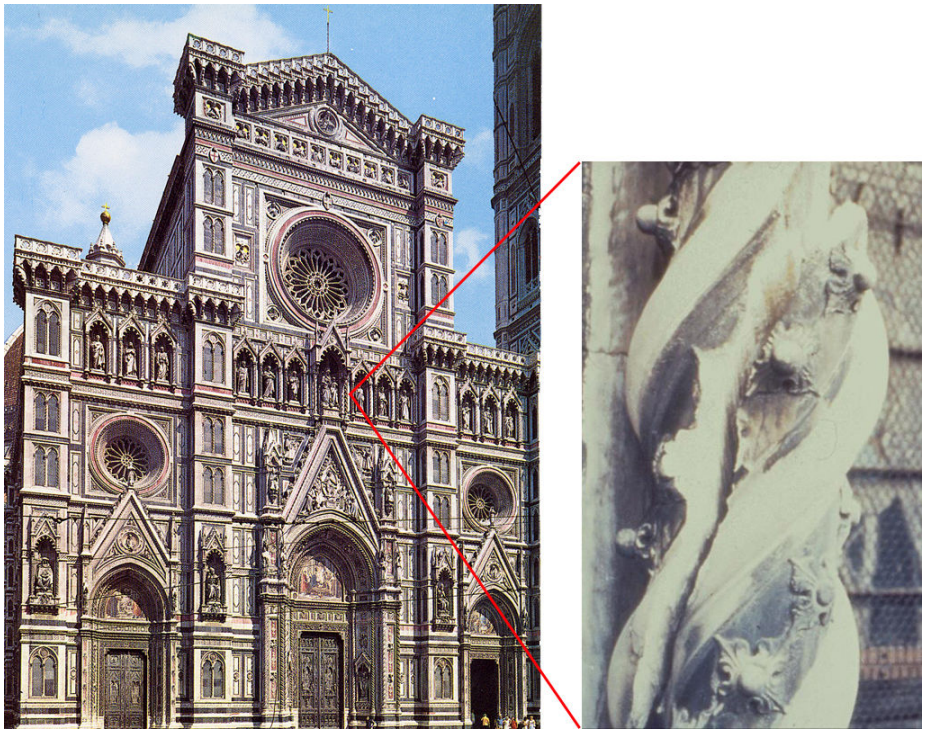

Fig.1.1 – Example of black crust on Santa Maria del Fiore, Cathedral of Florence - Italy

In general, mono-mineral rocks are more resistant if compared with the poly-mineral ones; on the other hand, calcareous stones, containing calcite and/or dolomite, are more sensitive to the chemical action of acidic pollutants normally present in urban areas, if compared to silicate rocks. The internal structure of the material (porosity, pores size distribution, degree of interconnection of the pores) is another factor that determines the behaviour of the stone and influences the processes of absorption, condensation, evaporation and migration of water: high porosity facilitates the absorption of water and thus the acceleration of the decay processes, while a high degree of pores interconnection can cause the diffusion of salt solutions inside the stone, extending the damaged areas. The transport of water through porous materials strongly depends on their capillary and (sub)micro structure: the capillary force increases as the

diameter of the pores decreases and, as a result, small pores (diameter around 1 μm) are characterized by a high capillary suction and a slower water evaporation, if compared with the bigger ones.

In all the weathering phenomena, water plays a crucial role [8]. In fact, water participates in different processes, such as the dissolution of stone constituents and the migration, solubilization and recrystallization of salts. Moreover, water increases the damage caused by the acidic air pollutants, such as NOx and SOx, which are more aggressive and prompt to react with stone in comparison with the correspondent dry deposition [3]. For these reasons, it is important to assess how water penetrates and moves inside the stone object. The majority of water comes from outside during the rain, but the rock can also uptake liquid by capillary absorption from the ground. In addiction to the liquid water absorption mechanism, another mechanism should be considered. Water vapour, which is almost always present in the atmosphere, penetrates into the pores and, due to the physical properties of porous systems, as well as to the variation of environmental conditions (e.g. temperature and relative humidity) in the body of the stone, it can later condense, leading to the formation of liquid water.

Stone weathering is a dynamic and complex process far from being a simple chemical reaction. In the modern concept, the deterioration of the rocks occurs in a variety of mechanisms which may proceed independently, but more often continuously and simultaneously, where synergic effects are very important and should be always taken into account.

1.2 Effect of soluble salts

Soluble salts can be originally present in the material, or they can also come from different external sources, e.g. soil by capillary rise and atmosphere by wet/dry deposition of gases and particles and sometimes by non-appropriate conservation treatments.

Soluble salts can be transported through the materials as aqueous solution, but the evaporation of water, caused by the changes of the environmental conditions, may lead to their precipitation. If crystallization takes place on the surface, efflorescences are formed, causing mainly an aesthetical damage (Fig. 1.2). This happens when the evaporation of the solution is slower than the migration to the surface. On the contrary,

if water evaporation is faster than the migration to the surface of the artefacts, the crystallization of the salts takes place in the inner part of the pores and subflorescences are formed (Fig. 1.3). The growth of the crystals produces high pressures into the cavities and the stone material is seriously weathered.

Fig. 1.2 – Salt effolorescences on stone surface

As a result of several cycles dissolution/crystallization, the rock can lose mechanical stability and the historical object can be damaged. These latter decay phenomena are also caused by salts with low solubility, such as $CaSO_4 \cdot ½ H_2O$ or Na_2SO_4, in which water molecules occupy a well defined position in the crystal structure. If the environmental conditions (i.e. temperature and/or relative humidity) change, these salts react changing the number of the molecules of water in their structure. The transition from one hydration state to another is associated with a change in volume and then these compression/expansion cycles can cause relevant and harmful mechanical stress into the stone pores.

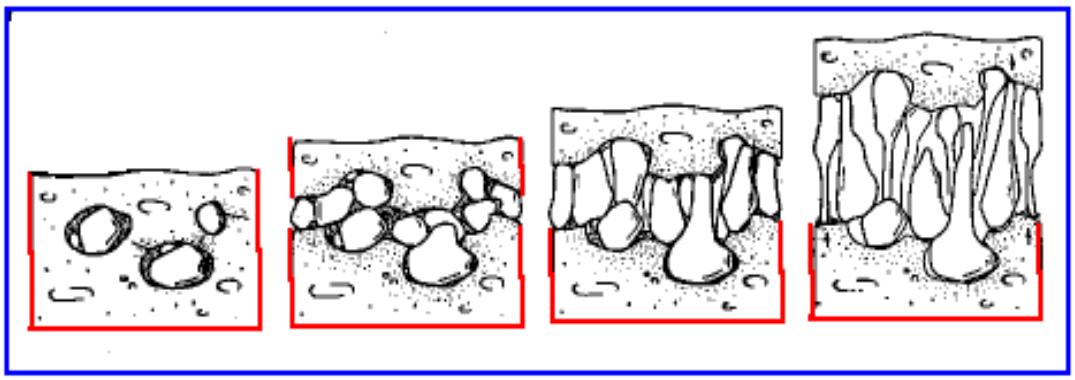

Fig. 1.3 – Mechanism of damage caused by crystallization of soluble salts inside the pores of stone building material [9].

In the special case of hygroscopic and deliquescent salts, such as nitrates, nitrites and chlorides, further effects have to be considered. Because of their chemico-physical characteristics, these compounds can increase and accelerate the uptake of the moisture of the rock from the environment, in some cases already starting from low values of equilibrium relative humidity (RH_{eq}%) (Tab. 1.1). The formed solutions contribute to keep the surfaces wet and then to make the stone more sensitive to the action of the atmospheric pollutants.

	Soluble salts			
	NaCl	$Mg(NO_3)_2 \cdot 6H_2O$	$Ca(NO_3)_2 \cdot 4H_2O$	$CaCl_2 \cdot 6H_2O$
Mineral	Halite	Nitromagnesite	Nitrocalcite	Antarcticite
RH_{eq}%, Equilibrium Relative Humidity	75.3	52.9	50.0	29.0

Tab. 1.1 – Equilibrium relative humidities (RH_{eq}%) of some saturated salt solutions at 25 °C [3]

Moreover, desorption of the condensed water is more difficult than its absorption, because hysteresis phenomena can take place. In other words, if RH% > RH_{eq}% the crystallized salts will dissolve, while even if RH% < RH_{eq}% the solution still exists in the pores [10].

1.3 Effects of atmospheric pollution

A pollutant is a substance that produces a change in the natural composition of air. According with this definition, it cannot be originally present in the atmosphere or exceed its natural concentration [11]. The sources of the atmospheric pollution can be both natural and anthropic. In the urban areas or in the industrialized sites, where the productive activities are largely developed and concentrated, the considerable emissions of pollutants can cause serious dangers both for human health and the environment. With “dry deposition” we mean all the transfer processes of pollutants from the atmosphere to the ground without including the role of water, while wet deposition are the other transfer processes where water is involved, such as precipitations and interactions of H_2O with the contaminants [12]. As shown in Fig. 1.4 the pollutants can undergo several processes of transportation and transformation.

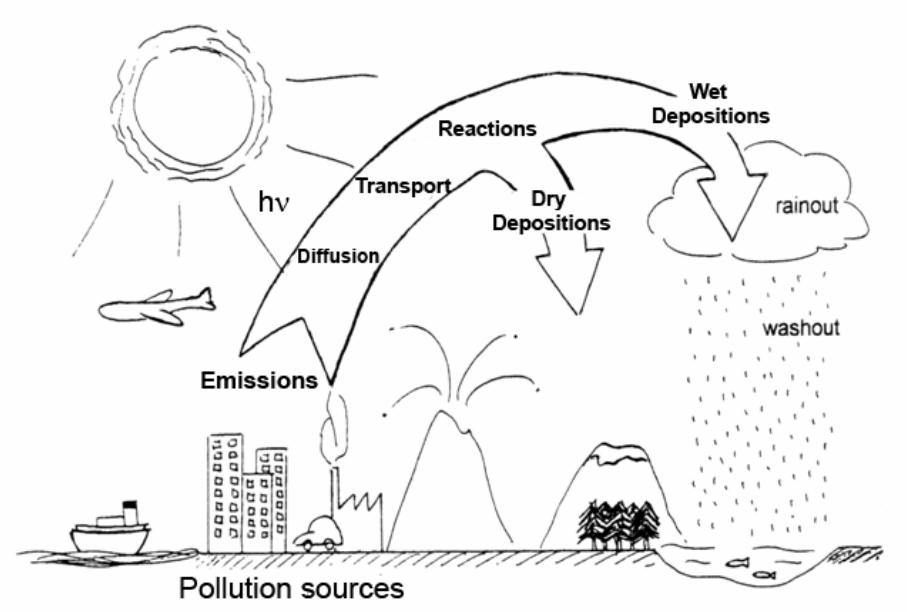

Fig. 1.4 Phenomena of transportation and transformation of pollutants

The Cultural Heritage, and especially stone artefacts, should be considered as a part of the ecosystem. This consideration implies that the object itself interacts with all the environmental factors and is subject to the action of the pollutants. Therefore, the acceleration of the decay process in the urban stone monuments, in the last decades, has been attributed to the relevant increase of atmospheric emissions due to human activities. Again, water is one of the key factors in the decay processes caused by these gaseous compounds. In fact, some undesirable weathering phenomena cannot occur without the presence of liquid water or vapour.

Among the atmospheric pollutants, carbon dioxide, sulphur oxides (SOx) and nitrogen oxides (NOx) are the major responsible of the stone material corrosion and decay.

Carbon dioxide is a natural constituent of the atmosphere but with its sharp increase in emission and concentration [13] it significantly contributes to stone artefacts erosion.

SOx have been studied for long time and they have demonstrated to have really harmful effects on the stone Cultural Heritage [14]. They enter the atmosphere mainly as SO_2 from both natural and anthropic sources. After oxidation, SO_2 is transformed into SO_3 which reacts with the carbonate substrate leading to the formation of gypsum precursor of black crusts [15]. However, the recent introduction of fuel with a low content of sulphur and of DeSOx (SOx removal) systems has caused a considerable decrease in SOx emissions.

The next section is dedicated to nitrogen oxides (NOx), a class of contaminants with remarkable acidic characteristic that can react in several ways in the atmosphere, mainly forming acids in the presence of water and/or oxidising agents. More information on other pollutant classes may be found in "Environmental Chemistry" by Mahan [16].

1.3.1 Nitrogen oxides (NOx)

Nitrogen, the most abundant gas in the atmosphere, is very stable. In fact, only in special conditions it can react with oxygen, forming nitrous oxide (N_2O), nitric oxide (NO) and nitrogen oxides (NO_2). N_2O is relatively unreactive and it does not significantly influence important chemical reactions in the lower atmosphere [16]. On the contrary, colourless, odourless NO and pungent red-brown NO_2 are very important in polluted air. These gases, collectively referred to as NOx, enter the environment from sources both natural, such as biological processes, and anthropic, such as industrial processes. These latter are much more significant, since the sources are concentrated in urban and industrial areas, where the concentration of these pollutants can cause severe problems to air quality.

Most of NOx are produced in combustion processes involved in energy production and transports, since at high temperature the following reaction occurs:

$$N_2 + O_2 \longrightarrow 2\ NO$$

NO undergoes several transformation processes, as shown in Fig. 1.5. It can be oxidized by ozone (O_3) or molecular oxygen, present in the environment, giving NO_2, according to these reactions:

$$NO + O_3 \longrightarrow NO_2 + O_2$$

$$2\ NO + O_2 \longrightarrow 2\ NO_2$$

Nitrogen dioxide is involved in several processes in the atmosphere. It is characterized by a great reactivity and it participates in the photochemical smog and

corrosion of the materials [16]. It can be also present as dimer, because of the establishment of the following equilibrium:

$$2NO_2 \rightleftharpoons N_2O_4$$

At room temperature N_2O_4 is the most abundant, since at temperature of 21,5 °C the ratio NO_2/ N_2O_4 is 0,001 [17].

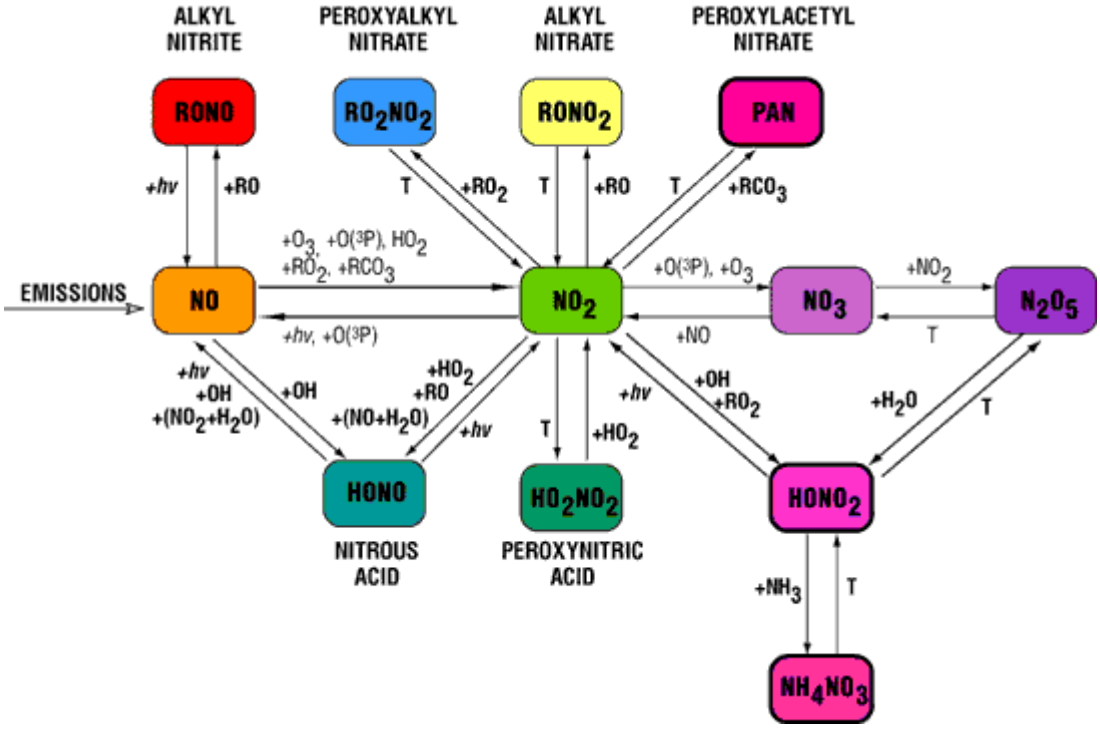

Fig. 1.5 – Transformation processes of NOx

In presence of water NO_2/N_2O_4 can be converted into nitrous (HNO_2) and nitric acid (HNO_3):

$$3NO_2 + H_2O \longrightarrow 2HNO_3 + NO$$

$$N_2O_4 + H_2O \longrightarrow HNO_3 + HNO_2$$

These acids can be formed in the atmosphere during precipitations - phenomenon called acid rain – and/or in other condition, such as droplet of the aerosols or fog, while the dry deposition of NOx has been found to be slower than the wet one [18].

The presence in the atmosphere of these strong acids can be very dangerous for stone materials, especially for limestones, where the carbonate minerals can be dissolved, according to the following reactions:

$$CaCO_3 + 2HNO_3 \longrightarrow Ca^{2+}\ 2NO_3^- + H_2O + CO_2 \uparrow$$
$$CaCO_3 + 2HNO_2 \longrightarrow Ca^{2+}\ 2NO_2^- + H_2O + CO_2 \uparrow$$

The damage due to NOx is not easily detected on the building façades, especially because nitrites and nitrates formed are high soluble and then they can be washed out by the rain or liquid water. As a consequence, the effects of nitrogen oxides have been not deeply investigated yet and therefore are also not well documented. On the contrary, the interactions of SOx with stone materials have been extensively studied, both in situ and through laboratory systems, because the formation of black crusts [19, 20] is one of the most evident rock decay phenomenon (see also Fig. 1.1). Nitrogen oxides have been often considered only as oxidants of SOx and in several works carried out from the late 70's till the 90's: NO_2, and more in general NOx, have been considered and proved to be promoters of the SO_2/SO_3 action [21].

Judeikis and Stewart carried out measurements of SO_2 depositions and they incorporated NOx to investigate the influence of NO_2 in SOx reactions [22]. Moisture was an important parameter for the conversion processes of SO_2, while the deposition of NOx was found to be independent from the relative humidity changes. A study on the interaction of SO_2 and NOx on stone materials by Johannson et al. [18] suggested that the presence of NO_2 greatly enhanced the conversion of SO_2, since the resulting corrosion products were predominantly gypsum. This is in reasonable agreement with the observations of other experimenters [23, 24]. The role of NO_2 and its conversion were, however, not clear and the formation of $Ca(NO_3)_2$ seemed to be unaffected by relative humidity.

In some works stone powders have been used in a variety of reaction devices in order to confirm the findings and to investigate the influence of porosity, RH% and stone composition. These and other laboratory studies have also enabled some estimation of the theoretical reaction kinetics [25-28].

The direct effects of NO and NO_2 and their deposition onto soil and cement has been studied by Judeikis and Wren [29]. Later, Johansson et al. [18] detected nitrites and nitrates on stone samples as a result of the exposure to an SO_2/NO_2 atmosphere.

Both authors did consider the action of nitrogen oxides and the formation of nitrogen salts as a minor effect. Other studies on the impact of acidic pollutants on natural rocks [30] and lime mortars [31] drew the same conclusion: here, the decay caused by NO_2 was found to be negligible if compared to other contaminants.

Recently, the effects of NOx on building materials have been evaluated, also taking into account the possible presence of conservation treatments [32]. Nitrogen dioxide induces two different harmful processes for limestone: in presence of water, NO_2 produces HNO_2 and HNO_3 that corrode calcareous materials because of their strong acidity; the salts (nitrites and nitrates) produced by these reactions and found on calcareous surfaces not directly washed by the rain, can directly and significantly contribute to the decay of the artefacts with the mechanisms already discussed in section 1.2.

1.4 Stone conservation

The conservation of stone Cultural Heritage has become over the last years a more and more complex problem that depends on several factors such as the characteristics of the rock and the environmental conditions of the area where the stone artefacts or buildings are placed. In addition to the natural causes of weathering, other decay factors, connected with the industrialization and the human activities, have appeared since the beginning of the XX century. Conservation is the whole set of actions taken to remedy and prevent the decay of Cultural Heritage. It embraces all acts that prolong and preserve the artistic and human message of the object, and in the case of stone artefacts, it involves several skills, such as architects, historians, engineers and of course conservators, supported by chemists, physicists, geologists and biologists.

Every restoration work should follow different phases: diagnosis, cleaning, consolidation (where necessary) and protection. The aim of preliminary investigations is normally to learn the history of the artefacts – in particular whether prior conservation treatments have been carried out – and evaluate its conservation state by means of chemical and physical analyses. Another crucial point is the knowledge of the environmental conditions, e.g. temperature, RH% and presence of pollutants around the object and then of the decay phenomena that may have taken place.

The treatment of the stone consists, on one hand, in the consolidation of the artefacts and, on other hand, in its protection, in order to reduce the damage caused by the ageing processes. Since, as already mentioned in sections 1.1 and 1.2, weathering is significantly enhanced by the water, it would be logical that the protective product must give high water repellent properties to the surfaces in order to avoid absorption of liquid water. For this reason, several organic products – mainly polymers – have been developed and studied, in order to reduce the absorption of water and moisture and, as a consequence, to preserve the material [33]. Both natural and synthetic polymeric materials, such as waxes, rubbers, vinyl polymers, acrylic resins, silicon-based products, epoxy resins, polyesters and polyurethanes, have been tried as conservation materials [3, 34]. Each product has well-defined characteristics depending on its composition and structure and it is hard to find one polymer which can, at the same time, fulfil all the needed requirements. Therefore, copolymers (polymers constituted by two or more different monomers) and blends (two or more polymers not chemically bonded to each other) have been introduced in the stone conservation field, in order to combine in the same product the properties of different molecules and obtain better performances [3]. In other cases, the polymers have been modified introducing fluorine (F) instead of hydrogen (H). Since the chemical bond C-F is stronger than C-H, 484 kJ/mol vs. 413 kJ/mol [35], the fluorinated polymers are more stable and chemically inert than the unmodified ones, so that the restoration treatment is more resistant to the ageing caused by pollutants, UV light and heating [36].

Also inorganic compounds, such as $Ba(OH)_2$ [3, 36] and $(NH_4)_2C_2O_4 \bullet 4\ H_2O$ [37], are used as consolidant/protective products, with the aim of reducing the exposed surface and/or reconstituting the natural binder and then increasing the mechanical strength of the material.

All the chemico-physical characteristics of the rock and other environmental conditions must be taken into account while planning a conservation treatment. In fact, because of the high variability of these parameters, a standard treatment does not exist and every conservation case must be considered as a unique problem. However, especially when organic molecules are employed, the surface must be completely water repellent after the application of the protective product, but the petrophysical properties of the material, such as the permeability to the water vapour, should not change drastically, in order to avoid the damages due to the entrapment of liquid water inside the stone. A drastic reduction of the permeability to the water vapour may occur when

superficial polymeric films are formed or a high number of pores are filled with the conservation materials.

The performance of the treatments depends not only on the choice of the product, but also on the application method, depending on the type of the surface, e.g. flat or sculptured, the dimension of the artefact, the porosity of the material and the desired penetration depth. Currently, four methods are the most used: (1) spraying and brushing, (2) absorption by capillary suction, (3) immersion at atmospheric pressure and (4) immersion at reduced pressure (under vacuum). Each method has its own advantages and drawbacks, depending on the object to be treated. The amount of the conservation product applied is relevant for obtaining a high efficacy of the treatments, but it should take into account that excessive amounts can cause pore blockage and harmful effects.

Also penetration depth and product distribution inside the rock pores are major parameters that strongly influence the final treatment efficacy. When the polymers penetrate deeply and are well distributed, the treatment gives a high hydrophobicity to the stone and the capability of the material to exchange water vapour from the rock to the environment is normally preserved.

The penetration and distribution of the treatments depend on several factors:

- porosity of the stone
- dimension and morphology of the pores
- chemical and physical properties of the conservation product
- choice of the solvent
- concentration and viscosity of the treatment solution
- application method and treatment condition

The presence of polar groups, such as –OH and/or –COOR, in the organic molecule can enhance the adhesion and the affinity between the treatment and the rock, leading to a more probable homogenous distribution. Other factors, such as polymer molecular weight, concentration and choice of the solvent, influence the viscosity of the solution. As a general trend, the viscosity of the treatment solutions increases as the molecular weight and concentration increase and the penetration depth decreases as the viscosity increases.

Last, the application method and conditions determine the time in which the solution is in contact with the substrate as well as the evaporation rate of the solvent: application by immersion or capillary absorption provide higher penetration and more

homogeneous distribution than brushing and spraying. An estimation of the conservation treatment effectiveness can be done by means of water repellence measurements. This quick and simple method gives indications about the surface behaviour and the stone capability of absorbing liquid water. The hydrophobic tests cannot help to deduce other information, i.e. the distribution of the polymer, the degree of protection against the atmospheric pollutants or the processes of diffusion and condensation of water vapour. For these reason, the complete evaluation of the conservation treatments should be based on different complementary techniques. Several test methods, such as measuring of the water droplet absorption time, visual observation of colour changes on wetting and drying, water vapour permeability or strength tests, try to determine the penetration depth by measuring superficial characteristics [38]. Other methods, both direct and indirect, are destructive, not very accurate or reproducible; they sometimes require a complicated sample preparation or the use of markers to highlight the presence of the treatment [38].

More difficult is the evaluation of the polymer distribution inside the stone material; Magnetic Resonance Imaging (MRI), an indirect and non-destructive technique, has been successfully applied to visualize the diffusion of liquid water in treated (hydrophobic treatment) and not treated stone samples [39]. Recently, also neutron techniques demonstrated to be useful for the localization of the conservation treatments [40].

The performance and efficacy of the treatments should be tested directly on sample of weathered stone, but this is seldom possible, then laboratory samples must be used. Laboratory samples can be also studied for the investigation of long term effects induced by the treatments on stone materials or the durability of the treatments themselves. To these aims, accelerate ageing systems can provide useful information about the behaviour and efficacy of the products when submitted to thermo-hygrometric cycles, UV radiation or exposition to aggressive pollutants. The knowledge of the modification that may occur on the treatments over time is necessary in order to assess whether the restoration compromises or not future conservation treatments.

The reversibility [41, 42], intended as the possibility to remove completely an old superficial treatment from an artefact, is a fundamental issue, since aged products can cause undesirable aesthetical and harmful effects [43], e.g. yellowing and/or acceleration of decay processes. The conservation treatments often become insoluble in any solvents, due to their chemical modifications after application and/or to the ageing

processes [44]; for these reasons they can be hardly removed from the surfaces, and in these cases, mechanical and physical methods (e.g. laser ablation) must be used [45].

Chapter 2

MATERIALS, METHODS AND EXPERIMENTAL CONDITIONS

2.1 Stone material: Lecce stone

For this research, Lecce stone - a biocalcarenite - has been chosen. This rock takes its name from the city of Lecce in the south of Italy, however it is a very common material in the entire Salento region. It has been used for a long time, especially during the Baroque period, for covering the façades of the most important and beautiful buildings of that area (e.g. Basilica of Santa Croce in Lecce, Fig. 2.1) as well as for sculptures. Nowadays, it is employed for the realization of decorative objects.

Fig. 2.1 – Façade of the Basilica of Santa Croce in Lecce (Italy)

The petrographic study has been carried out on thin sections (Fig. 2.2b) observed in transmitted polarized light by means of optical microscopy. These observations were necessary to determine the petrographic classification of the rock, to estimate the grain size and to recognize the type and amount of bounding material. Lecce Stone reveals to be made of a grain mixture of microfossils, fossil fragments and shells, with dimensions ranging between 100 and 200 μm. The bioclasts are constituted prevalently by planctonic foraminifera and secondarily by shells. The macroporosity is relevant and mainly due to empty foraminifera chambers, while the microsparitic matrix is constituted essentially by calcium carbonate. This mineral is the basic component, with

a total percentage of 93-97%, while small amounts of granules of quartz, glauconite, feldspars and clay minerals (i.e. kaolinite, illite, smectite) have been detected by x-ray powder diffraction.

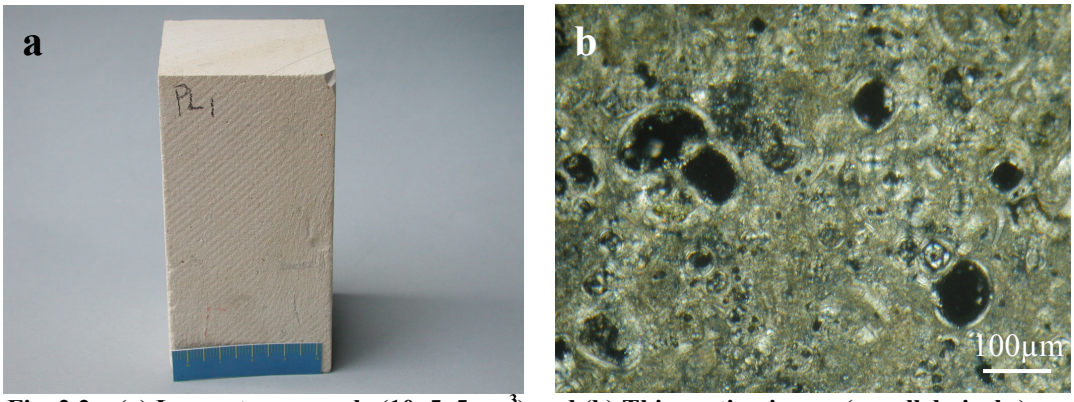

Fig. 2.2 – (a) Lecce stone sample (10x5x5 cm^3) and (b) Thin section image (parallel nicols)

Petrographically, in Dunham's classification this stone is named as wackstone and in Folk's classification as biomicrite.

The physical parameters of Lecce stone, such as porosity and density, have been measured by means of different techniques commonly used for the characterization of rocks. As shown in table 2.1, Lecce stone demonstrates to have a high open porosity.

Lithotype	Real density (g/cm^3)	***Bulk density*** (g/cm^3)	Total open porosity (%)	Water porosity (%)	Meso-porosity (%) (0.007-300 µm)
Lecce stone	2,70 ± 0,10	1,42 ± 0,20	47,4 ± 1,2	39,0 ± 0,2	35,8 ± 2,1

Tab 2.1 – Physical parameters of Lecce stone

The total open porosity and the density values have been obtained by a helium pycnometer (Quanta Chrome).

The porosity accessible to water (WP%) is calculated according to the method ISO 6783 [46], with the following equation:

$$WP\% = \frac{(M_3 - M_1)}{(M_3 - M_2)} \times 100$$

Where M_1, M_2, M_3 are the dry, hydrostatic and wet weight of the sample.

The mesoporosity, defined as pores with diameter range 0.007-300 µm, has been measured by means of a Thermofinnigan mercury porosimeter (Pascal 140 and 240

units). This technique also allows to estimate the pore size distribution, reported in Fig. 2.3.

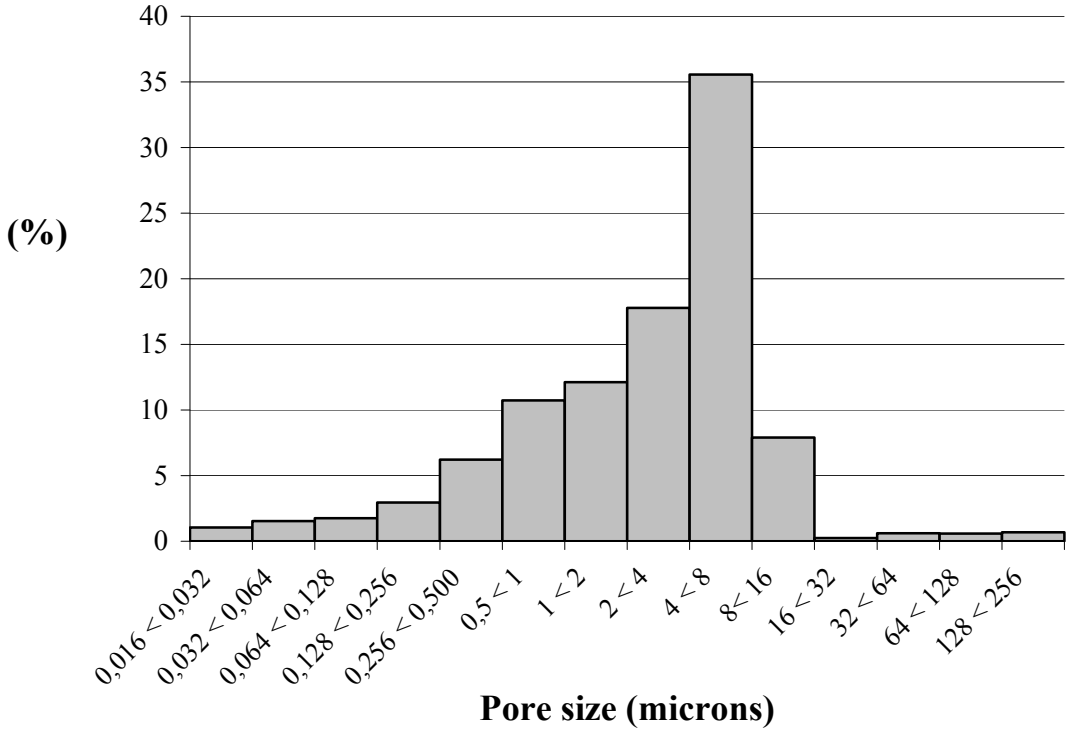

Fig. 2.3 – Pore size distribution estimated by mercury intrusion porosimetry

2.2 Sample preparation and characterization

Samples, with dimensions 5 x 5 x 1 cm^3, have been scraped off with a grinding paper of granulometry P-180 using a lapping machine RemetLS2 (30 seconds at 100 rpm), in order to give uniform surfaces and to delete cutting imperfections. Subsequently, they have been washed with water so as to remove the dust deposits. These specimens have been characterized by means of several techniques, such as capillary absorption test, colour measurement and surface analysis.

Other samples, with dimensions 3 x 3 x 10 mm^3 and 1 x 1 x 10 mm^3, suitable for micro computed tomography (μ-CT) and synchrotron radiation computed tomography (SR-CT), have also been prepared (fig. 2.4).

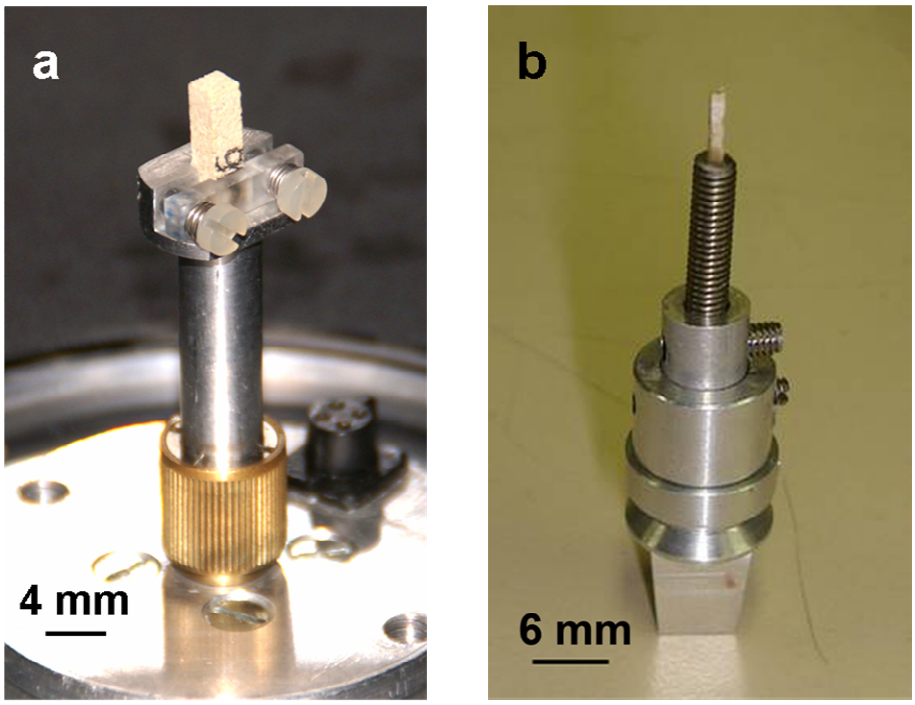

Fig. 2.4 – Lecce stone samples for (a) µ-CT and (b) SR-CT

2.2.1 Capillary absorption tests

The measurements of water capillary absorption have been performed according to the UNI method [47]. The samples have been dried in a desiccator with $CaCl_2$, until constant weight (± 0.001g) has been reached, and then put on a stack of fifty filter paper saturated with distilled water, as shown in Fig. 2.5.

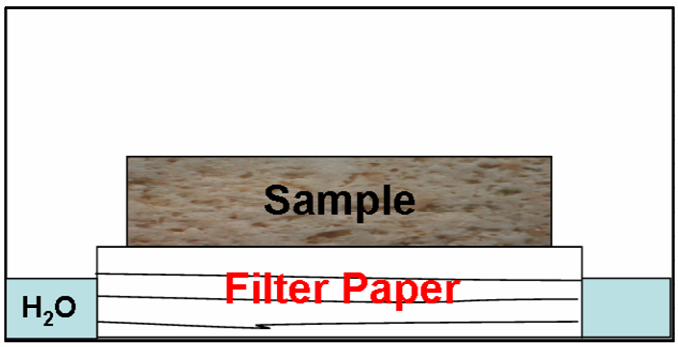

Fig. 2.5 – Scheme of capillary absorption test

After 15' the samples have been weighted and the amount of water absorbed (A) has been calculated by difference between the wet (W_{Wet}) and dry (W_{Dry}) weight:

$$A = W_{Wet} - W_{Dry}$$

The absorption measurements have been repeated on each sample 5 times. These measurements, taken before the treatment, allow the selection of samples with homogeneous behaviour and with a constant ability for absorbing water. In fact, only the samples showing a percent error (Er%) < 10% have been selected. E% was calculated as follows:

$$Er\% = \frac{A_{Max} - A_{Min}}{A_{Med}} \times 100$$

where A_{Max}, A_{Min} and A_{Med} are the maximum, the minimum and the average amount of water absorbed by the sample in the absorption tests, respectively.

2.2.2 Colour Measurements

The aesthetic aspect of the façades and stone artefacts is one of the major issues in stone conservation. Colour measurements have been carried out, according to the NORMAL method [48] by a Minolta CR-200 chromameter, based on the acquisition of reflectance patterns of the rock surface. The data are represented using a colour solid (Fig. 2.6), where every colour can be defined by three coordinates: L*, brightness ranging from 0 (black) to 100 (white); a*, hue from -60 (green) to +60 (red); b*, saturation from -60 (blue) to +60 (yellow).
The chromatic data can also be expressed as E:

$$E = \sqrt{L^{*2} + a^{*2} + b^{*2}}$$

The measurements have been carried out only on the 5 x 5 x 1 cm^3 samples, analyzing the same area, in order to highlight colour changes that may occur because of the conservation treatments or ageing.
These variations are calculated as follows:

$$\Delta E = \sqrt{\Delta L^{*2} + \Delta a^{*2} + \Delta b^{*2}}$$

Normally, the colour changes appreciable by the human eye have values of $\Delta E \geq 3$.

Fig. 2.6 – L*a*b* colour representation

Colour measurements have been performed before and after the application of the conservation treatment and ageing, in order to highlight surface changes that may occur.

2.3 Conservation treatments

Several chemicals have been used for stone conservation, both organic and inorganic, as consolidants (to restore the mechanical properties of the artefacts) and protectives (to prevent the deterioration action by physical and chemical agents).

A good treatment should have the following characteristics [49]:

- Water repellence
- Non-reactivity with stone

- Stability over time to heat, UV radiation, environmental agents and pollution
- Reversibility
- Good adhesivity to rock
- Do not block completely the natural porosity
- Do not cause chromatic changes the stone surface
- Solubility in solvent non-dangerous or tossic

Four products, widely used for stone conservation, have been selected for the research carried out in this PhD thesis: Paraloid B 72 (PB 72, acrylic resin), Hydrophase Superfici (Sil, alkyl alkoxy silanes), a Fluorinated rubber (NH) and ammonium oxalate (Ox). Some of these products, such as acrylates, are employed as consolidants and protectives, depending also on the application method, which determines the penetration of the treatment itself. On the contrary, the fluorinated rubber and alkyl alkoxy silanes have mainly a protection function, while ammonium oxalate is normally used as a consolidant.

The most relevant characteristics of polymers influencing the performance of the treatments are the glass transition temperature (Tg) and the average molecular weight (M_W).

The glass transition temperature is a relevant characteristic of the polymeric products. It is defined as the temperature at which an amorphous solid, such as a polymer, becomes brittle on cooling, or soft on heating [50]. Below the glass transition temperature amorphous solids are in a glassy state and most of their joining bonds are intact. Organic polymers above Tg become soft and are able to give plastic deformation without fractures. This has two aspects: a polymer which is too soft will lead to a sticky surface or a dirt pick-up coating; while a polymer which is too stiff may crack when stressed or may not be able to respond to the movements in the object, such as thermal dilatation/contraction cycles of the artefacts [34].

The average molecular weight (M_W) influences the distribution of the polymers in the stone structure: a high molecular weight may give less uniform distribution than polymers with lower molecular weight. This is due to the dimension of the molecules, that may be larger than the stone pores, and to the viscosity and solubility of the products. As a general trend, in fact, the viscosity of the treatment solutions increases as the molecular weight increases, while the solubility of polymers decreases as the molecular weight increases.

2.3.1 Paraloid B72 (PB 72)

Acrylates, both as homopolymers and copolymers, have been employed in conservation field since a long time, not only for stone artefacts, but also for paintings, wood, paper and textiles [34].

The choice of monomers strongly influences the chemico-physical properties of the resulting products. In fact, the poly acrylates are generally more flexible than the poly metacrylates, while the rigidity increases as the number of carbon atoms in the alkoxy group decreases. For example, the poly methyl methacrylate is more rigid than the methyl acrylate and the poly methyl acrylate is harder if compared with the corresponding poly ethyl acrylate. Paraloid B 72 (Fig 2.7) is an acrylic *co*-polymer formed by ethyl methacrylate (70%) and methyl acrylate) (30%). It provides a good combination of rigidity, resistance and adhesion, but it has also some drawbacks, as the treated surfaces become yellow because of its oxidation by UV radiation [51] and its water repellence decreases over time [36].

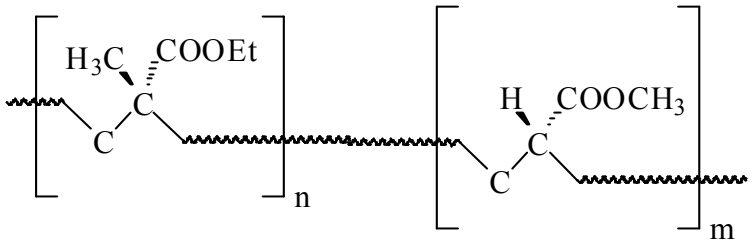

Fig. 2.7 – Structure of Paraloid B72. Et = ethylic group

Paraloid B 72 has a M_W = 91000 amu and a Tg = 43 °C. It has been applied in acetone solution with a concentration of 2% (w/w).

2.3.2 Fluorinated rubber

Fluorinated rubber, also called NH (Fig. 2.8), is a copolymer hexafluoropropene-*co*-vinylidenefluoride, with a content of fluorine = 65% (w)/w).

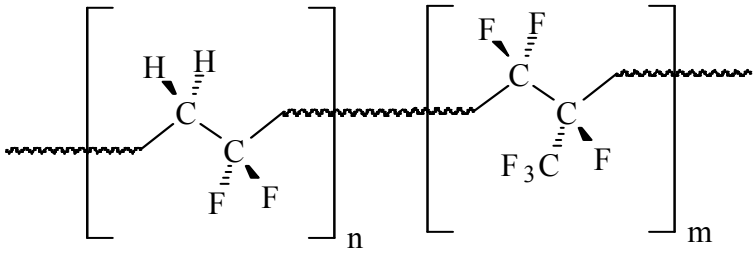

Fig. 2.8 – Structure of Fluorinated rubber

This conservation product has good solubility in organic solvents with medium polarity, such as ketones, and other major properties:

- High stability to UV radiation, due to the presence of C-F bonds (not easily oxidized as C-H);
- Reversibility, since chains cannot cross link and the polymer is still soluble after application and ageing;
- High water repellence.

NH with its high molecular weight, i.e. M_W = 350000 amu, is normally suitable for the treatment of stones with high porosity, such as Lecce stone, while the presence of small pores, such as in marbles, makes the penetration of the polymer difficult [36]. Moreover, Tg is -18 °C, meaning that cracks caused by mechanical stresses cannot occur. On the other hand this may results in remarkable dust and dirt deposition.

Fuorinated rubber has been applied in acetone solution with a concentration of 1% (w/w).

2.3.3 Hydrophase Superfici

Hydrophase Superfici is a commercial solution of alkylalkoxysilanes oligomers in 2-propanol (40%, w/w). Because of their small molecular size, the oligomers can easily penetrate inside the stone structure and, after the evaporation of the solvent, they polymerize in situ forming the effective protective product with the mechanism shown in Fig. 2.9. Since the formation of the actual treatment involves processes of hydration (step 1) and subsequent condensation (step 2), the time and degree of polymerization depends on the environmental parameters, e.g. temperature and relative humidity: step 1 is enhanced by high humidity, step 2 requires dry conditions.

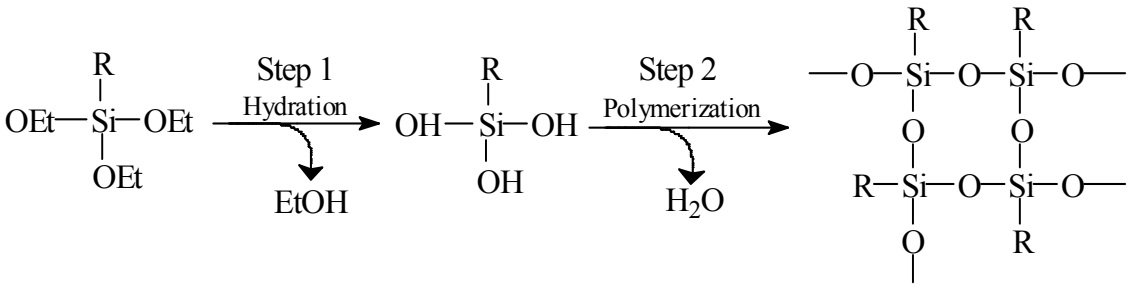

Fig. 2.9 – Mechanism of polymerization of alkyl alkoxy silanes. R = organic chain (typically methyl or ethyl) ; Et = ethylic group; EtOH = ethanol

The resulting treatment is also influenced by the amount of alkoxy group present in the oligomers: the higher the number of –OR group, the higher the degree of cross-linking and therefore the rigidity of the polymer.

This treatment has generally good adhesion properties due to the hydrogen bonds between the oxygen of the chain and the rock, as well as strong water repellence due to the alkyl groups oriented to the air/solid interface.

Hydrophase Superfici is more expensive than PB 72 and after application it becomes insoluble in any solvent, so that it can be removed from the surface only with mechanical methods. It has been applied as supplied.

2.3.4 Ammonium Oxalate

The treatment with ammonium oxalate is based on criteria radically different from those of water repellent and polymeric protective agents applied on the surface of stone artefacts, since it is a not hydrophobic treatment. It has been originally developed for the consolidation of wall paintings [52] and consists in the application of a saturated solution of ammonium oxalate which can react with the carbonatic substrate leading to the formation of whewellite ($CaC_2O_4 \cdot H_2O$), as follows:

$$CaCO_3 + 2\ NH_4^+(aq) + C_2O_4^{2-}(aq) \Longrightarrow CaC_2O_4 \cdot H_2O + 2NH_3 + CO_2$$

The whewellite coats the pores walls and gives a consolidant and/or protective effect, without changing the original characteristic of the rock, such as its wettability. However, it should be taken into account that the heterogeneous reaction with contemporary formation of insoluble product (whewellite), associated to the complicate

stone structure and the uncontrollable condition may cause the precipitation of the calcium oxalate in powdery form, without an efficient coating and distribution into the rock pore network.

Another issue is the colour changes induced by the oxalate. In fact, an excess of solution on the surface can cause a whitening of the object.

This treatment has been performed with a solution of concentration = 5% (w/w) exclusively by capillary absorption.

2.3.5 Application methods and conditions

For Lecce stone samples with dimensions 5 x 5 x 1 cm^3 two application methods have been used: brushing and capillary absorption.

Bushing is one of the most common methods for treating building façades and large objects. The evaporation rate of the solvent depends on the environmental conditions, but it is normally quick and thus the penetration of the solution is rather limited to few millimetres. Brushing is generally cheap and requires a limited amount of product if compared with other methods.

Capillary absorption can be used to realize a better penetration, applying a compress to the artefact surface, e.g. cellulose pulp soaked with the treatment solution. As compared to brushing, this method allows to better control the treatment parameters and penetration, but it requires a higher amount of product and solvent and it produces a considerable amount of wastes. For laboratory samples, the capillary absorption treatments were performed putting one of the 5 x 5 cm^2 faces of the samples on stacks of 10 sheets of filter paper saturated with the polymer solution, until the samples were completely soaked. Table 2.2 shows the optimized experimental conditions of the treatment.

The samples with dimensions 3 x 3 x 10 mm^3 and 1 x 1 x 10 mm^3, analyzed by μ-CT and SR-CT respectively, have been treated by vacuum impregnation. The specimens have been put in a Schlenk flask connected to a membrane vacuum pump for 2 h in order to eliminate air and moisture inside the pores and afterwards the treatment solution was added using an addition-funnel. After 20 h, the samples were drawn out and dried at room temperature. This different method has been used because the

treatment of small samples is more complicated and the capillary suction is not enough to guarantee and effective absorption of the solution.

Product	Application method	Conditions
PB 72	Brushing	3ml, 2% (w/w) in acetone
	Capillary absorption	2% (w/w) in acetone, 7h
NH	Brushing	3ml, 1% (w/w) in acetone
	Capillary absorption	1% (w/w) in acetone, 17h
Ammonium Oxalate	Capillary absorption	5% (w/w) in H_2O, 28h
Hydrophase Superfici	Brushing	3ml
	Capillary absorption	3h

Tab. 2.2 - Conditions of conservation treatment application

2.3.6 Evaluation of the protective treatments

The treatments of the 5 x 5 x 1 cm^3 have been evaluated measuring the capillary absorption of the specimens before and after the products application and calculating the protective efficacy (PE%) as follows:

$$PE\% = \frac{A_B - A_A}{A_B} \times 100$$

Where A_B and A_A are the amounts of water absorbed by the sample before and after the treatment respectively. The decrease of water uptake helps to estimate the effectiveness of the treatment.

The values of permeability to water vapour have been calculated as mass of water vapour crossing the stone surface unit in 24 h, according to the NORMAL method [53] and expressed as Residual Permeability (RP%):

$$RP\% = \frac{P}{P_0} \times 100$$

where P and P_0 are the permeability to water vapour of the treated and untreated sample, respectively. This value gives an idea of the decrease of the vapour exchange capability and the pore blockage, caused by the polymer application.

Other investigations have been done by means of 2D/3D neutron imaging and x-ray μ-, nano- and SR-computed tomography, with the aim of studying the penetration and distribution of the polymers. A description of these techniques, instruments and experimental conditions is provided in chapter 3.

2.4 Accelerate ageing system

An accelerate ageing system (Fig. 2.10) has been set up with the aim of exposing stone samples to atmosphere with NOx and study the reactions and decay processes in which these contaminants are involved.

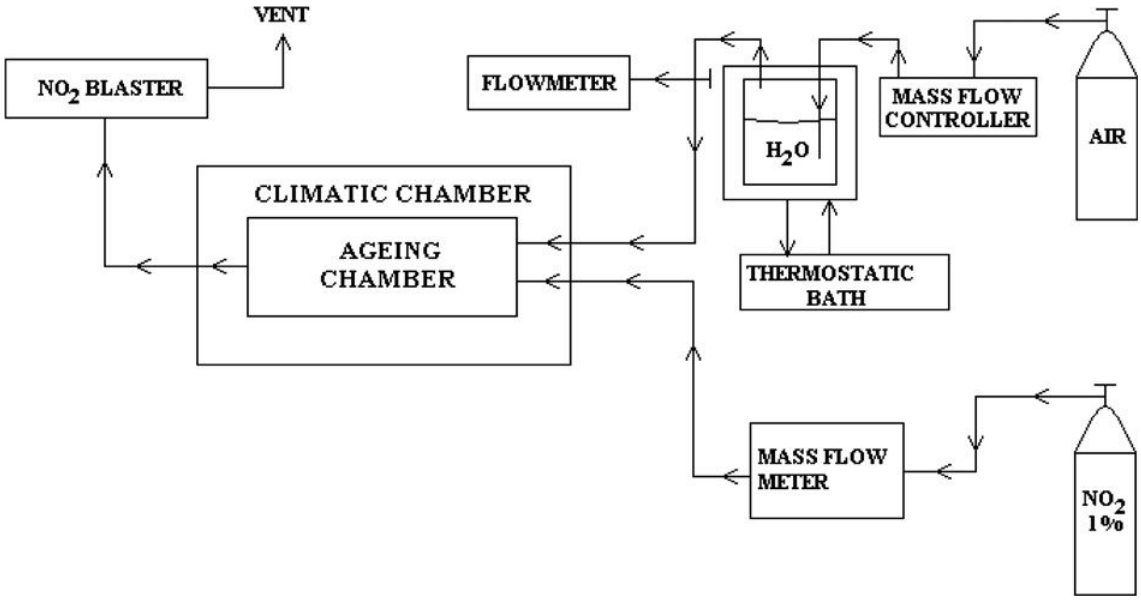

Fig. 2.10 – Scheme of accelerate ageing process of rock materials with NOx

To simplify this study, NO_2 was chosen as representative of NOx, considering that NO, in the troposphere, is readily converted into NO_2, a very reactive and significant species in urban areas [16].

The ageing chamber (Fig 2.11) is a box of stainless steel AISI 316 (American Iron Steel Institute) fitting in a climatic chamber (Mazzali Climatest) which allows to

perform thermo-hygrometric cycles, in order to simulate day/night environmental conditions.

The flow of NO_2 (1% mol/mol in N_2) is regulated by a mass flow meter AALBORG GFC171s (operating range 0.00 - 10.00 ml/min); while air is used to dilute NO_2, to achieve the desired concentration and to regulate the humidity. In fact, the air flow bubbles through water, kept at constant level and temperature (30 °C), in order to obtain constant and repeatable humidity inside the ageing chamber.

The gases enter from the top (NO_2) and the bottom (air) of the box through a metallic gas diffuser and they are mixed by three fans. NO_2 concentration is constantly monitored with a sensor (ThermoGas Tech Mod. Screamer) calibrated in the range of 0 - 10 ppm, with sensitivity = 0.1 ppm.

Several tests have been performed in order to optimize all the parameters and ageing conditions [54], in order to simulate a real polluted environment. The artificial ageing process does not include liquid water, so that the research on the samples is mainly representative of the behaviour of stone artefacts sheltered from the direct rain effects and/or low precipitation seasons.

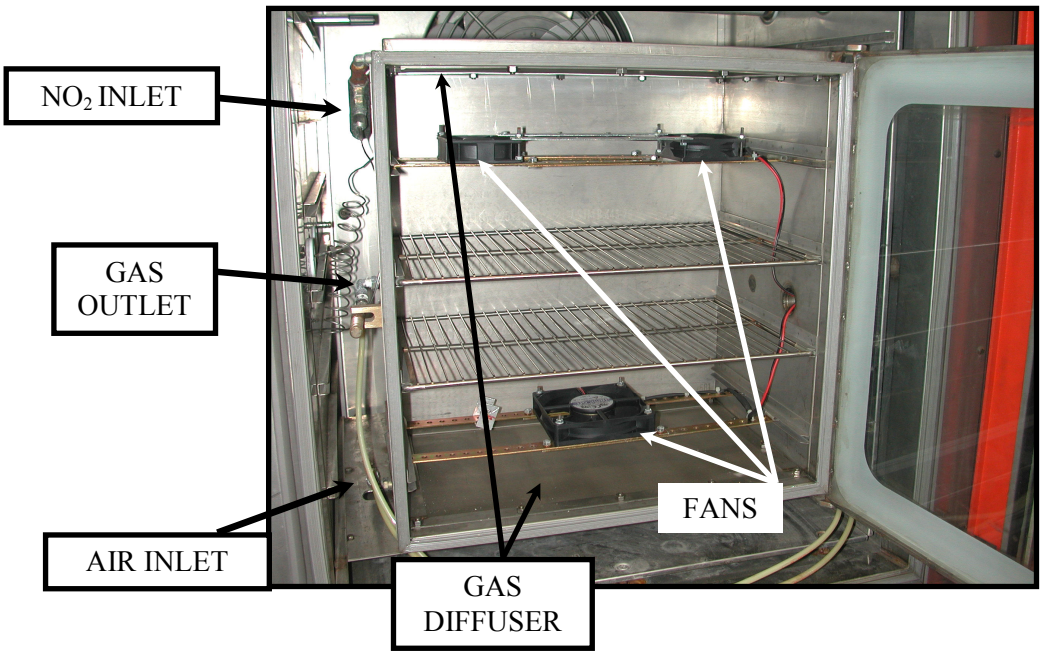

Fig. 2.11 – Ageing chamber

Forty samples 5 x 5 x 1 cm^3 (five untreated and thirty-five treated with the selected products; for each product and application method five samples have been

used) and fifteen samples 3 x 3 x 10 mm^3 (five untreated, five treated with PB 72 and five treated with NH) have been aged with the following experimental conditions:

- Temperature ranging from 5 to 30 °C and Relative Humidity (RH%) from 50% to 90% during 330 min cycles, as displayed in Fig. 2.12 (1 cycle = 5.5 h)
- Air flow = 120 ml/min @ 3.5 bar
- NO_2 flow = 2.00 ml/min @ 2 bar
- [NO_2] = 0.9 - 1.1 ppm. It assures to speed up the ageing, but without drastic conditions. In fact, this concentration is around ten times the concentration limits for air quality imposed by the Italian law (DM 60/2.4.2002)
- Temperature of the thermostatic bath = 30 °C

The chosen temperature, RH% and [NO_2] are possible conditions in urban areas where most of the stone artefacts are located. The intent of the research is to accelerate the ageing processes and not to expose the materials to drastic conditions. To use drastic conditions may lead to results not representative of the actual action of NO_2.
The samples have been analyzed at different steps, in order follow the ageing process and investigate its mechanism.

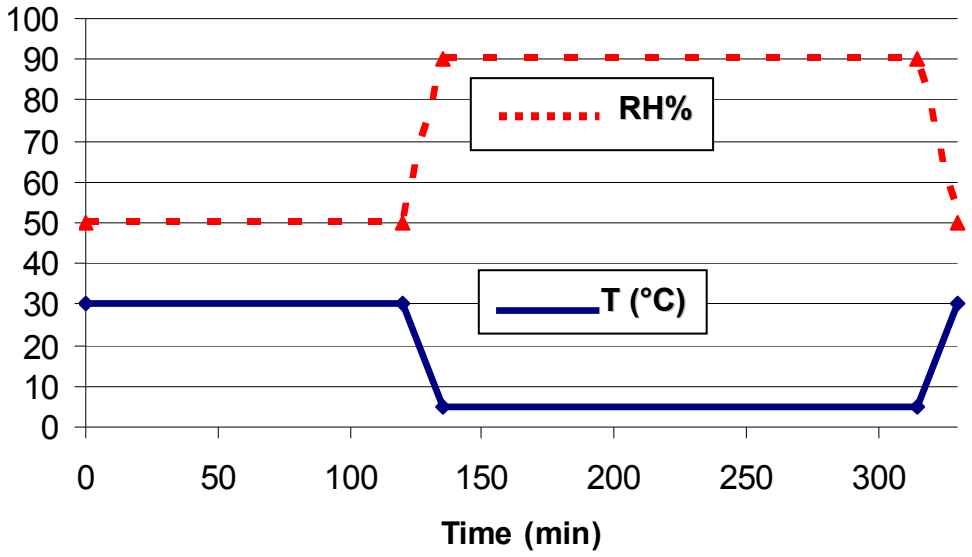

Fig. 2.12 – Thermo-hygrometric condition of ageing

2.4.1 Monitoring of the ageing

The ageing process of Lecce stone samples have been monitored by means of several techniques. The surfaces have been analyzed by Environmental Scanning Electron Microscopy (ESEM) and laser µ-profilometry which allow to highlight the erosion and morphological changes caused by NOx.

ESEM is particularly useful, since it is a non-destructive technique and it is possible to achieve high resolution in the images. "Environmental" indicates that the instrument can work in low vacuum mode (around 10 torr) instead of the high vacuum (10^{-5} - 10^{-7} torr), necessary in the conventional electron microscopes. One of the advantages of ESEM is finally the possibility to analyze non-conductive samples, as stone is, without special or complicated sample preparation, such as metallization, thus the samples can be preserved and investigated at different ageing steps.

A laser µ-profilometry is also a non-destructive techniques and it has been used to acquire images and profiles of the surfaces with high precision and spatial resolution (up to 1 µm). This system has been developed at the National Institute of Applied Optics (INOA) of Florence and it is based on a commercial laser distance- meter (Optimet Conoprobe) fitted on two high precision (0.1 µm) power-driven slides [55]. The equipment and sample holder have been put on an anti-vibration table and an area of 1 cm^2 has been scanned with a sampling pitch of 20 µm (Fig. 2.13).

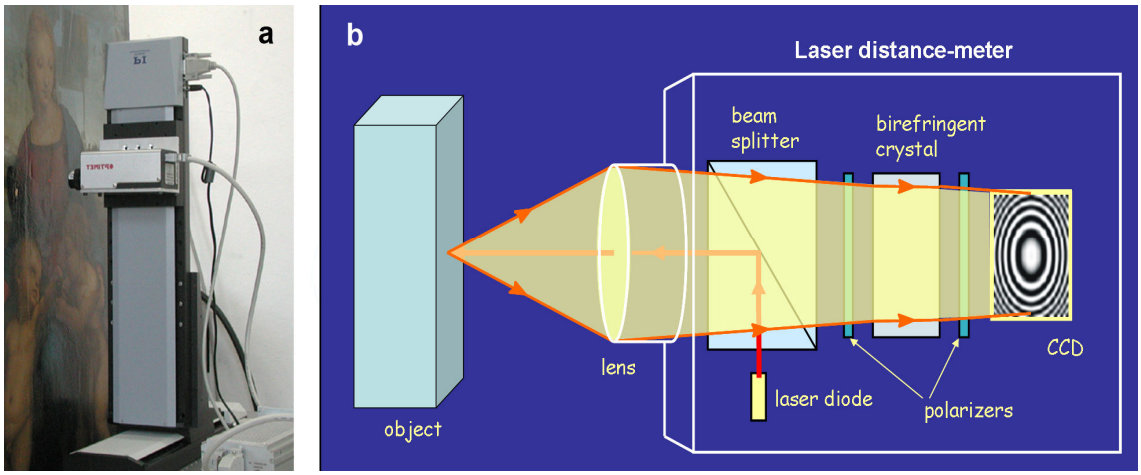

Fig. 2.13 – Laser µ-profilometry system. (a) In situ application and (b) optical scheme. (courtesy of Dr. Pampaloni)

In the case of the ESEM it is very difficult to investigate exactly the same area of the sample at different ageing steps. The images, taken at different magnifications,

are qualitatively evaluated to highlight morphological changes of the surfaces and/or of the calcite crystallites. On the contrary, the same profiles of the samples at different ageing steps can be acquired and compared by laser μ-profilometry.

In addition to these surface investigations, the colour measurements (see section 2.2.2) of the samples have been performed, with the aim of highlighting colour changes due to the ageing processes.

Since the action of NOx leads to the formation of nitrates and nitrites in Lecce stone specimens, these soluble salts have been extracted, by washing the aged samples with bidistilled water, in order to estimate the damage caused by the exposure to these contaminants. The presence of the conservation treatments (hydrophobic products) on the samples, makes the extraction process difficult, thus several consecutive extractions are required. Each extraction has been performed with 130 ml of water, under constant magnetic stirring, using a closed glass device previously cleaned with chromic mixture and dried at 60 °C. The efficacy of the extracting procedure has been tested by grinding the samples and washing the obtained powder for 70 hours: no significant amounts of nitrites and nitrates have been found in these solutions.

The amount of NO_3^- and NO_2^- has been determined by ionic chromatography under the following conditions:

Chromatograph: Dionex DX 500 chromatography system

Detector: ED50 Electrochemical

Analytical column: AS14

Guard column: AG14

Eluent: Na_2CO_3 3.5 mM/$NaHCO_3$ 1.0 mM

Moreover, 2D/3D neutron imaging experiments have been performed with the aim of evaluating and quantifying the impact of NOx on the rock, while x-ray μ-CT has been used to investigate the changes of morphological parameters induced by the exposure to the contaminants. More details about these techniques and the experimental conditions are provided in chapter 3.

Chapter 3

X-RAY TOMOGRAPHY AND NEUTRON IMAGING TECHNIQUES

3.1 X-ray tomography

The three-dimensional (3D) structures of objects and materials can be studied by means of two-dimensional (2D) or 3D imaging. 2D investigations are normally made on polished flat planes or thin sections, and they can help to understand structure and morphology. However, 2D representations are rather limited, as a section is only a part of the whole object. A 2D analysis is not enough when direct 3D information is needed; for instance, the number of objects per surface area cannot be linked to the true 3D number of objects per unit volume, since objects in a 2D section might appear separated whereas they are connected in 3D. The size distribution of phases with complex shape in the material cannot be simply estimated from a 2D section; the same happens for the connectivity of phases which is a 3D parameter [56].

Any method that reconstructs mathematically the internal structural information from a series of projections within a specimen is called tomography [57]. Tomography takes its name from old Greek word "tomos", meaning section or slice. This is a technique that allows to visualize inner sections of an object without cutting it and thus, to access and investigate its 3D structure.

Computed tomography (CT) provides three-dimensional information of the sample by recording a set of two dimensional radiographs imaged at different angles: each radiograph is a map of the attenuation of the x-ray photons caused by the sample. The attenuation is related with different factors, such as elemental composition and thickness of the phases present in the object.

Starting from the stack of the 2D projections it is possible, using mathematic algorithm, to reconstruct a data set of the transversal sections, corresponding to a full 3D map of the linear attenuation coefficient.

The first CT instruments have been developed in 1972 by Hounsfield [58] and used for long time only for medical purposes. Later, they have been successfully applied also in other research fields, such as geosciences [59].

Photographic films have been used for a long time to record radiographies, but nowadays the most common detectors for x-ray radiography and tomography are the systems with scintillator and charge-coupled device (CCD) camera. The image is then obtained by converting the x-rays into visible light using a scintillator and projecting them onto a CCD. In other words, when the x-ray hits the scintillator it produces a visible radiation, recorded by the camera and proportional to the amount of photons.

Each element of the camera is called pixel and it records a small part of the 2D projection. Pixel is also used with meaning of picture element; in fact it corresponds to a single point in a graphic image or the smallest single component of an image [60].

In CT, resolution is expressed as pixel size, indicating not the physical size of the single element of the CCD, but the dimension of the scanned object recorded by one pixel. When the tomographic datasets are analyzed 3D, voxel (volume element) can be also used instead of pixel.

Resolution strongly depends on the spot size of the x-ray source, the characteristics of the detector and the scanner geometry. In the medical CT scanners, the patient is fixed and the source and detector are rotating around him, and the maximum resolution achievable nowadays is a pixel size of 250-100 µm. With the diffusion of compact microfocus x-ray tubes, new CCD cameras and more powerful calculation resources, desktop micro-CT (µ-CT) instruments have been developed in the 90's [61]. In these instrumentations, the x-ray source and the detector are fixed and the sample is mounted on a motor stage in order to rotate it (Fig. 3.1). This different geometry, x-ray sources and detectors allow to achieve a resolution in the order of microns.

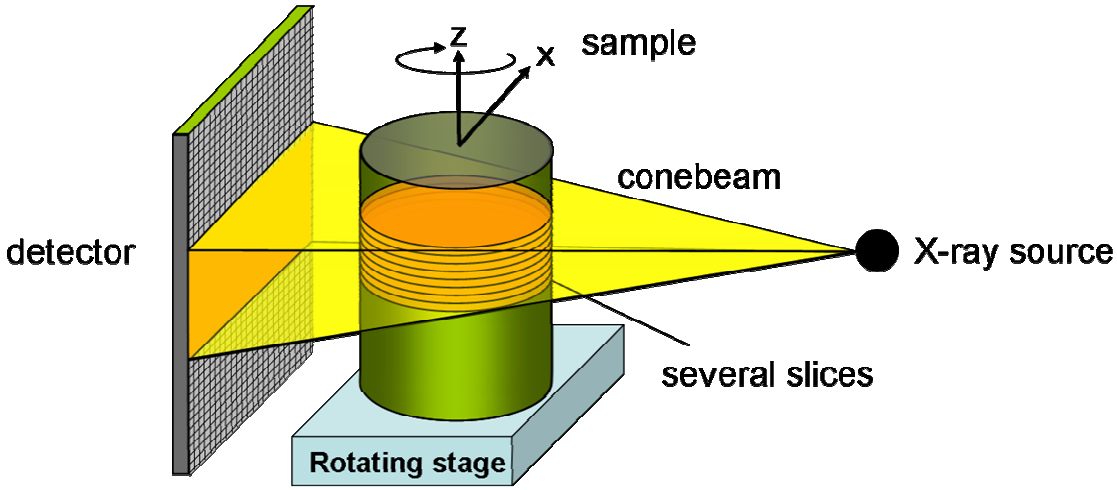

Fig. 3.1 – Scheme of laboratory µ-CT instrument geometry

Presently, the desktop µ-CT systems are really improved thanks to advances in detector technology, more accurate rotation stages and new acquisition geometries, and they can achieve higher pixel resolutions (up to 0.8 µm). Furthermore, thanks to new x-ray sources with sub-micron spot size, instruments for x-ray computed tomography with

sub-micron resolution, called nano-CT, have been developed. With the latter, it is possible to achieve a pixel resolution of 150 nm, but only small sample (typically 0.5-2 mm) can be scanned.

3.1.1 Interaction of x-rays with matter

When an incident X-ray beam passes through the matter several processes take place. The intensity of the beam decreases because of the scattering of the photons, i.e. deflection, or of their absorption, i.e. complete loss of their energy. A brief description of the physical phenomena involved in the interactions of x-ray with matter is here presented with the intent to give a simple overview. An extensive description of these processes can be found in different books [62].

Compton Effect

The Compton scattering or the Compton effect occurs when an incident x-ray interacts with the external-shell electrons of the atoms. The incoming photon is scattered incoherently, so the emerging photon is deflected by an angle related to the loss of energy and a wavelength increased by a value, called the Compton shift.
The photons are scattered in a different direction from the original one and part of their energy is transferred to the electrons.

Rayleigh Effect

The Rayleigh effect occurs when the interaction between an x-ray photon and electron of the absorbing compound is elastic, i.e. without loss of energy. This process is also called coherent scattering, thus the photon does not lose energy, but it is just deflected by the electrons.

Photoelectric Effect

The photoelectric effect is a quantum electronic phenomenon in which electrons are emitted from matter after the absorption of energy from x-rays.

The energy of the incoming photon is transferred to an internal-shell electron that is ejected. In the meantime, another electron from the external-shell fills the vacancy in the internal-shell and emits a radiation with a characteristic energy.

Pair Production

Pair production refers to the creation of an elementary particle and its antiparticle. In nuclear physics, this occurs when a high-energy photon interacts with an atomic nucleus, allowing it to produce an electron and a positron without violating conservation of momentum.

In order to generate a pair, the photons need to have energy above 1.022 MeV, thus the pair production effect is negligible because the sources we used for CT cannot achieve this energy.

3.1.2 Attenuation

During the CT scans it is not possible to distinguish the single contributions of the different phenomena because of the interactions of the x-ray with the object. In fact, the detector records the attenuation of an incoming beam of intensity (I_0) depending on its path through the sample, as shown in Fig 3.2.

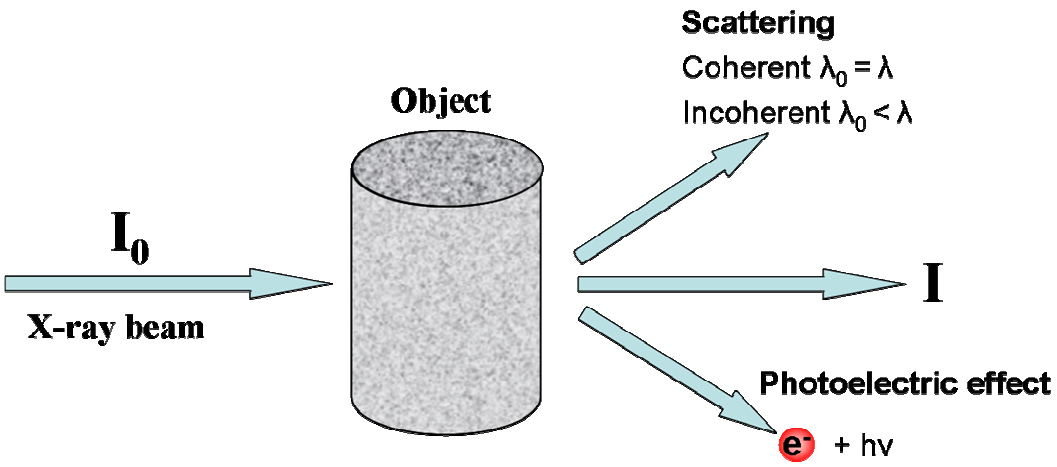

Fig. 3.2 - Scheme of the interactions of x-rays with matter

In the simplest case, in a monomaterial hit by a monochromatic beam, the initial (I_0) and final (I) intensities are related by the Lambert – Beer's Law:

$$I = I_0 e^{-\mu x}$$

Where μ is the linear attenuation coefficient of the object and x the length (in cm) of the paths of the x-rays in the object. The linear attenuation coefficient is a quantity which describes how the intensity of the beam is reduced as it passes through a specific material.

If the material is composed by i-compounds, Lambert – Beer's Law can be modified taking into account the different values of μ_i and x_i for every compound:

$$I = I_0 e^{\Sigma-\mu i x i}$$

In the case of laboratory instruments, the source produces a polychromatic x-ray beam in a wide energy range. Since the linear attenuation coefficient depends on the energy (E), the general equation that describes the attenuation of x-rays by an object is:

$$I = \int I_0(E)\ e^{\Sigma-\mu i(E)\, xi}\, dE$$

Each pixel of a CT image contains information about the linear attenuation coefficient, which can be related to the material by electron density (ρ) and atomic number (Z) by the following equation:

$$\mu = \rho\,(a + bZ^{3.8}/E^{3.2})$$

where "a" is the energy-independent Klein-Nishina coefficient and "b" is a constant [63]. The first term stands for the Compton scattering, predominant for energies above 100keV, while the second one accounts for photoelectric absorption, which becomes more relevant at energies below 100 keV.

3.1.3 Image reconstruction and artefacts

After the acquisition, the radiographs have to be processed in order to obtain the reconstructed cross-section of the scanned object. There are several pieces of software, both commercial and free, based on different algorithms, which can be used depending on the system geometry, i.e. parallel or cone beam.

In the CT images, there may be a variety of defects in the projection sets that propagate errors – or, better, artefacts - into the reconstructed cross sections.

Beam hardening is the most common artefact in CT results [57]. Using a polychromatic source, the x-rays with lower energy are preferentially attenuated by the sample, so that the effective attenuation coefficient of a voxel changes depending on its position in the object. In the reconstructed images this will cause more attenuated areas close to the edges of the sample and less attenuated ones in those in the centre. To reduce beam hardening effects filters, generally aluminium or copper foils of suitable thickness can be applied in order to remove to the x-ray tube spectrum the low-energy part. Another solution is to employ a monochromatic source, such as synchrotron radiation (see section 3.2).

Other defects which often affect CT images are ring artefacts. They appear as full or partial circles centred on the rotation axis and they are related to the inaccuracies of some pixels in the detector. These artefacts can be reduced by optimizing the scanning parameters, such as rotation step, exposure time, frame averaging, and/or by means of software processing, which can significantly enhance the quality of the images.

3.1.4 Applications of CT in geosciences and stone conservation

The first CT investigations on stone in the field of Cultural Heritage have been carried out by conventional medical scanners for the study of sculptures, moisture distribution in porous rock and to monitor physical and biological weathering of stone [64, 65]. The results were very promising, although the achieved resolution was not enough to entirely assess the decay processes. Later, μ-CT has been used for

quantitative and qualitative analysis in geosciences, e.g. for the study of porosity of rock and soil samples [66, 67].

As already mentioned in chapter 1, a detailed knowledge of these phenomena is a prerequisite to the restoration action and the effectiveness and durability of the conservation treatments should be evaluated. To this respect, μ-CT, with its non-destructive and non-invasive character, is a powerful tool, suitable to monitor and investigate the deterioration and restoration processes.

μ-CT instruments have been successfully used for the characterization of natural building stone, in particular for the study and quantification of petrographic parameters, such as porosity and pore network [68-70]. The main advantages of this technique are the easy sample preparation, since no special procedures are required, other than preparing the samples to the appropriate dimensions to allow sufficient transmission of the x-ray beam and good magnification, and the possibility to access the full 3D structure. This latter aspect is crucial to visualize and study the actual shape of the pores - very often modelled as spheres or cylinders - and their interconnectivity.

Tomographic analyses also allow to map the conservation treatments [71]: the images reconstructed from CT analyses performed at two different times, e.g. before and after the application of restoration products, can be compared in order to highlight the changes induced by the products and deduce information about their distribution [72]. Generally, the application of conservation treatment causes an increase of the x-ray attenuation due to the partial and/or complete filling of empty pores. However, at the spatial resolution delivered by μ-CT, it is not always possible to visualize directly the polymer in the reconstructed images also because of the low contrast given by the focal spot size of the source and low attenuation of x-rays by the water repellent. Moreover, the conservation products fill pores too small to be detected and create very thin films around the grains of the stone, which are very difficult to be distinguished at a micrometric resolution. In order to improve the contrast between the stone and the product, a contrast medium can be added to the treatment solution [73], or radio-opaque markers (e.g. bromine or iodine) can be chemically bonded to the polymer chains [71]. Unfortunately, these methods allow to estimate only the penetration depth and not the way in which the pores are filled by the conservation treatment.

3.1.5 Experiments with laboratory µ-CT systems

The µ-CT measurements have been performed by a SkyScan 1172 system. This desktop system consists of an x-ray micro focus tube, with tungsten reflection target and a CCD camera 4000 x 2096 as detector.

The samples have been scanned applying the following conditions:

- X-ray tube parameters: voltage = 100 kV, current of 100 µA
- Rotation step = 0.4° (over 180° rotation)
- Frame averaging = 4
- Detector: CCD camera of 4000 x 2096 pixels binned to 2000 x 1048 with a pixel size resolution of 2.6 µm.
- Filter copper 0.038 mm + aluminium 1 mm

The choice of frame averaging = 4 and rotation step = 0.4 significantly enhances the quality of the images and leads to a good signal to noise ratio. Moreover, the applied filter allows to reduce the beam hardening artefacts and to obtain a better air-stone contrast. The 2000 x 1048 camera provides good balance of resolution, time for acquisition and reconstruction and size of the datasets. CCD camera 4000 x 2096 has been used to achieve a higher resolution (600 nm pixel size) and compare the results with those obtained with SR.

The tomographic cross-sections have been reconstructed by means of NRecon software package based on modified Feldkamp cone-beam algorithm [74]. In addition to the optimization of the reconstruction, this software also includes the possibility of correcting the images from beam-hardening and/or ring artefact.

Subsequently, the obtained data sets have been processed and analysed with the CTAn software package in order to create a complete 3D representation of the internal microstructure of the stone. CTAn also allows to calculate relevant morphometric parameters of the specimens within a selected region of interest (ROI):

- Porosity, as a percentage of the empty spaces on the volume of interest (VOI)
- Pore size distribution
- Surface-to-volume ratio. This parameter gives an idea of the complexity of the internal structures.
- Structure model index (SMI), giving an estimation of the average shape of the pores (0 correspond to an ideal plate, 3 to a cylinder and 4 to a sphere). The

calculation of the SMI is based on a dilatation of the 3D voxel model, which is artificially adding one voxel thickness to all pore surfaces [75].

First, the repeatability of the μ-CT measurements has been checked: the same sample has been scanned five times, in order to estimate the errors caused by the repositioning of the sample and the instrumental uncertainty. The porosity values, calculated from the five data sets, have been then compared.

Other experiments have been carried out to investigate the changes on stone materials caused by the conservation treatment application and/or NOx exposure. Since Lecce stone is a sedimentary rock, which very often shows differences in porosity and composition from one block to another, the estimation of the porosity should be based on a sufficiently large number of samples. For these reasons, 21 samples (3 x 3 x 10 mm^3) have been investigated to obtain a statistically meaningful average of all the basic morphological parameters, such as porosity, pore size distribution and wall thickness distribution.

The same samples have been scanned at different steps, i.e. prior to any treatment, after product application and after ageing with NOx, taking advantage of the high repeatability of μ-CT measurements and the non-destructive character of this technique.

The 21 samples have been divided in 3 groups: Set 1 (samples 1-7), Set 2 (samples 8-14) and Set 3 (samples 15-21). Set 2 and Set 3 have been treated by vacuum impregnation with Paraloid B72 (2% in acetone) and the Fluoroelastomer (1% in acetone), respectively.

In addition to the calculation of the morphological parameters, a further statistical data analysis was carried out by calculating the differences in porosity (Δ_i) of the same sample before and after the treatment and ageing. The averages of the differences ($\overline{\Delta}$) of the same group have been compared with a Student's t-test for paired samples, in order to determine whether the protective product or ageing have caused significant changes at a given level of significance, α [76]. By means of the t-test it is possible to verify whether the null-hypothesis is statistically valid. Indicating δ as the average of the population of the differences, the null hypothesis (H_0) is that there are no significant differences ($\delta = 0$) in porosity values before and after treatment or ageing; on the contrary, the alternative hypothesis (H_1) is $\delta \neq 0$.

The standard deviation (σ_Δ) of the same set of samples is calculated as follows:

$$\sigma_{\Delta} = \sqrt{\frac{\sum_{i=1}^{n} \left(\Delta_i - \overline{\Delta}\right)^2}{n-1}}$$

The experimental value of t_{calc} calculated according to the following formula

$$t_{calc} = \frac{\overline{\Delta}}{\sigma_{\Delta}}\sqrt{n}$$

has been compared with that tabled (t_{tab}): if $t_{calc} > t_{tab}$ H_0 is rejected and there are significant differences between the two averages, i.e. the treatment or ageing do not change the stone porosity, otherwise H_0 is accepted and the two averages come from the same population. If H_0 is rejected, it is possible to calculate the averaged difference and its confidence interval as follows:

$$\delta = \overline{\Delta} \pm \frac{t_{tab} \cdot \sigma_{\Delta}}{\sqrt{n}}$$

Pore size and wall thickness distribution graphs, as well as their average values before and after treatment and ageing, have been also compared, in order to evaluate more in detail the changes of the stone structure and properties.

3.1.6 Experiments with nano-CT systems

For the nano-CT experiments, a SkyScan 2011 system was used. This instrument employs a different x-ray source from the 1172, consisting in an open-type x-ray source with a LaB6 cathode and a gold transmission target. The small spot size provided by this source (< 400 nm) allows to achieve a maximum spatial resolution of 150 nm.

The samples have been scanned with a pixel resolution of 580 nm, keeping the voltage at 25 kV and the current at 200 μA. Due to the different x-rays characteristic, no filter has been applied and a frame average of 15 has been chosen, in order to obtain projections of acceptable quality and good signal-to-noise ratio. The cross sections of

the sample have been reconstructed by NRecon software, the same used in micro-CT scans.

The images have been evaluated qualitatively, in order to test the possibility of detecting the conservation products inside the stone structure.

3.2 Synchrotron Radiation (SR)

It is beyond the aim of this thesis to give a comprehensive review about synchrotron radiation (SR) and its properties. Some basics on SR are presented below, for more information the reader is then directed to other books [77, 78].

3.2.1 Basics of Synchrotron Radiation

As charged particles are forced on a circular orbit while traversing a magnetic field, they emit an electromagnetic radiation tangential to their path [79]. This radiation, called synchrotron radiation, has been first observed in 1947 [80] and it has been later advantageously used for spectroscopic investigations, thanks to its broad energy distribution, i.e. from infrared to hard x-rays.

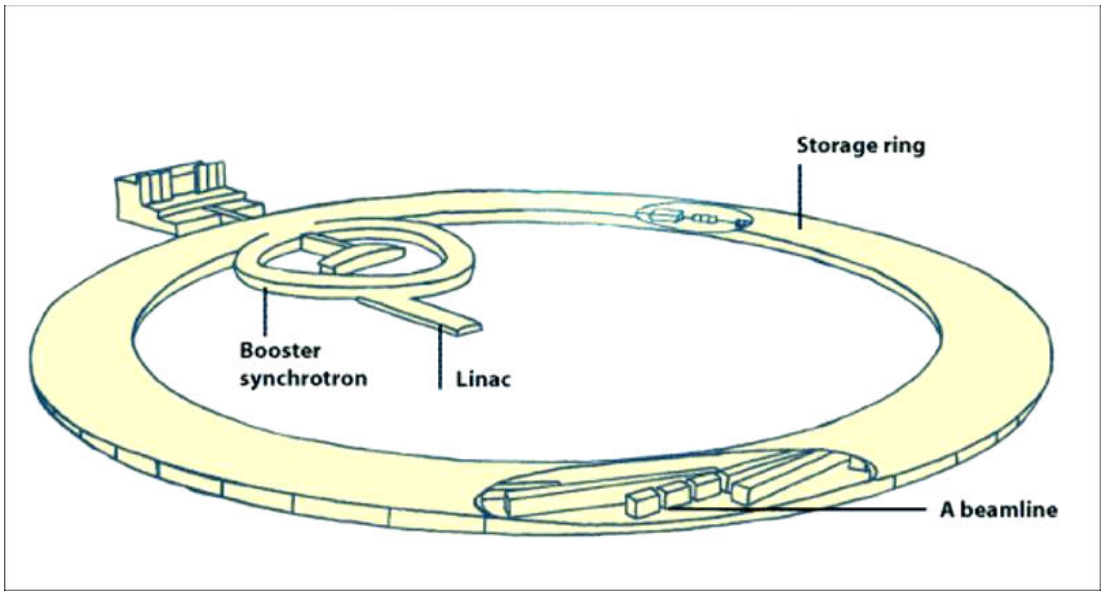

Fig. 3.3 - Scheme of a synchrotron [81]

A synchrotron is a round accelerator of particles, generally composed by different parts, as shown in Fig (3.3): linear accelerator, a booster synchrotron, a storage ring which includes different devices, such as bending magnet and undulators and the beamline, i.e. the end stations where the experiments are carried out.

In order to generate a radiation, electrons are produced and accelerated in a linear accelerator (Linac) and injected in the booster synchrotron where they achieve a speed close to light speed. The electrons are then injected in the storage ring where the bending magnets, undulators and wiggler force them to follow a precise trajectory. Bending magnets maintain the electrons in the ring, giving a curve direction, while undulator and wiggler, constituted by linear arrays of dipole magnets alternating in orientation, give to the electrons a zigzag trajectory (Fig. 3.4). Undulators lead to low amplitude of the sinusoidal electron motion and produce well-collimated and high flux radiation; wigglers have a larger sinusoidal electron path and produce a relatively wide fan of radiation, covering horizontal angles of few degrees.

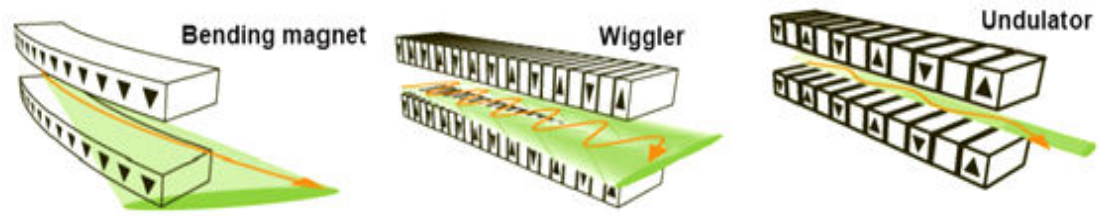

Fig. 3.4 – Magnetic devices used in the storage ring. The black arrows indicate the orientation of the magnetic field, while red and green are the electron trajectory and the fan of the SR, respectively [81]

The properties of the produced radiation depend on the experimental parameters and set up, one of the main differences and advantages, respect to conventional x-ray tube, is the possibility to obtain monochromatic beams with high brilliance. Brilliance is the unit that characterizes the SR, taking into account not only the flux (number of photons per second in a certain bandwidth (BW)) but also the x-ray source size and collimation. It is calculated as the flux normalized to a solid angle of 1 $mrad^2$ and a source size of 1 mm^2.

The performances of different generations of synchrotrons and x-ray tubes over the last century are presented in the 3.5. Currently, the third-generation storage rings are

able to achieve a maximum brilliance of 10^{20} photons s^{-1} (0.1% BW) mm^{-2} $mrad^{-2}$. Synchrotron with such performances are for instance European Synchrotron Radiation Facility (ESRF) in Grenoble (France), Swiss Light Source (SLS) in Villigen (Switzerland), Advanced Photon Source (APS) in Argonne (IL, USA) and Super Photon ring-8GeV (SPring-8) in Hyogo (Japan).

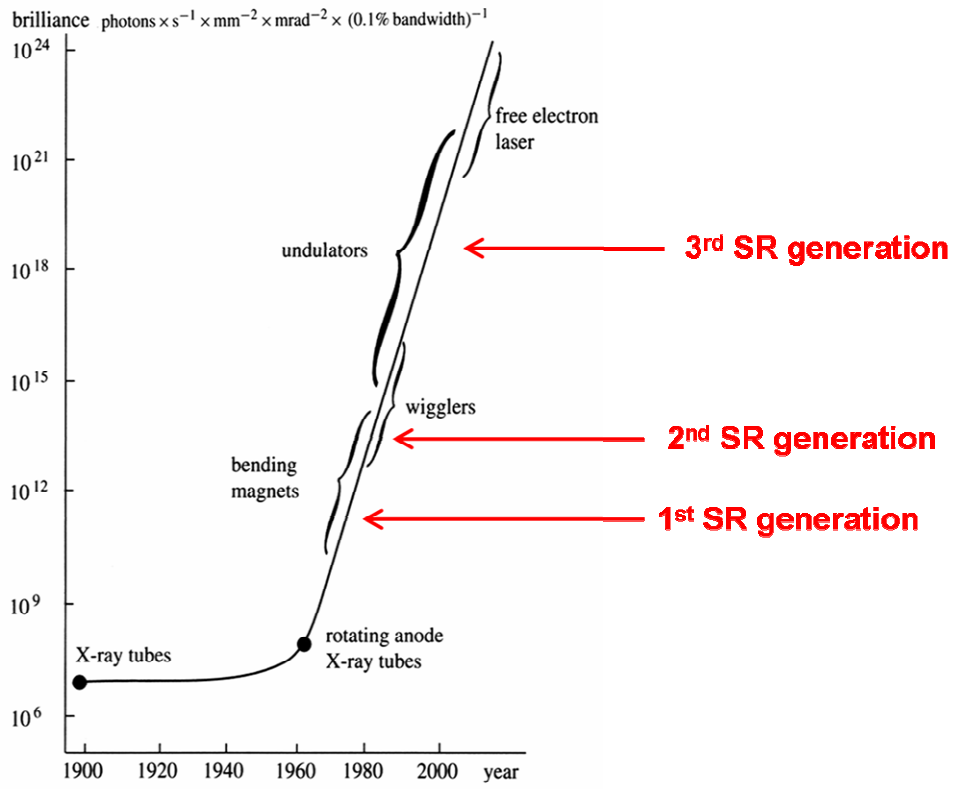

Fig 3.5 - Brilliance of x-ray sources and different SR generations [79]

3.2.2 X-ray tomography with SR (SR-CT)

Imaging with hard x-rays, i.e. above 1.8 keV [82], has evolved dramatically over the last decade with the appearance of third generation synchrotrons. Nowadays, micrometric resolutions are common for instruments using detectors based on optically coupled scintillation-CCD cameras. In situ studies can be performed on samples from different fields such as astrophysics, biomedicine and materials sciences. The functionality of complex structures and the evolution of processes can be investigated in real time, while precious samples can be analyzed non-destructively and thus preserved.

The setup of tomography with synchrotron radiation (SR-CT) is not conceptually different from the laboratory systems: the sample, mounted of a rotating stage, is illuminated by the x-ray beam and the projections are acquired by a CCD camera (Fig. 3.6).

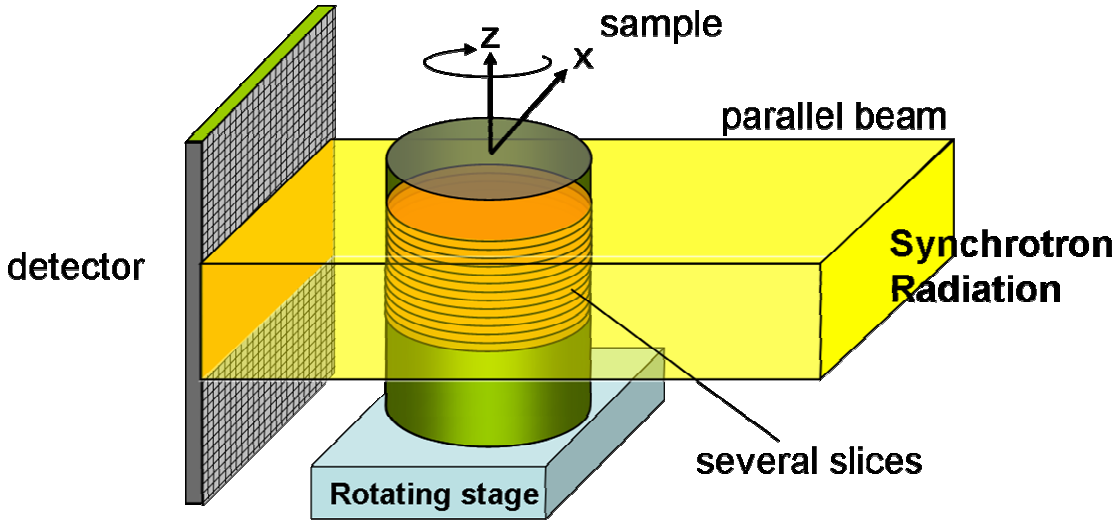

Fig. 3.6 - X-ray tomography setup with synchrotron radiation

Compared to laboratory systems, in SR-CT there are some additional devices, such as monochromators, normally constituted by a double silicon (Si) crystal or multilayer coated mirrors [79]. The use of monochromatic and energy tuneable x-ray beam allows to enhance the contrast between different phases present in the object and to reduce reconstruction artefacts [83].

A third generation synchrotron source can produce extremely intense nearly parallel x-ray beams that can be monochromatized, leading to high quality absorption scans without beam hardening effects or geometric artefacts, which are due to the polychromatic x-ray spectrum and the cone beam geometry used in most laboratory microtomographic systems. Moreover, the parallel beam geometry and the high signal-to-noise ratio due to the high flux of SR, significantly improve the quality of the reconstructed images: for the same nominal pixel size, with SR smaller details are visible and distinguishable [83].

Fig. 3.7 illustrates the differences in image quality between laboratory and synchrotron μ-CT scans of one sample, recorded with approximately equivalent scan parameters, e.g. same voxel size and angular step. SR also allows fast scan acquisition

times: in the case presented in Fig 3.7, to scan the sample with a laboratory system and SR took 3.75 and 0.75 h, respectively [83].

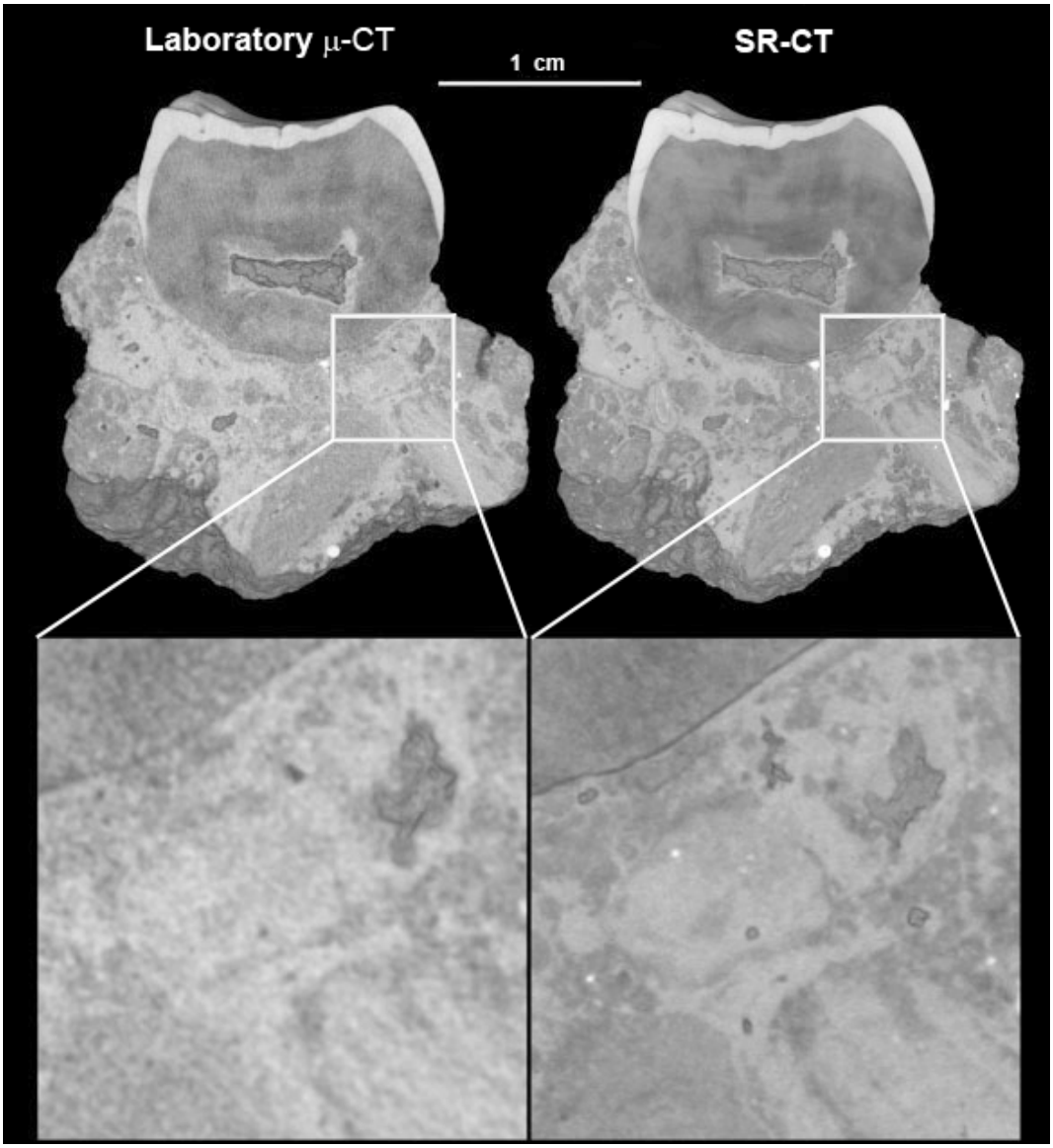

Fig. 3.7 - Comparison between cross sections of the same sample (fossilized Pongo molar) obtained with laboratory μ-CT system and SR-CT at the same nominal resolution [83]

With the advances in nano-science and technology, interest has grown in imaging, in particular, for increasing the spatial resolution. With parallel setup the resolution is largely determined by the spatial resolution of the x-ray image capture system. The scintillators, optical efficiency, and diffraction of visible light place a limit on the resolution of the x-ray image capture system [84]. In order to overcome the detector-limited micrometer resolution, several approaches have been considered. They are mainly based on the principle of projecting a magnified x-ray image of the object onto the detector. The x-ray magnification is either achieved with a microscope or with

a diverging x-ray beam (Fig. 3.8 and Fig. 3.9, respectively). If the beam is essentially parallel, as delivered by certain synchrotron beamlines where the source-to-object distance, z_1, is large (e.g. ID19 at the ESRF [85]), the magnification can be obtained using an optical microscope, in order to magnify the visible images coming from the scintillator (Fig. 3.8).

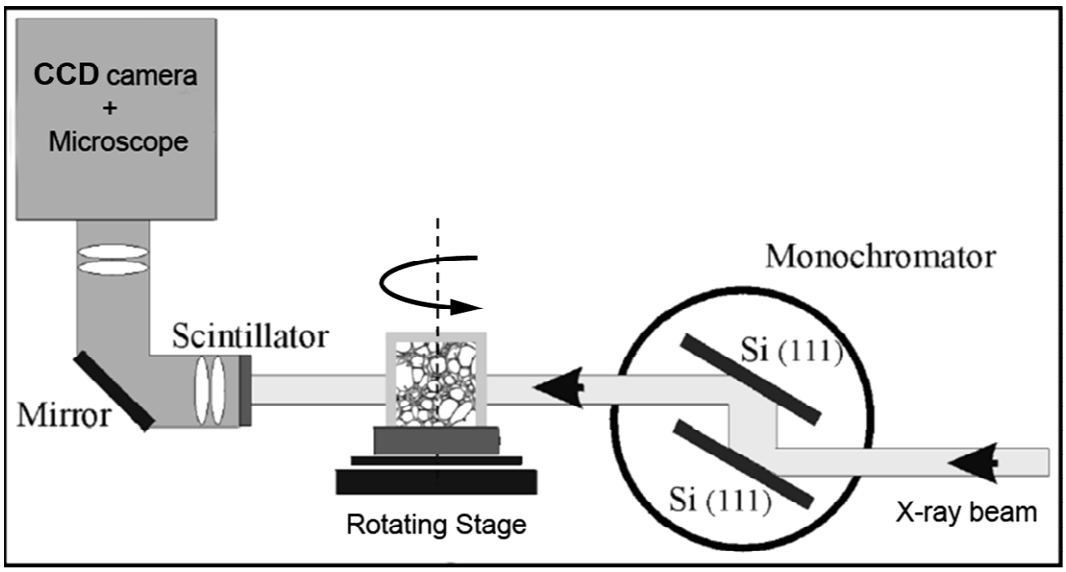

Fig. 3.8 - SR-CT setup with scintillator-CCD camera-microscope system

This setup is simple; on the other hand, cone beam geometry can also be successfully adopted using synchrotron radiation: the beam is focused into a small spot, which serves as a secondary source (Fig 3.9). The sample is illuminated by the diverging secondary source and the magnified x-ray shadow is recorded at a large sample-detector distance (z_2). In this case, the spatial resolution is limited by the penumbra effects caused by the source spot size (Fig. 3.9). This effect of blurring can be limited by reducing the source spot size, while the resolution can be improved acquiring images at small source-to-object distance. The cone beam can be obtained by focusing SR with x-ray lens-based systems [82].

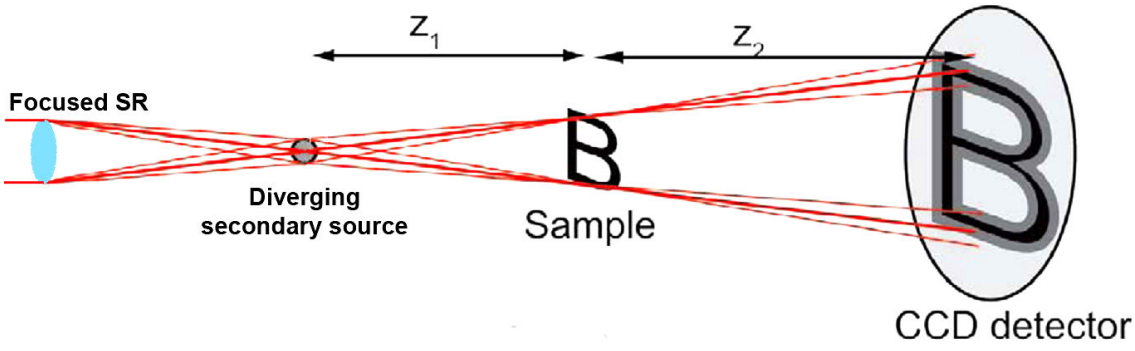

Fig. 3.9 - SR-CT with cone beam setup [82]

The highly coherent radiation available at third generation synchrotron sources offers also possibilities for new phase contrast techniques. Phase contrast imaging makes micro-structures with low absorption contrast become visible [86, 87]. The great advantage of this new type of imaging is the increased sensitivity it provides, either for light materials such as polymers, or for composites made up of materials with neighbouring densities. A first use of the phase images, called edge enhancement, relies on the visualization of the phase jumps that occur at the edges between different phases, having a different index of refraction. A more sophisticated quantitative approach, called phase retrieval or holotomography, also allows to extract information about the density of the materials present in the object [88].

3.2.3 SR-CT experiments at ESRF

The experiments of SR-CT have been performed at ID 19, one of the beamlines of ESRF dedicated to x-ray imaging. At this end station it is possible to carry out measurements by means of different techniques, such as microtomography (absorption and phase contrast imaging), laminography [89] and diffraction imaging. ID 19 is a long beamline (145 m), so that the experimental hutch is located out of the ring of the experimental hall. This long source-sample distance and the small source size (30 µm vertical x 120 µm horizontal) allow to have a radiation with relevant spatial and temporal coherence and a beam size which can range from mm scale to 100 nm.

The monochromaticity, obtained either with a double Si (111) crystals (BW = 10^{-4}) or a multilayer mirror (BW = 10^{-2}), and the wide range of photon energy (6 – 120 keV) considerably contribute to improve the contrast between the different phases present in the sample.

Lecce stone samples (1 x 1 x 10 mm^3) untreated and treated with conservation products, have been analyzed with the aim of investigating the polymer distribution.
In the experimental set up (fig 3.10), the samples have been mounted on a rotation motor which also allows the adjustment of the rotation axis, and a FRELON (Fast Readout Low Noise) camera 2048 x 2048 has been used as a detector. This is a 14-bit depth resolution CCD camera developed at ESRF, which allows a fast acquisition of radiographs, a high magnification thanks to the optics system, assuring a good quality of the images.

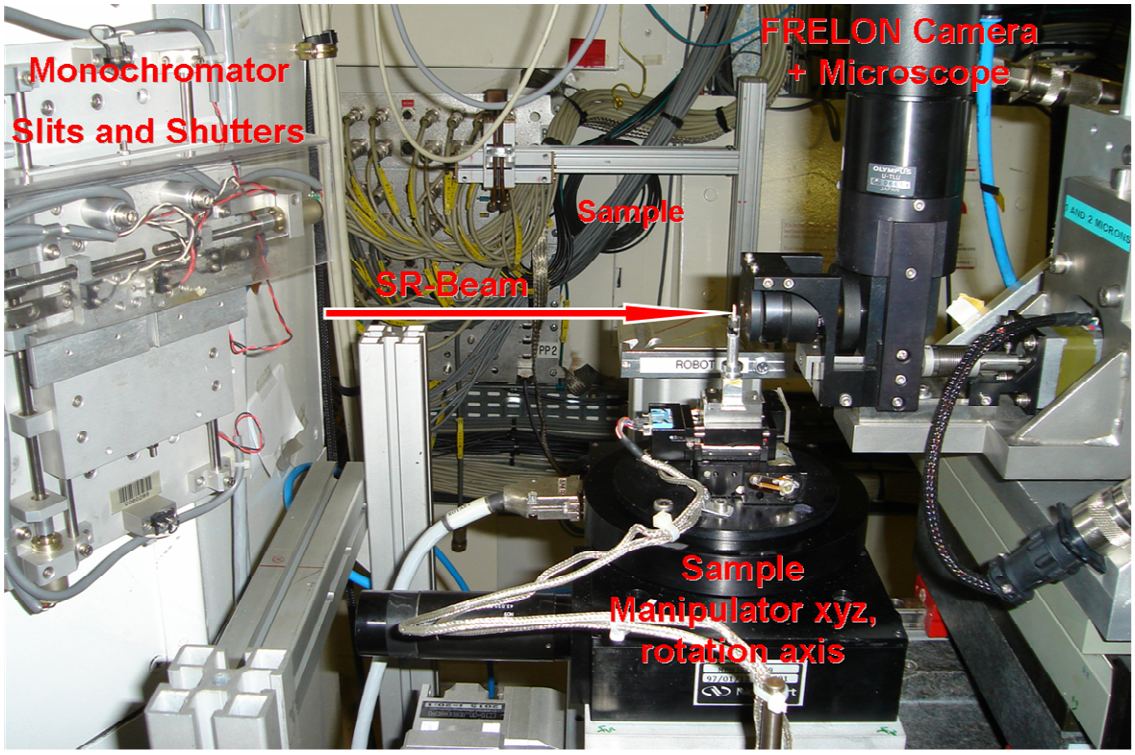

Fig. 3.10 – Setup of the tomography experiments at ID 19 of ESRF

Some preliminary tests have been done to define the experimental parameters. The samples have been scanned with a beam energy of 19 keV which allows a transmission of about 30%. With the used optics configuration, for each tomography scan, 1500 projections over a 180° rotation (rotation step = 0.12°) have been acquired

with a pixel size of 700 nm. These conditions provide a good balance between quality of the reconstructed images and scanning time (one scan takes about 20 minutes).

The images have been qualitatively evaluated to highlight the presence of the conservation treatments and the manner in which they coat the stone pore walls.

3.3 Neutron radiography and tomography

Neutron is a subatomic particle with no net electric charge and a mass of 1.6749 $\times 10^{-27}$ kg (slightly more than a proton). Neutrons have been used for many kinds of material investigations by transmission analysis [90]. Neutron radiography (NR) and tomography (NT) are techniques that provide two- or three-dimensional maps of the attenuation coefficient distribution within an object. In neutron radiography the information about the attenuation coefficient is projected onto a 2D transmission image, while with tomography information is reconstructed in 3D, as in the case of x-ray CT. NT can help to investigate the morphology and/or the structure of objects non-destructively, reconstructing the cross sections of the sample from a series of transmission measurements taken from different rotation angles. This procedure for neutrons is based on the same method used for conventional x-ray CT.

Although basic principles are known since decades, this technique became more used in recent times, due to the availability of digital neutron detectors and devices. Modern neutron imaging detectors provide at the same time high sensitivity and sufficient spatial resolution. Thus, objects in the size of few millimetres up to tens centimetres can be scanned in reasonable time.

A transmission NT setup essentially consists of a neutron source, a digital neutron detector system and a rotary table, which allows to acquire neutron radiographs at small angular steps over 180° or 360°.

The main differences between NT and x-ray CT are due to the different radiation-matter interactions, discussed in the next section. There are many advantages of neutrons compared to x-rays, e.g. the possibility to investigate non-destructively thick objects made of metals or high atomic number elements and to detect hydrogen with a high sensitivity: these differences make x-ray CT and NT complementary techniques [91].

3.3.1 Neutrons vs. x-rays

Since the development of intense neutron sources (typically $10^6 – 10^7$ cm^{-2} s^{-1}), neutron imaging has become possible. Nowadays neutrons have found their application into several areas of science, e.g. geology, biology, material science and medicine. Neutrons can be divided in different groups, depending on their energy:

- high energy neutrons (E > 100 MeV),
- fast neutrons (E ~ 1 MeV),
- epithermal neutrons (E > 1eV),
- thermal neutrons (E ~ 25 meV),
- cold neutrons (E ~ 4 meV),
- ultra-cold neutrons (E ~ 100 neV).

When a neutron beam passes through the matter several processes can take place [92]:

a) the neutrons may be deflected with loss of energy (incoherent scattering);
b) the neutrons may be deflected without loss of energy (coherent scattering);
c) the neutrons can be captured by the atomic nucleus (absorption process), emitting γ-ray, α particle (i.e. nucleus of ^4He) or a proton.

As in the case of x-rays, in NR or NT experiments the different interaction processes are not distinguished, and the detector records the intensity of the neutron beam attenuated by a sample depending on composition and thickness of the material, according to Lambert-Beer Law.

X-rays interact with electrons and their attenuation increases as the atomic number (Z) of the elements present in the specimens increases (Fig 3.11). Unlike x-rays, neutrons interact with nuclei and there are no standard rules to determine their cross-section: the attenuation of hydrogen is large if compared to other elements, e.g. silicon, oxygen, calcium, aluminium and iron, as shown in Fig 3.11.

Thermal or cold neutrons can be used for imaging purposes. Imaging experiments performed with fast neutrons are less common due to their low detection probability and the limited number of facilities which produce this type of neutrons [93].

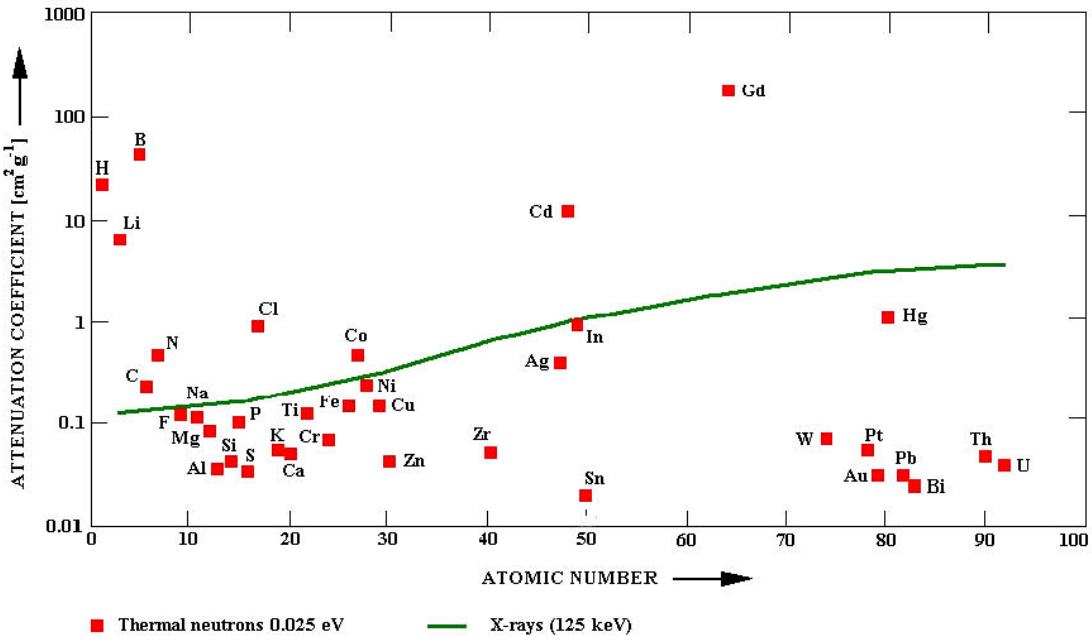

Fig. 3.11 – Attenuation coefficient for x-rays at 125 keV (green line) and thermal neutrons at 25meV (red spots) vs. atomic number [94]

An example of the differences between x-ray and neutron imaging is given in Fig 3.12 where radiographs of a photo camera have been acquired with both methods. In the x-ray images the metallic parts are clearly visible, while neutrons show to be more useful for the detection of the plastic materials.

Indeed neutrons guarantee a good penetration in the objects which are too thick to be analyzed with x-rays; however, despite significant improvements over the last year, the achievable spatial resolution with NR and NT is nowadays 20-100 microns [95] depending on the detector system, actually not comparable with the (sub)micrometric one, reached by x-rays. This makes neutrons more suitable for the investigation of bulk objects instead of the micro structure of small samples.

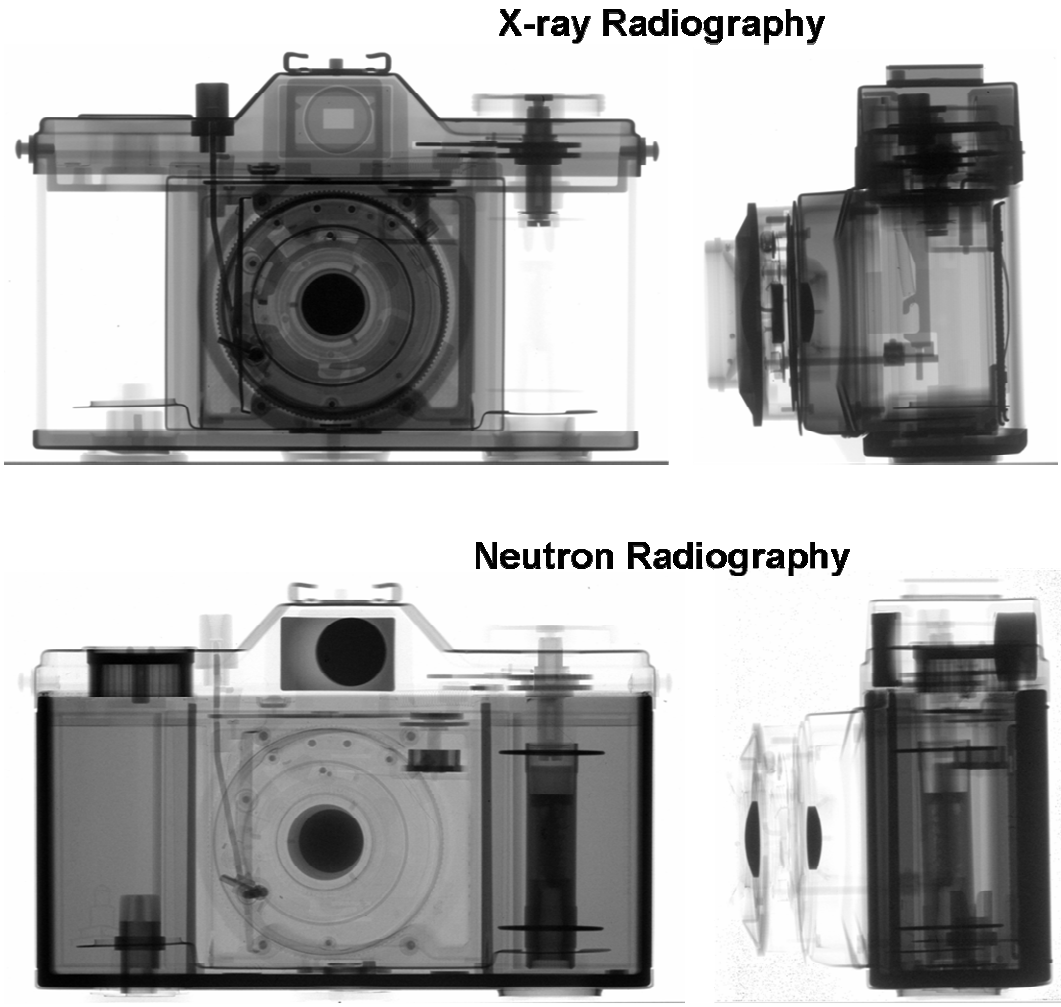

Fig. 3.12 – Radiographs of a photo camera acquired with x-rays and neutrons (courtesy of Dr. Lehmann)

In contrast with x-ray imaging, the possibilities of neutrons for imaging are less known. There are indeed fewer neutron sources and they are much more complicated. Moreover, neutrons normally require large facilities and high safety standards, as they are very harmful for human health. The most used facilities for neutron imaging are nuclear research reactors, followed by neutron spallation sources, which are particles accelerators where high-energy protons are accelerated and used to break-up heavy nuclei into lighter elements, neutrons and protons. Table 3.1 illustrates the main types of neutron sources and their characteristics.

Source type	nuclear reactor	neutron generator	spallation source	radio isotope
Reaction	fission	D-T fusion	spallation by protons	gamma-n-reaction
used materials	U-235	deuterium, tritium	high mass nuclides	Sb, Be
gain: primary neutron intensity [1/s]	1,00E+16	4,00E+11	1,00E+15	1,00E+08
beam intensity [cm^{-2} s^{-1}]	10^6 to 10^9	10^5	10^6 to n*10^7	10^3
neutron energy	fast, thermal and cold	fast, thermal	fast, thermal and cold	24 keV, thermal
limitation of use	burn up	life time tube	target life time	half life Sb-124
typical operation cycle	1 month	1000 h	1 year	0,5 year
costs of the facility	high	medium	very high	low

Tab. 3.1 – Characteristics of different neutron sources (courtesy of Dr. Lehmann)

It is well known that x-ray radiography and tomography have several common applications, such as medical diagnostics. The human body is more or less transparent to x-rays due to the high content of hydrogen and other light elements. Bones or even metals have much higher attenuation coefficient for x-rays and can easily be distinguished from the soft tissue.

In material testing with samples of technical or technological relevance (e.g. search for defects and material changes), where mostly metals or radio-opaque materials are involved, the penetration of x-rays is often limited. If metals are to be investigated, few millimetres are sufficient to shield the x-ray beam completely. At this point, neutrons become valuable due to higher penetration for most of the relevant high atomic weight elements. On the other hand, the attenuation of thermal neutrons caused by hydrogen is remarkable, so that thin layers of hydrogen-containing materials can provide high contrast.

For the investigation of a variety of museum objects, such as bronze statues, it is clear that metals are more transparent for neutrons than for x-rays. On the other hand, the study of materials with organic origin like leather, wood, wax or textiles gives much higher contrasts with neutrons than with x-rays. Since the composition and the inner structure of archaeological objects are often unknown, the availability of two complementary images of the same sample is very useful for the evaluations and the study of historical artefacts [93].

Because of the different properties of neutrons and x-rays, they may be used for a wide range of applications. Due to the different nature of interactions and the complementary Z-dependent cross sections, x-rays are mainly employed to investigate

materials and samples with high resolution, whereas neutrons are interesting probes for the investigation of samples containing light elements such as hydrogen, lithium, and boron or where high penetration in sample containing heavy elements is needed.

3.3.2 Neutron imaging applications in stone conservation

Neutron tomography has a large potential to monitor fluid dynamics in various types of porous rocks such as natural building stones, and it has the advantage to be a non-destructive technique. Neutron radiography has been used to visualize fluids in porous media [96-98], and also to study the uptake of water repellents and consolidants inside the stone [40].

If application of conservation products is planned, it is crucial to determine the penetration depth of restoration products into natural building stones. Since the contrast between hydrogen and elements normally present in stone materials (e.g. calcium, iron, aluminium) is high, it is also possible to study water and polymeric material distribution inside the rock structure. In fact, stone results almost transparent, while the neutrons are highly attenuated by water and the organic compounds.

Neutron radiography and tomography are also ideal tools to study dynamical processes, if a high neutron beam flux is provided. Real-time experiments have been performed to follow water migration [99] and conservation treatment solution diffusion [40] in stone materials.

3.3.3 Neutron experiments at PSI

The neutron imaging experiments have been carried out at the beamline NEUTRA of the SINQ facility at the PSI of Villigen (CH). SINQ is a spallation source where a proton beam with energy of 590 MeV and current up to 1.8 mA, is used to break heavy nuclei to produce neutrons. The targets are currently a series of lead (Pb) rods, enclosed in stainless steel tubes and placed in the centre of the concrete and steel shielding (FIG 3.13). The beamlines, where different types of experiment can be carried out, are located radially to the proton beam.

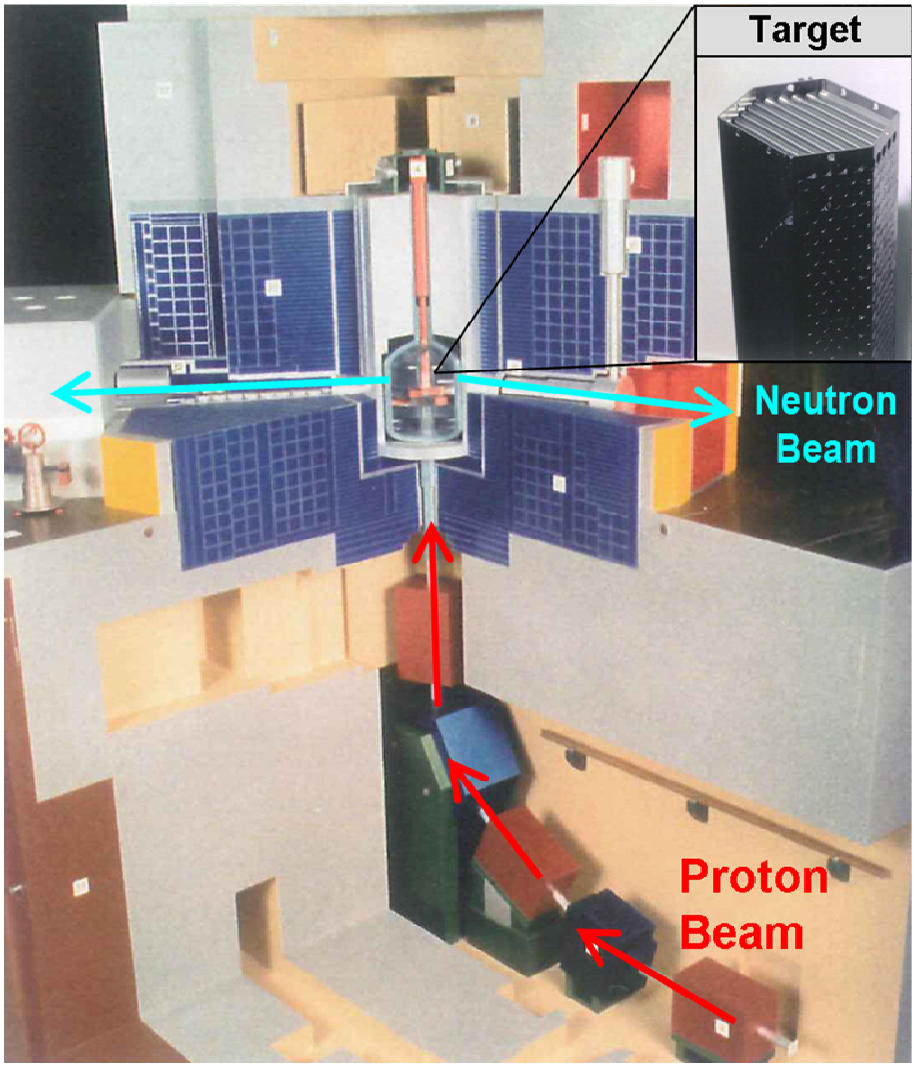

Fig. 3.13 – Model and cut section of SINQ neutron source [94]

A proton beam of 1 mA produces about 3 to 6 $\cdot 10^{16}$ high energy neutrons per second, which need to be slowed down to thermal energy (~ 25 meV). For this purpose a moderator tank of about 2 meters in diameter filled with heavy water surrounds the targets and allows the neutron guides to convey the neutrons to the different end stations.

The experiments have been carried out at NEUTRA (NEUtron Transmission Radiography), the beamline dedicated to imaging with thermal neutrons, established in 1997 at SINQ. The view of the beamline from the top (Fig. 3.14) shows that three measuring positions are possible: position 1, close to the target, is used for time resolved experiments when the spatial resolution is not the major issue; position 2 is normally suitable for the investigation of radioactive samples; position 3 is where the best spatial resolution can be achieved.

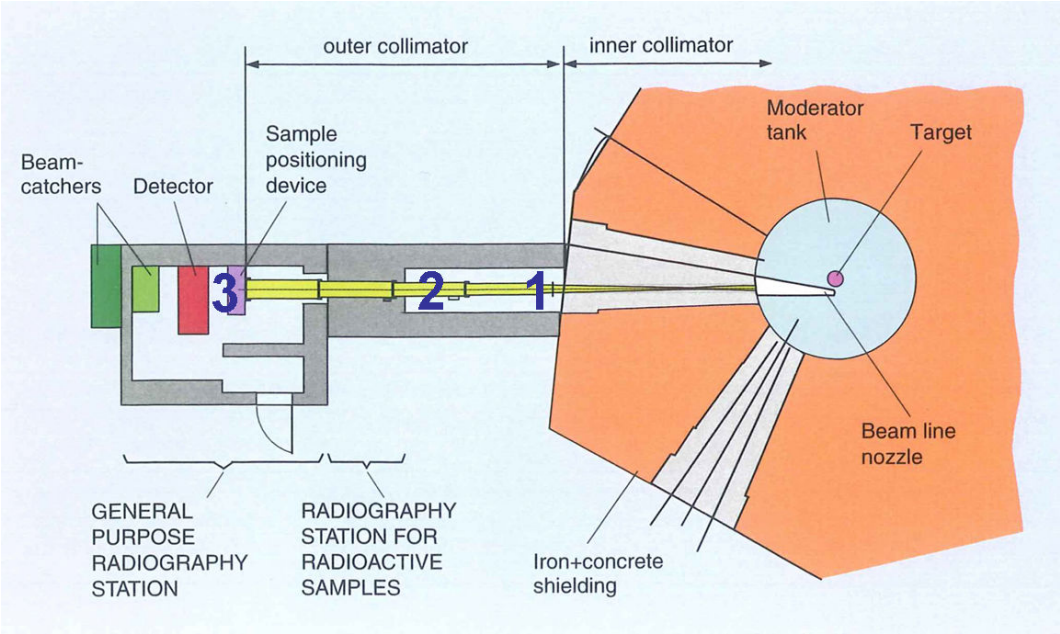

Fig 3.14 – View from the top of NEUTRA beamline. 1, 2 and 3 indicate the possible measuring positions [94]

The Lecce stone samples have been analyzed at position 3, where the neutrons are well collimated and the beam has its minimum divergence. Images with a pixel size resolution = 115 μm have been acquired by a detector based on the combination of a scintillator with a CCD camera (1024 x 1024) with exposure time of 60 seconds.

Both radiography and tomography have been performed fixing the specimens in an aluminium sample holder which also allow to add liquids, such water and/or treatment solutions. Aluminium is normally used since it is a low absorbing and diffracting material for neutrons, so it does not interferes with the scans.

Different experiments have been performed:

1. NR and NT of Lecce stone samples (5 x 5 x 1 cm^3) treated with H-containing conservation products (PB 72 and Hydrophase), in order to detect them and estimate their distribution.
2. NR and NT of Lecce stone samples (5 x 5 x 2 cm^3) untreated and impregnated with a known amount of $Ca(NO_3)_2 \cdot 4H_2O$. The samples have been put in a box at RH% = 100% and then scanned at different steps, in order to follow the moisture uptake vs. time. These experiments have been performed to demonstrate that the presence of the nitrocalcite in the stone structure brings to and increase of moisture uptake, as opposed to natural rock.
3. NR and NT of Lecce stone samples (5 x 5 x 1 cm^3) untreated and treated with conservation products, aged for 3000 hours in the ageing system described in

section 3.4. The aim is to investigate how the conservation treatments influence the moisture uptake and to estimate the amount of nitrates and nitrites formed in the ageing process, since the amount of moisture absorbed depends on the amount of salts (nitrates and nitrites).

The tomographic reconstructions have been performed by a piece of software implemented in IDL (Interactive Data Language) that allow to normalize the projections (this is necessary because of the instability of the beam intensity) and to correct them from other defects due to the detector and the spatial non-uniformity of the beam. Further corrections have been also done using QNI – Quantitative Neutron Imaging software [100], implemented in IDL as well, that corrects the defects due to the neutron scattering.

Tomographic cross-sections have been also successfully reconstructed using NRecon software (SkyScan NV), normally used for laboratory x-ray μ-CT data processing.

Chapter 4

EVALUATION OF CONSERVATION TREATMENTS: RESULTS & DISCUSSION

4.1 Efficacy and permeability tests

Lecce stone is a lithotype with high open porosity. The short time (15') capillary absorption tests show that the amount of water absorbed by the samples ranges from 8 to 13 g for 100g of rock.

The evaluation of the protective efficacy (PE%) of the conservation treatments applied on the 5 x 5 x 1 cm^3 specimens has been carried out by repeating the absorption test before and after the product application. These experiments give an estimation of the reduction of the rock's capability to absorb liquid water. PE% estimation has not been performed on samples treated with ammonium oxalate, since this product is not hydrophobic and it does not give any water repellence to the stone surface.

Another relevant measured parameter is the residual permeability to water vapour (RP%). The applied protective products can partially or completely block the open pores, so the water vapour exchanges between stone and environment may be significantly reduced. PE% and RP% should be evaluated and interpreted taking into account the actual amount of product deposited in the rock structure, normally determined by weight difference between the dry weights of the sample before and after treatment.

In Tab. 4.1 the results obtained with different treatments - brush (B) and capillary absorption (CA) – are presented. The values are averaged on five samples. It can be noticed that the procedure followed to choose the stone samples allowed to select specimens with homogeneous behaviour, so the averages of the amounts of product deposited on different stone samples, using the same application procedure, have low standard deviations. This is an essential condition to obtain reproducible results, not only for treatments, but also for the ageing step.

Regarding the characteristics of the polymers tested, they drastically change the wettability of the Lecce stone, as shown by the protective efficacy values. In the case of PB 72 and NH, the application by capillary absorption is more effective than that by brush. However, PB 72 shows always higher PE% values than NH, justified by the higher amount of protective product applied. These differences may be explained also by the different penetration of the polymers inside the stone: the lower molecular weight of PB 72, in comparison with NH, and the application method (capillary absorption instead of brush) increase the penetration.

	CONSERVATION TREATMENTS						
	PB 72-B	**PB 72-CA**	**NH-B**	**NH-CA**	**Sil-B**	**Sil-CA**	**Ox-CA**
Product mg/100g rock	238±2	422±5	106±2	150±7	141±24	290±19	238±9
PE (%)	97±2	98±1	90±1	93±1	100±1	100±1	**----**
RP (%)	85±2	67±2	82±2	74±1	74±1	71±2	81±2

Tab. 4.1 - Amount of protective product applied, Protective Efficacy (PE%) and Residual Permeability to water vapour (RP%) determined on Lecce stone samples treated with Paraloid B 72 (PB 72), Fluoroelastomer (NH), Hydrophase Superfici (Sil) and ammonium oxalate (Ox), applied by brush (B) and capillary absorption (CA). The values and their standard deviation have been calculated on five samples.

Hydrophase Superfici makes the surface of the rock completely water-repellent, with a protective efficacy of 100%. The application method of this product does not significantly influence the PE%, since the small size of the oligomers and the low viscosity of the solution allow a good penetration depth by both capillary absorption and brush. Generally, when the treatments are performed by capillary absorption, the rock is longer in contact with the solution and the evaporation rate of the solvent is slower, so that the amount of product deposited and the penetration depth is higher. On the other hand, a high amount of product also implies higher occlusion of pores and reduction of the water vapour permeability.

In the case of PB 72-CA and Sil-CA, the high penetration associated with a great amount of product applied may cause a partial blockage of the pores, as demonstrated by the substantial reduction of the permeability to water vapour. For NH treatments, comparable RP% values are obtained, but with much lower amount of polymer, in comparison with PB 72 and Sil. Fluoroelastomer may be not well-distributed because of its high molecular weight and it can preferentially form a film on the surface with a partial pore blockage, leading to a decrease in the water vapour permeability.

In general, the reduction of water vapour permeability is higher for the treatments performed by capillary absorption. In all the cases studied, however, the samples maintain an acceptable transpirability.

4.2 Colour measurements

The application of the conservation treatment should not cause any colour and aesthetical changes. Chromatic variations are normally due to the formation of a polymeric film on the surface and/ or to the refraction index of the products which may induce a glossy or shiny effect on the rock artefacts.
The results of colour measurements performed on 5 x 5 x 1 cm^3 samples are presented in Tab. 4.2.

Treatment	ΔL*	Δa*	Δb*	ΔE
PB72-B	-2.71±0.41	0.43±0.2	2.64±0.69	3.81±0.75
PB72-CA	-6.38±3.0	1.31±0.72	5.24±2.41	8.36±3.88
Ox-CA	-2.41±0.63	0.14±0.67	2.74±0.35	3.65±0.66
Sil-B	-0.59±0.27	-0.13±0.02	0.24±0.16	0.65±0.28
Sil-CA	-1.62±0.83	0.24±0.15	1.38±0.72	2.14±1.1
NH-B	-0.88±0.43	0.06±0.03	1.39±0.48	1.64±0.63
NH-CA	-0.68±0.1	0.06±0.07	0.99±0.11	1.20±0.13

Tab. 4.2 - Colour variations of Lecce stone samples due to the conservation treatment application. (Sil = Hydrophase Superfici; NH = fluoroelastomer; PB 72 = Paraloid B72; Ox = ammonium oxalate; B = brush; CA = capillary absorption).

NH and Sil-B does not significantly change the appearance of the samples, while other treatments, i.e. Sil-CA and Ox-CA induce a slight whitening of Lecce stone specimens appreciable also by visual inspection. The most evident variations have been detected in samples treated with Paraloid B72 as shown in Fig. 4.1.
The darkening effect induced by this acrylic polymer has been reported by other authors [3], especially in case of treatment of rocks with high porosity, as Lecce stone is.

Fig. 4.1 - Lecce stone samples. Untreated (on the left) and treated with PB 72 by brush (on the right)

4.3 X-ray tomography

X-ray tomography has been used to investigate Lecce stone samples with dimension ranging from 3 mm to 0.5 mm, depending on the resolution and instrument, with the aim to take as much information as possible about the rock structure and the applied conservation treatments.

4.3.1 Basic characterization of Lecce stone by μ-CT

Several Lecce stone samples 3 x 3 x 1 mm^3 have been analyzed by μ-CT at a 2.6 μm resolution. The reconstructed images have been evaluated both qualitatively, looking at their appearance, and quantitatively, by calculating the three-dimensional parameters of the material.

The 2D cross sections confirm that Lecce stone has a very complex internal structure, as the thin sections and environmental scanning electron microscopy (ESEM) images suggested. Several inclusions, such as shells with different shapes and sizes (from few μm up to 1 mm, e.g. foraminifera in Fig. 4.2) can be clearly distinguished. These fossils are embedded in the calcite matrix and constitute the major part of the macro porosity.

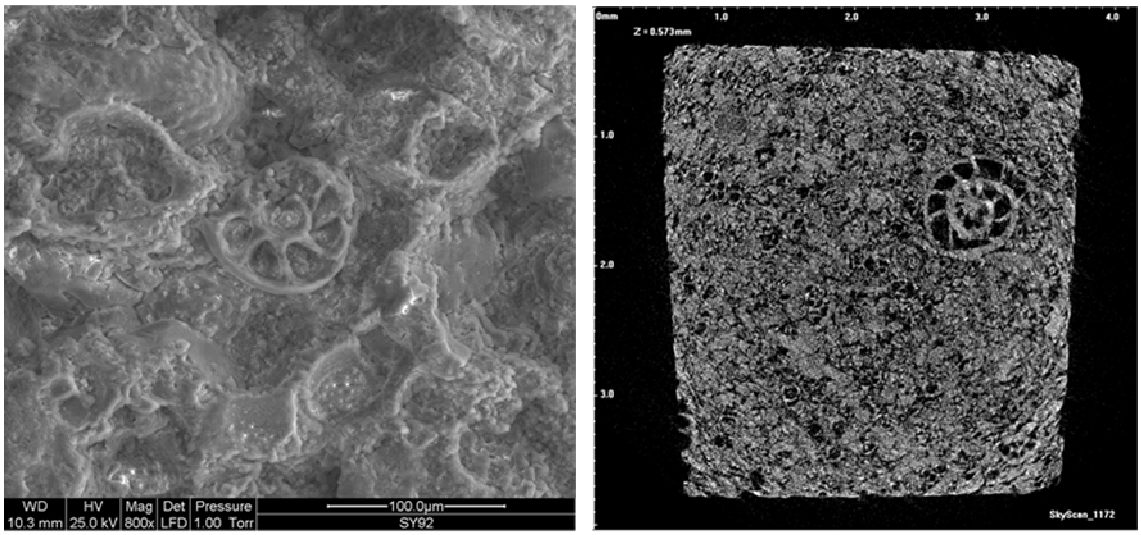

Fig. 4.2 - ESEM image (800x) of Lecce stone surface (on the left) and Lecce stone cross section (2.6 µm pixel size) reconstructed from µ-CT data (on the right)

The average surface-to-volume ratio of the pores calculated with CTan software is 275 mm^{-1}, indicating a very intricate shape of the pores. This last result is also confirmed by 3D rendering of a small portion of the pore network (Fig. 4.3), which gives an idea of the complexity and interconnectivity of the internal structure.

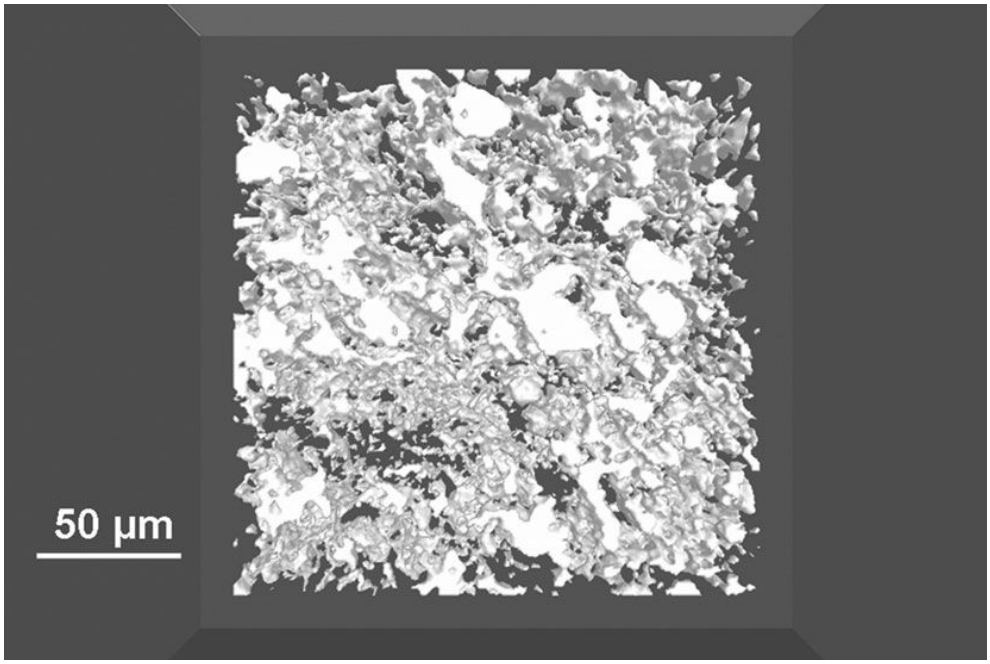

Fig 4.3 - Three dimensional rendering of the pore network of a cube of 150µm

The renderings are useful for a qualitative evaluation of the data, and give a complete three-dimensional visualization of the rock structure which may look different by the simple evaluation of the tomographic slices. The 3D model in Fig. 4.3 has been

created by CTan software and it is a representation of a selected part of the sample, because, in the case of rock, a big model where a lot of features and details are visible could be difficult to interpret. Moreover, big models have to be stored in large files (in the order of hundreds Mbytes) and therefore further elaborations, i.e. geometric operation, such as rotation, cuts, may require powerful calculation resources.

A quantitative characterization can be performed by calculating the three-dimensional parameters. The images (Fig. 4.2) reconstructed from the projections have an 8-bit depth: this means that the x-ray absorption of the samples is represented by a grey scale from 0 (black) to 255 (white). The calculation of the 3D parameters is based on binary images, in which the material and the pores are represented in black and white, respectively (Fig. 4.4). The binarization is done by selecting a threshold in the distribution of the grey levels, as shown in Fig. 4.4. The histogram corresponds to a certain area of the sample called the region of interest (ROI). The ROI should be as large as possible but completely inside the sample in order to avoid an overestimation of the porosity.

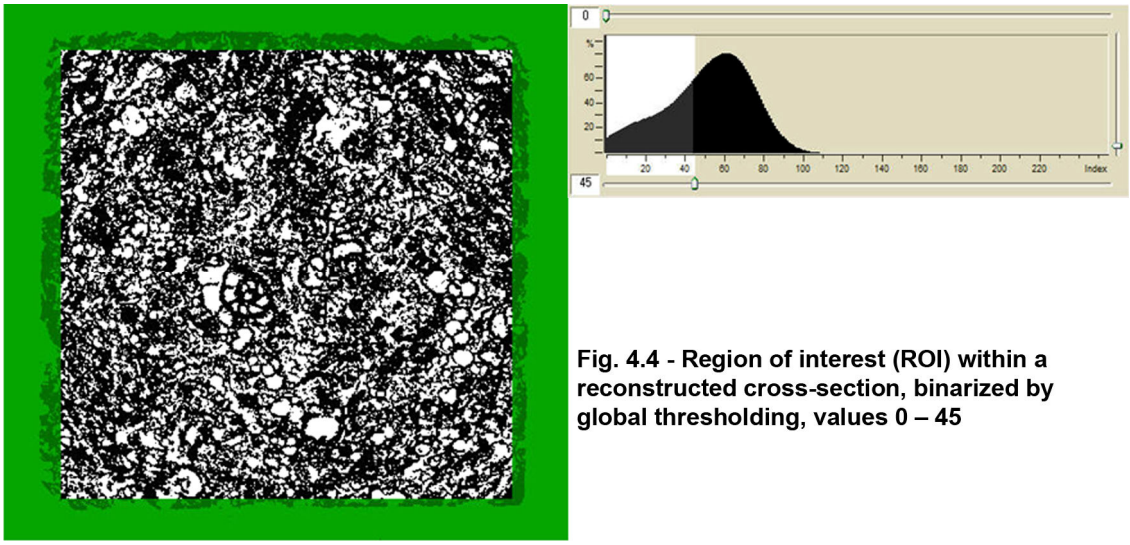

Fig. 4.4 - Region of interest (ROI) within a reconstructed cross-section, binarized by global thresholding, values 0 – 45

The threshold should be chosen carefully, as it influences the calculated morphological parameters. The choice of a too low threshold can increase the noise, resulting in an underestimation of the porosity, a false visualization of pore/channel connectivity and an unrealistic evaluation of the pore size distribution. On the other hand, a too high threshold would result in an overestimation of the porosity and a wrong visualization of the rock structure, with pore walls appearing thinner than in reality. In our case, an appropriate threshold of the grey values is 0 - 45. An example of the

appearance of the cross sections at different grey values threshold is given in Fig. 4.5. In general, there is no standard procedure to select the threshold value. An optimal value is normally set by trying different values and by a visual inspection of the appearance of the cross-sections.

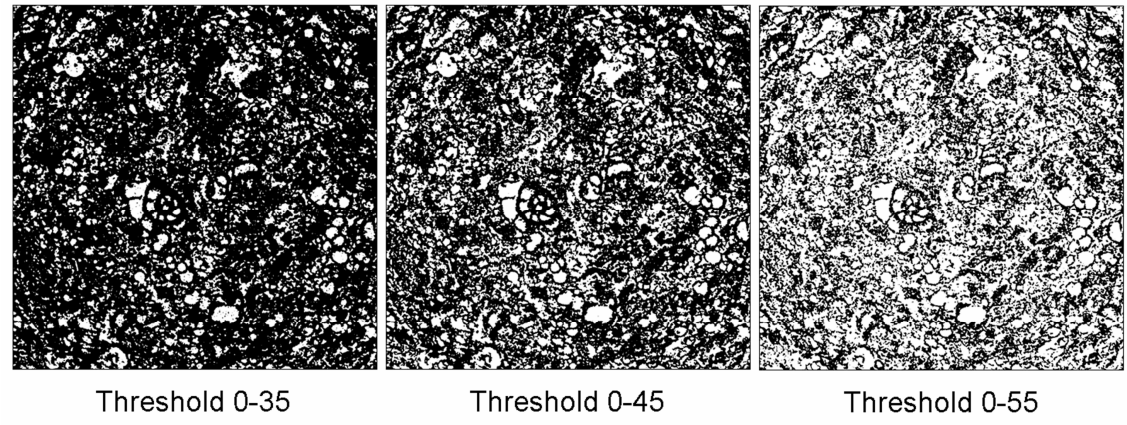

Fig. 4.5 - Binary cross sections obtained at different grey threshold values

If the aim of the analysis is to compare samples before and after treatment, it is important to keep the threshold value fixed, so that all the 3D parameters are calculated under the same conditions and only a systematic underestimation or overestimation of the porosity always affects the results in the same manner. Thus, all the 3D calculations have been performed using a global threshold [57] to obtain binary images and no additional filtering operation has been performed on the reconstructed images.

The average porosity calculated over 21 samples is 39.5 ± 1.1 %, which is in good accordance with the results from other techniques (reported in section 2.1). The pore size distribution (Fig. 4.6a) shows that the diameter of most of the pores ranges from 8 to 29 μm and the pore diameters between 3 and 8 μm are not abundant. These results are not in accordance with the pore size distribution evaluated with mercury intrusion porosimetry (MIP), where most of the pore diameters range from 1 to 8 μm (see Fig. 2.3). These contradictory results may be explained with the different physical principles on which the two techniques are based. The biggest limitation of the μ-CT is the intrinsic spatial resolution: according to the Nyquist theorem [101], pores with diameter smaller than 5 μm (twice the pixel size) cannot be distinguished. On the contrary, MIP can detect pores with radius higher than 0.0037 μm. However, as well-known, narrowing (bottleneck effect) may greatly influence the evaluation of the pores size distribution [102].

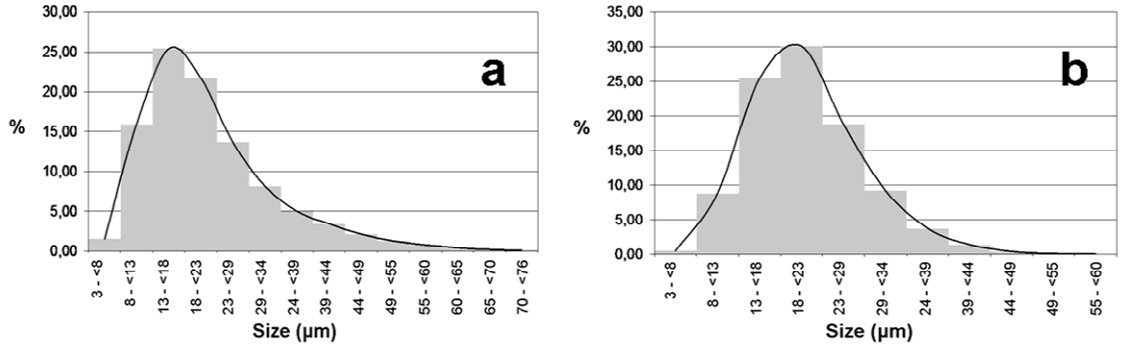

Fig. 4.6 - (a) pore size distribution and (b) wall thickness distribution of Lecce stone. The values have been calculated by averaging twenty-one samples

Wall thickness distribution (Fig. 4.6b) shows that the thickness of Lecce stone walls ranges from 13 to 29 µm, and that thicker walls (up to 60 µm) can be found, probably corresponding to fossils and shells, visible in the rock structure.

The average structure model index (SMI) calculated with CTan is 1.9. This means that the average shape of the pores is supposed to be between a plate (SMI = 0) and a cylinder (SMI = 3), i.e. similar to a flattened cylinder. This is an important result, because all the other techniques allow us to investigate the pore size distribution, but not their actual shape. In some cases, the pores are modelled like spheres or cylinders in order to obtain the pore size distribution.

4.3.2 Repeatability of µ-CT measurements

If compared with other methods, the main advantages of µ-CT are the simple preparation of the sample and the non-destructivity of the analysis. This allows to compare the characteristics of the same samples at different steps, e.g. before and after treatment or ageing.

In order to exclude that variations of morphological parameters are due to the instrumental precision or to the manipulation of the specimens, the repeatability of the measurements has been tested by scanning the same sample for five times and calculating the porosity values. The scans have been performed by removing/repositioning the sample from the scanner every time.

No. Scan	1	2	3	4	5	Average
Porosity (%)	38.1	37.5	37.1	37.6	37.5	37.6±0.4

Tab. 4.3 - Reproducibility test: porosity values of the same sample calculated from five different μ-CT measurements

The variations values in Tab. 4.3 show that the porosity ranges from 38.1 % to 37.1 %, thus the difference between the maximum and minimum value is 1%. It is then possible to monitor the porosity changes of samples induced by conservation treatments and/or ageing, but it should be taken into account that variations within 1% may be due to measurement uncertainty and only changes higher than 1% are significant.

4.3.3 Evaluation of the Paraloid B 72 treatment by μ-CT

As shown by the results in Tab. 4.1, the treatments give very high water repellence to the stone. At the resolution of 2.6 μm it is not possible to detect directly the polymers simply by comparing the cross sections of the samples before and after the treatment. In fact, the protective products normally have a low x-ray attenuation coefficient, in comparison to the rock; moreover, they may be distributed in very thin films around the grains of the stone and on the walls of the pores. On the other hand, although the conservation treatments are not directly visible, they can cause significant variations of the morphological parameters, such as porosity, pore size and wall thickness distribution. Therefore, samples of 3 x 3 x 10 mm^3 dimensions have been scanned by μ-CT before and after treatment with Paraloid B72 (Set 2, samples 8-14) and Fluoroelastomer (Set 3, sample 15-21) in order to highlight the differences in the 3D parameters. A Student's t-test has been applied in order to evaluate the statistical significance of these differences (see section 3.1.5).

Porosity values obtained from Set 2 are presented in Tab. 4.4. The two averages, before (39.4±1.3 %) and after (36.3±1.6 %) the polymer application, show that PB 72 has caused a slight decrease of the total open spaces. The t-test demonstrated that PB 72 induced a significant decrease in porosity, estimated to be 3.1±1.5 %. In fact, the experimental value of t (t_{calc} = 7.659) was greater than the tabled one (t_{tab} = 3.707) for a 2 tailed test with a probability of 99% (α = 0.01). The null hypothesis (H_0) is therefore rejected, i.e. the two averages are statistically different.

	Set 2 - Samples treated with PB 72							
	8	9	10	11	12	13	14	Average
Porosity Before Treatment (%)	38.5	38.6	41.0	38.1	38.9	39.5	41.3	39.4±1.3
Porosity After Treatment (%)	37.1	35.1	36.4	33.9	36.3	36.7	38.8	36.3±1.6
Difference (Δ_i) Before-After (%)	1.4	3.5	4.6	4.2	2.6	2.8	2.5	3.1±1.5

Tab. 4.4 - Porosity values and standard deviations of Set 2 before and after treatment with PB 72

The porosity is not the only morphological parameter that changes. The wall thickness distribution graph shown in Fig. 4.7 shows that there is a small decrease in the thinner walls (arrow A) and a slight increase in the thicker ones (arrow B) after the treatment.

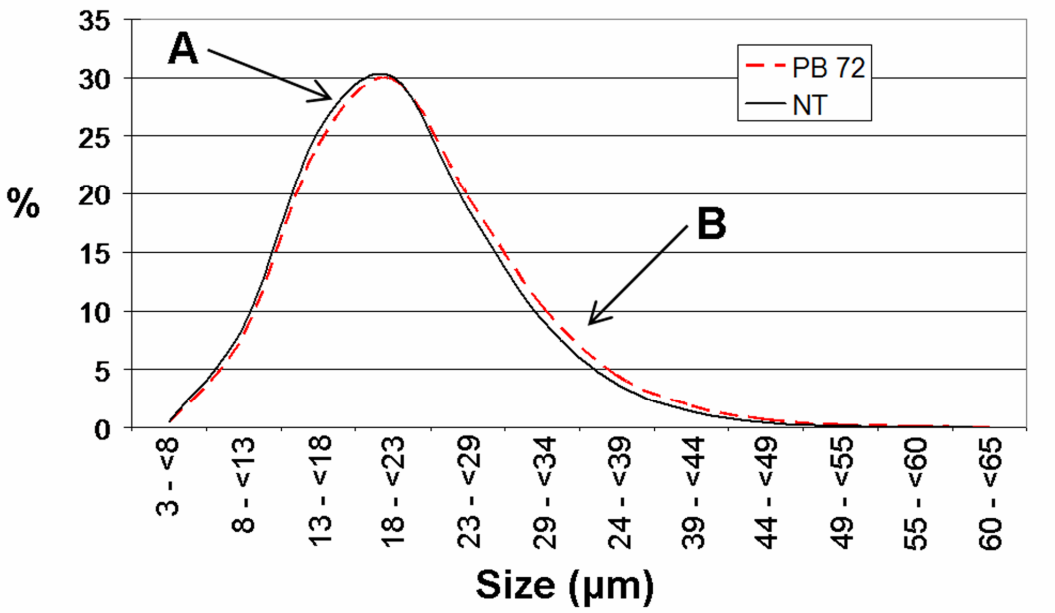

Fig. 4.7 - Wall thickness distribution of Set 2 untreated (continuous line) and treated with PB 72 (dotted line). The profiles have been calculated on an average of 7 samples

By forming a protective film along the walls of the pores, PB 72 has probably caused a wall-thickening effect. These slight changes have been noted also in the average wall thickness, since this value, after treatment, increased from 21 µm to 23 µm: again, the t-test reveals that the two averages of the wall thickness are significantly different.

Unexpectedly, only small differences have been found in the pore size distribution before and after the treatment (Fig. 4.8). PB 72 is probably distributed in thin films around the grains or on the pore walls of the Lecce stone, inducing an increase in smaller pores (arrow A) and a decrease in the larger ones (arrow B). Since the pore size is calculated as the diameter of the largest sphere that can be inscribed in the cavities [75], it is possible that, in some cases, the polymer fills small cavities and irregularities bringing to an increase of the wall thickness, without changing the pore dimension.

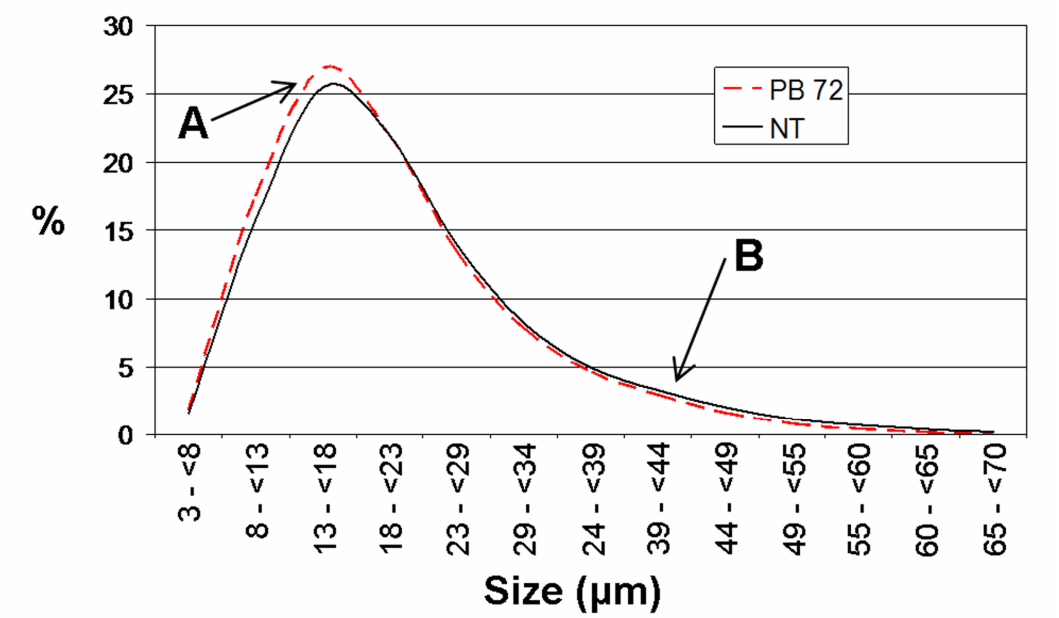

Fig. 4.8 - Pore size distribution of Set 2 untreated (NT, continuous line) and treated with PB 72 (dotted line). The profiles show a slight increase of the smaller pores (A) and a slight decrease of the larger ones (B)

Indeed, Paraloid B 72 provides the stone with good water repellence, without drastically changing the natural characteristics of Lecce stone. Harmful effects due to the occlusion of the open porosity and/or to the formation of a continuous film on the surface of the artefacts should therefore be avoided. However, it should be taken into account that these values are probably subject to an underestimation due to the distribution of the polymer in thin films and its low attenuation coefficient for x-rays in comparison with the rock.

4.3.4 Evaluation of the Fluoroelastomer treatment by µ-CT

The same protocol used for Set 2 has been employed for Set 3, and the samples have been analyzed by µ-CT before and after treatment with NH. The calculated porosity values presented in Tab. 4.5 show that the polymer application caused a significant decrease of the open spaces. The statistical comparison of the porosity before (39.6±1.2 %) and after (31.2±1.8 %) the treatment by a t-test (t_{calc} = 22.114, t_{tab} = 3.707 at 99% or α = 0.01) prove that there are significant differences between the two averages. In other words, the null hypothesis H_0 is again rejected, meaning that the two averages are significantly different and that NH caused a decrease in porosity, estimated in 8.4±1.4 %.

	Set 3 - Samples treated with NH							
	15	**16**	**17**	**18**	**19**	**20**	**21**	**Average**
Porosity Before Treatment (%)	39.7	37.7	39.6	40.9	39.9	38.4	41.1	39.6±1.2
Porosity After Treatment (%)	33.3	28.9	30.3	32.4	31.7	29.1	32.9	31.2±1.8
Difference (Δ_i) Before-After (%)	6.4	8.8	9.3	8.5	8.2	9.3	8.2	8.4±1.4

Tab. 4.5 - Porosity values (%) and standard deviation of the Set 3 before and after treatment with NH

The decrease of porosity induced by the Fluoroelastomer is higher than that induced by the Paraloid B 72 treatments (8.4 % vs. 3.1%). This quantitative discrepancy may be explained with a different distribution of the polymers in the stone structure. A uniform distribution of products with high molecular weight, such as NH, is more difficult than polymers with lower molecular weight, such as PB 72. Moreover, the acrylic polymer (PB 72), thanks to its esteric functional groups, has more affinity with the rock than the fluorinated one, and these interactions may improve the uniformity of distribution inside the pores in a thin layer.

The wall thickness distribution graph (Fig. 4.9, right part) shows a strong decrease in the amount of the thinner walls and a considerable increase in the thicker

ones. The NH treatment has induced a thickening effect due to the coating of the pores and the grains of the rock. The same behaviour has not been observed in pore size distribution, where no appreciable changes of untreated vs. treated have been found.

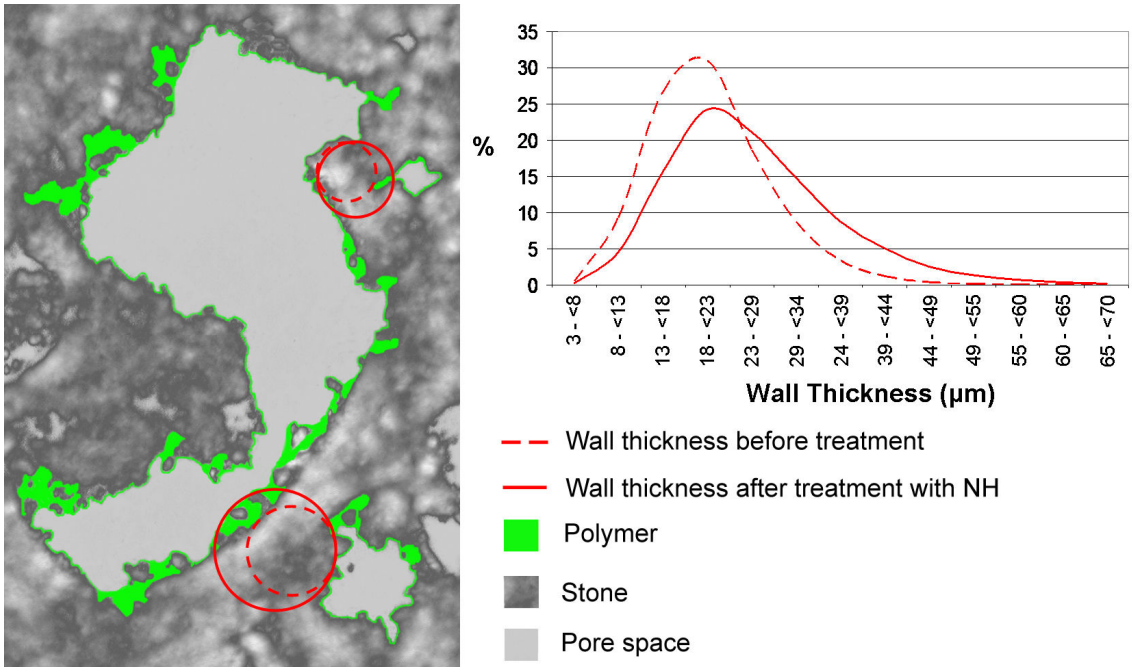

Fig. 4.9 – On the right: wall thickness distributions of Set 3 untreated (dotted line) and treated with NH (continuous line). On the left: a possible model of polymer distribution in the stone structure, with thickening of the walls without drastic pore size variation

It is possible that the application of the product has changed the wall thickness distribution and the total porosity, causing a very small variation of the pore dimension distribution (Fig. 4.9, left part). This small variation, associated with the appreciable decrease in porosity, also suggests that part of the cavities could be completely filled by the polymer.

According with the pore size and wall thickness distribution graphs, the initial average pore size (22 µm) has not changed after the treatment, whereas the average wall thickness has increased from 21 µm to 26 µm after the application of the polymer.

4.3.5 Nano-CT: untreated vs. treated

A nano-CT system has been used with the aim of testing the applicability of this technique in stone conservation. This instrument allows to achieve higher resolution, but it requires some limitations in the sample size.

Small pieces of irregular shape of around 0.5 mm, taken from 5 x 5 x 1 cm^3 samples untreated and treated with Hydrophase Superfici, have been analyzed at a 580 nm resolution. The image of the untreated sample (Fig. 4.10) shows more details compared to the μ-CT and a better description the internal structure of the stone. In the case of the sample treated with Hydrophase Superfici (Fig. 4.11), it is also possible to visualize the product which fills the pores - sometimes completely, but more often partially. These observations are more evident in the enlarged images, where the empty pores in the untreated stone (Fig. 4.10) can be clearly distinguished from the pores filled with the polymer in the treated one (Fig. 4.11).

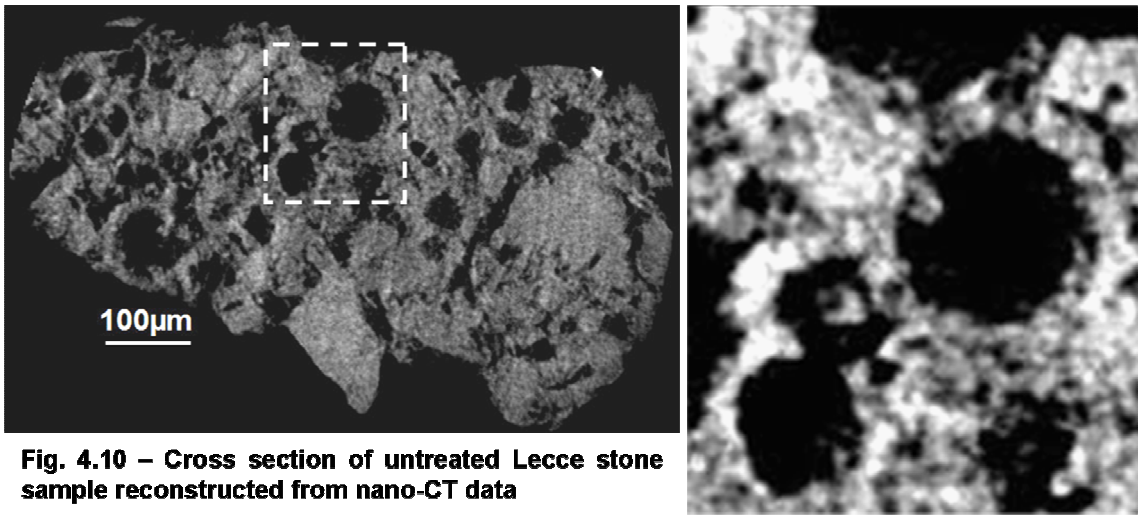

Fig. 4.10 – Cross section of untreated Lecce stone sample reconstructed from nano-CT data

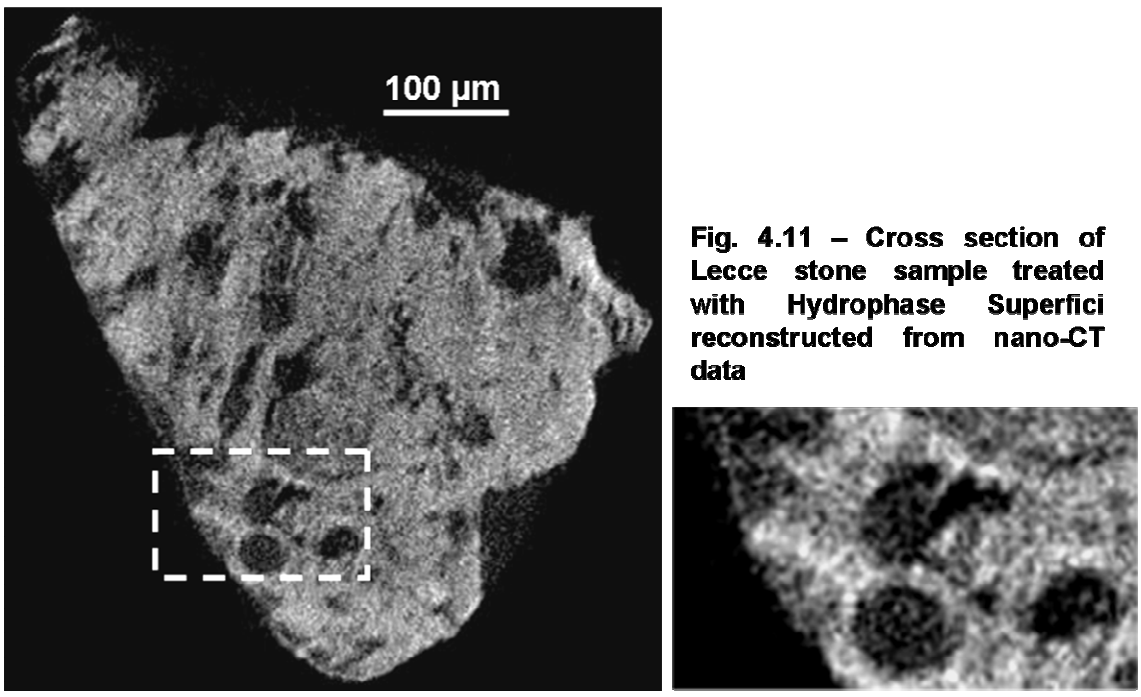

Fig. 4.11 – Cross section of Lecce stone sample treated with Hydrophase Superfici reconstructed from nano-CT data

The irregular shape of the samples makes an appropriate selection of a ROI difficult. Moreover, the calculation of the morphological parameters is not useful, since such small specimens are actually not representative of the general petrographic characteristics of Lecce stone. Thus, the nano-CT images have been evaluated only qualitatively, without any further elaborations.

The three-dimensional rendering of a small part of the untreated sample (fig. 4.12) is particularly interesting, which gives a detailed idea of the stone structure and of the remarkable relevance of the CT data processing. The present 3D model has been created by means of VGStudio MAX software [103], a commercial program for voxel visualization and analysis.

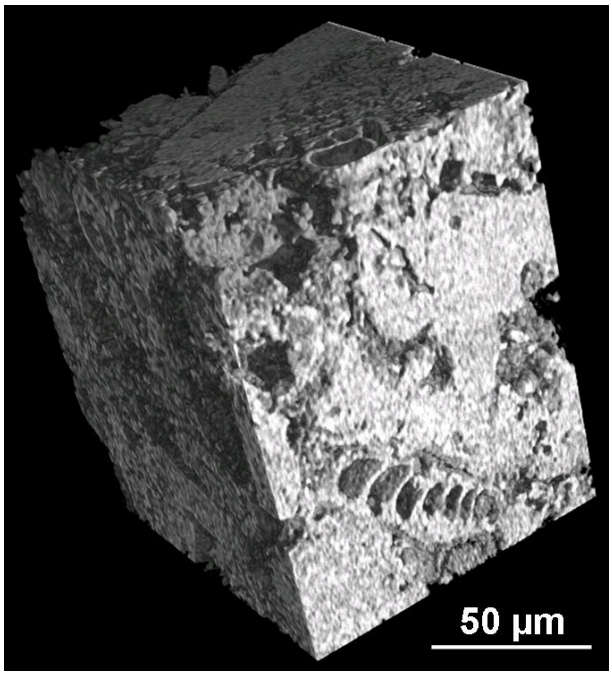

Fig. 4.12 - 3D rendering of portion of Lecce stone sample reconstructed from nano-CT data (image created by Dr. Veerle Cnudde)

Nano-CT can be useful to visualize and study the distribution of the products inside the pores, and to analyze samples taken from big treated specimens or real walls of historical buildings. For example, the penetration of the treatment can be estimated by taking samples at different depths from the treated surface.

4.3.6. Evaluation of conservation treatments by SR-CT

Lecce stone samples of 1 x 1 x 10 mm^3 dimensions, treated with Paraloid B 72, Fluororubber and Hydrophase Superfici, have been scanned by synchrotron radiation tomography at the beamline ID 19 of ESRF. The quality and the monochromaticity of

the x-rays enhance significantly the contrast between stone and protective products in the reconstructed images. In the nano-CT results, the treatment appears as a shadow and its borders are not completely defined. Examples of SR-CT analysis on stone treated with polymers are reported in Fig. 4.13 and Fig. 4.14, where PB 72 and Sil are directly visible.

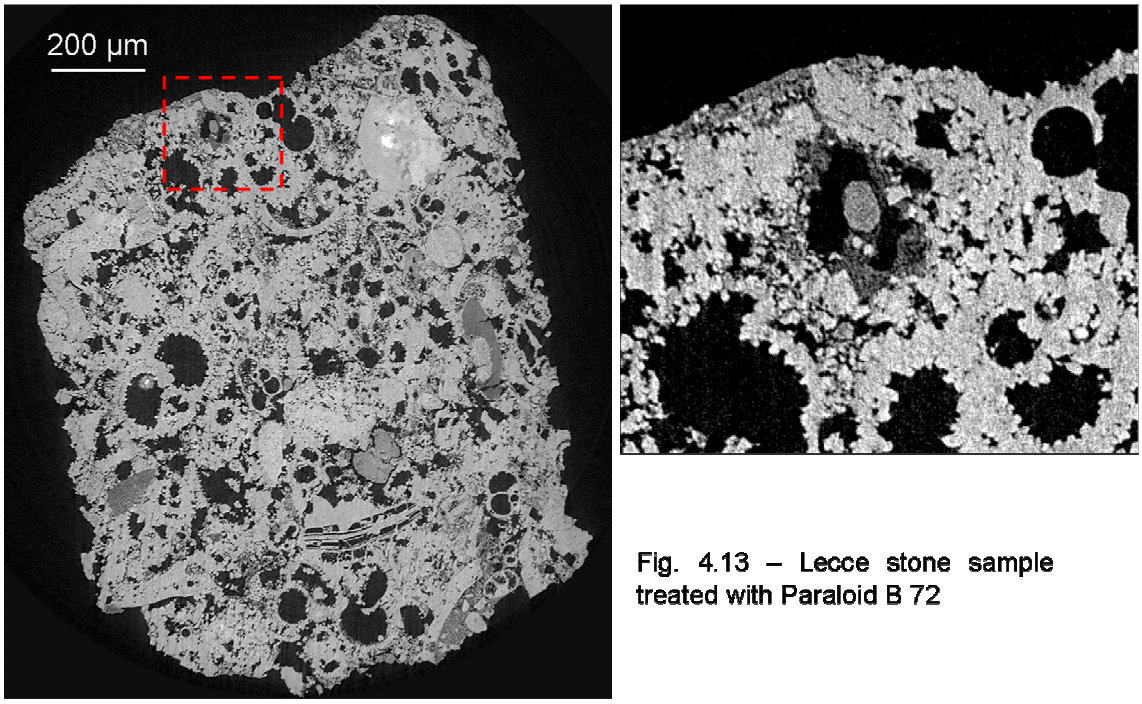

Fig. 4.13 – Lecce stone sample treated with Paraloid B 72

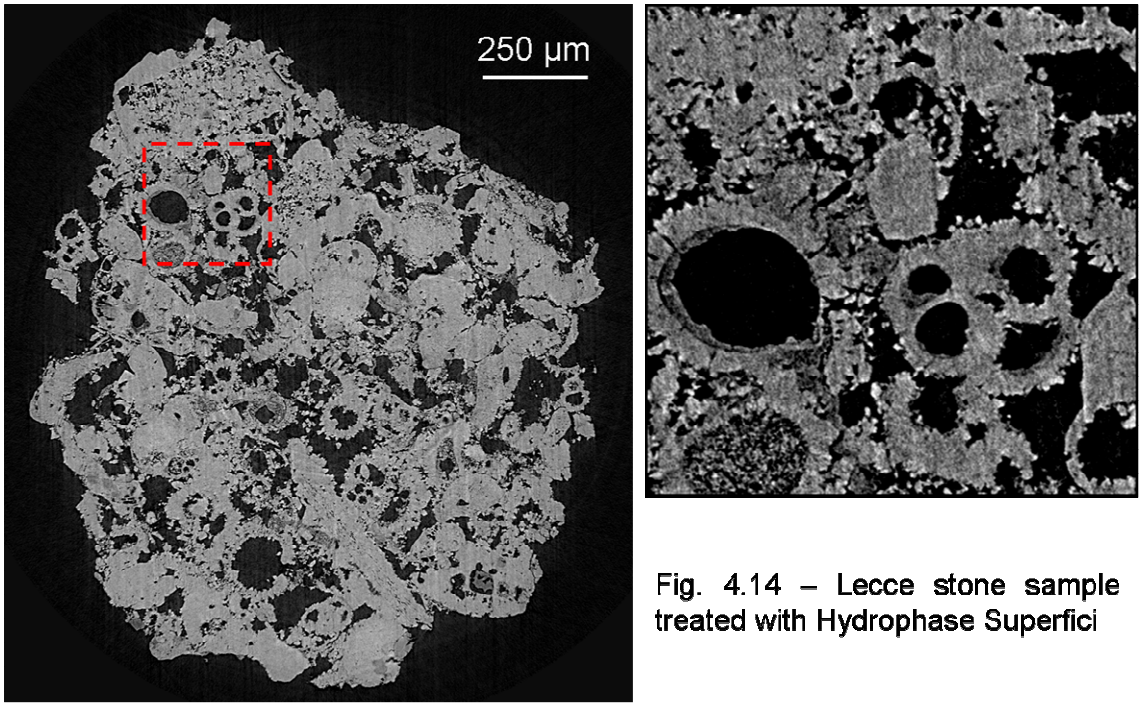

Fig. 4.14 – Lecce stone sample treated with Hydrophase Superfici

The protective products are distributed in thin films around the grains of Lecce stone and on the walls of the pores. On the other hand, there are areas in the samples where the polymer is not present. This may be due to the small size of the specimens (1 mm), so that the capillary suction and the treatment uptake are rather limited. Despite the application by impregnation under reduced pressure, the amount of product deposited in the stone structure seems to be quite modest.

However, these results show that SR-CT can be successfully used to visualize conservation treatments, their distribution and the manner in which they coat the pores. Therefore, since the treatment procedure of these samples is not completely effective and/or representative of actual treatments, the evaluation and estimation of the products penetration and distribution would probably be more reliable if the investigation could have been carried out on small specimens sampled from larger sample, as made in the case of the Nano-CT tests.

4.4 Neutron experiments

Neutron radiography (NR) and tomography (NT) experiments have been performed on Lecce stone samples (5 x 5 x 1 cm^3) with the aim of mapping the distribution of the conservation products. Since the neutrons are strongly attenuated by hydrogen, water and polymers containing hydrogen atoms, such as Paraloid B72 and Hydrophase Superfici, can be detected. Fluoroelastomer presents in its structure few hydrogen atoms, though not sufficient to produce a good contrast between stone and treatment. An example of NR experiment is given in Fig. 4.16 where the capillary rise of water in an untreated Lecce stone sample can be followed acquiring neutron radiographs at different time steps.

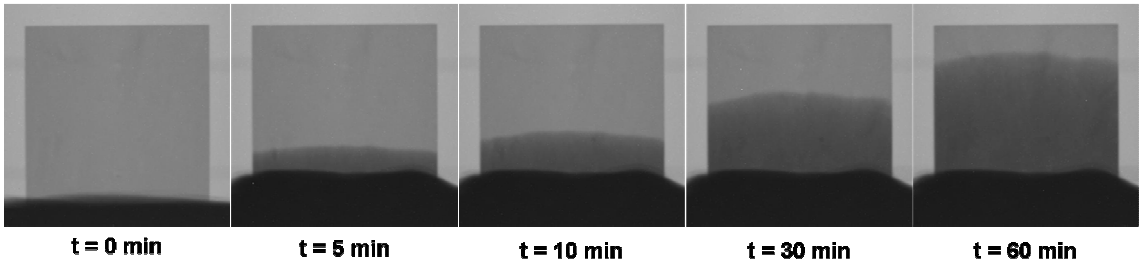

Fig. 4.16 – Capillary rise of water in Lecce stone sample followed by neutron radiography

Neutron tomography has been used to scan samples treated with Hydrophase Superfici by capillary absorption: the 3D rendering of a sample treated for 24 hours is presented in Fig. 4.17. The silicon-based product is mainly distributed on the surface that was in contact with the solution and on the side walls where the capillary suction is stronger. These treatment conditions lead to a quite homogenous superficial distribution, with a penetration depth of 1-2 millimetres. However, small amounts of Hydrophase Superfici, under the detection limit of neutron tomography, may be also present in the bulk of the sample.

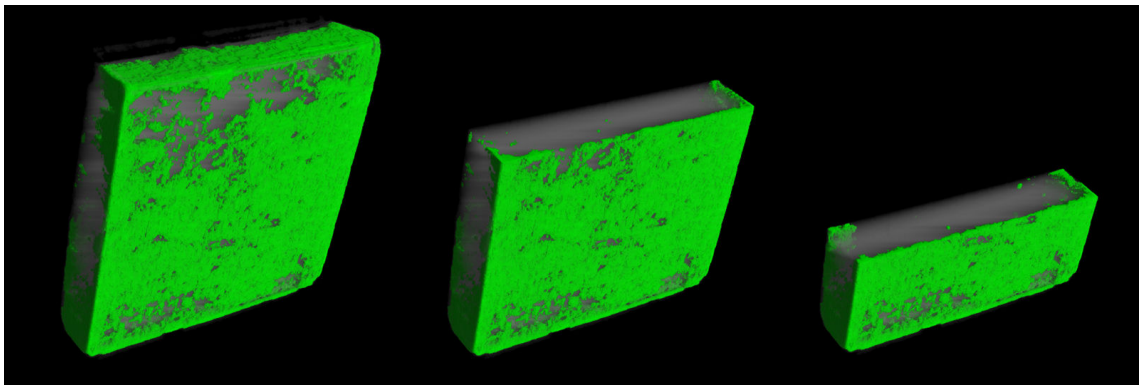

Fig. 4.17 - 3D rendering of a Lecce stone sample (5 x 5 x 1 cm^3) analyzed by neutron tomography. In green colour Hydrophase Superfici applied by 24h of capillary absorption

The same treatment with Hydrophase Superfici has been performed, keeping the sample in absorption for 48 hours. These different treatment conditions have been used to evaluate the importance of the treatment parameters.

The 3D rendering of the neutron tomography data presented in Fig. 4.18, shows a different distribution of the product, in comparison with the 24 hours treatment. The polymer is distributed not only on the surface that was in contact with the treatment solution, but also on the other side. The penetration depth is higher (2-4 mm), but the inner part of the sample is not coated by the product. This behaviour may be explained by the mechanism of solvent evaporation: when the samples start drying, the solvent migrates close to the surface and it hauls the product towards the sample edges. This effect on the product distribution is normally more evident when the solvent evaporation rate is slow.

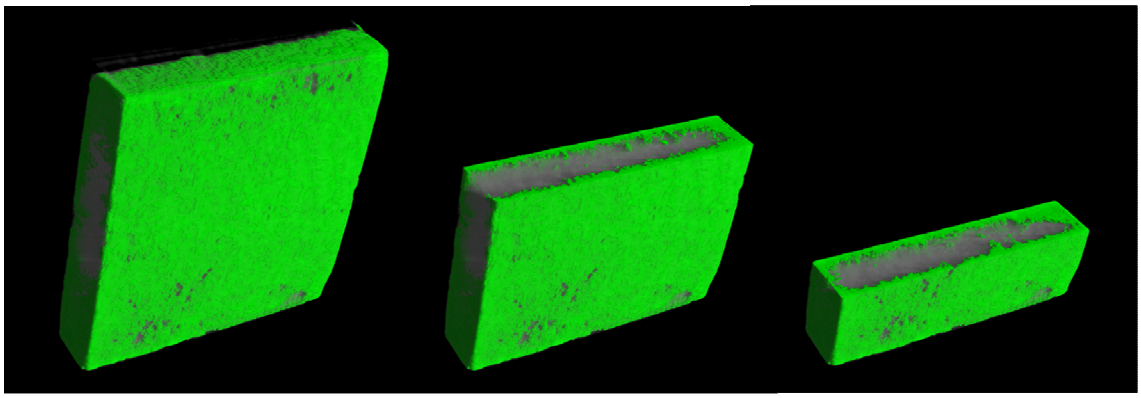

Fig. 4.18 - 3D rendering of a Lecce stone sample (5 x 5 x 1 cm^3) analyzed by neutron tomography. In green colour Hydrophase Superfici applied by 48h of capillary absorption (48h)

A sample treated with PB 72 has also been analyzed by neutron tomography. In the 3D rendering of Lecce stone specimens treated by capillary absorption (Fig. 4.19) and brush (fig. 4.20), differences in amount of polymer and its distribution can be observed.

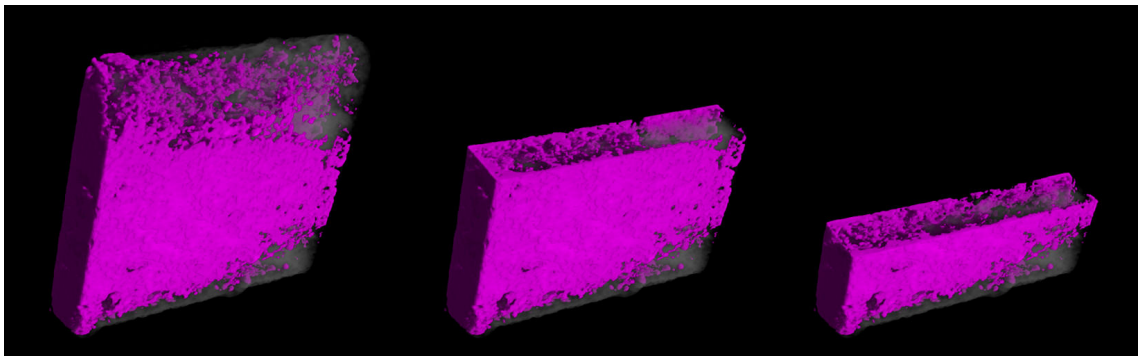

Fig. 4.19 – 3D rendering of a Lecce stone sample (5 x 5 x 1 cm^3) analyzed by neutron tomography. In magenta colour the PB 72 applied by capillary absorption.

The treatment by capillary absorption allows to deposit a higher amount of Paraloid B72 (as also found by the gravimetric data reported in Tab. 4.1), which is essentially distributed on the surface of the specimens, with a penetration depth of few millimetres.

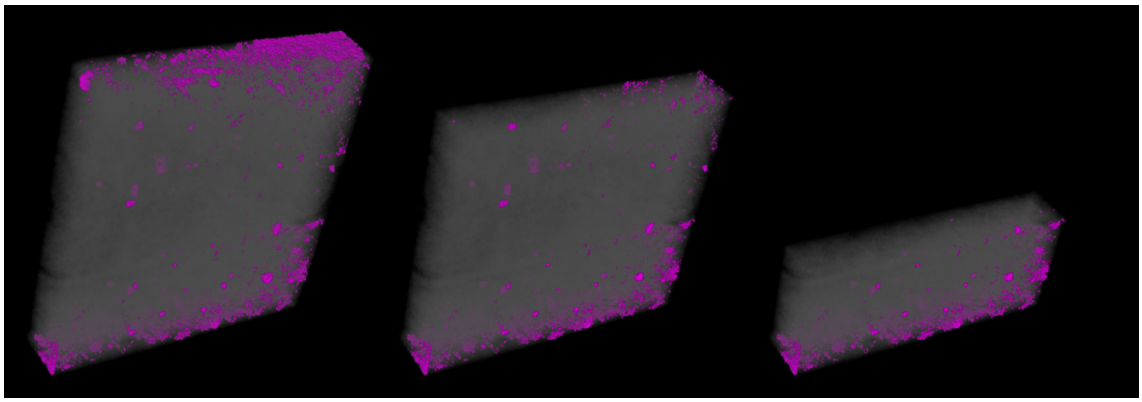

Fig. 4.20 – 3D rendering of a Lecce stone sample (5 x 5 x 1 cm^3) analyzed by neutron tomography. In magenta colour the PB 72 applied by brush.

On the other hand, the sample treated by brush has considerable water repellence; this means that the amount deposited on the surface is sufficient to give hydrophobic properties to the rock, but it is probably under the detection limit of neutrons. Fig. 4.20 also shows that the treatment is sometimes concentrated in spots inside the stone structure and/or close to the edges of the sample, as in the case of application by means of capillary absorption.

Chapter 5

EVALUATION OF THE IMPACT OF NOx: RESULTS & DISCUSSION

5.1 Environmental-SEM and laser μ-profilometry

The surfaces of Lecce stone samples have been monitored during the ageing with NOx by means of electron microscopy (ESEM) and laser μ-profilometry, in order to detect the morphological changes induced by the action of the pollutant.

ESEM images have been acquired at different ageing steps. Fig 5.1 shows the surface of an untreated Lecce stone not aged and after 3000h of exposure to NO_2. Qualitatively, the morphology of the rock has not changed. At higher magnification (2400x) the shape of the crystallites of calcite looks intact without any sign of corrosion.

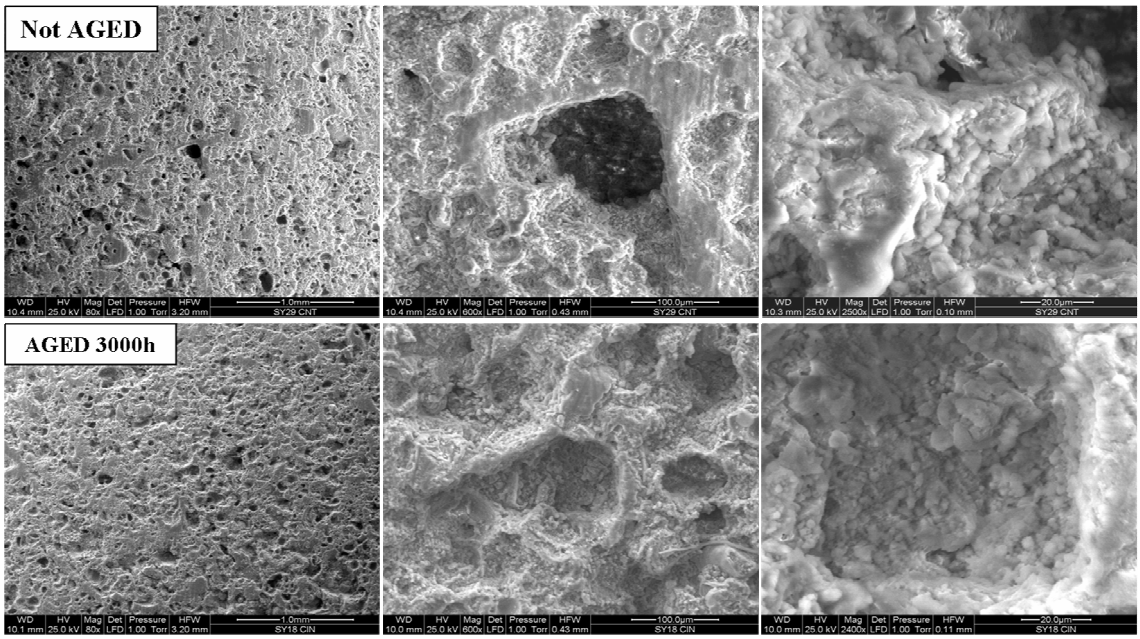

Fig. 5.1 – Images of untreated Lecce stone sample, not aged and aged 3000h, acquired by Environmental Scanning Electron Microscopy (ESEM) at different magnifications (80x, 600x, 2400x).

The same considerations can be done for aged samples treated with conservation products. In fact, superficial changes have not been detected on these samples in the ESEM images, not even where inclusions in the calcite matrix, such as shells and foraminifera, are present.

These results, in contrast with the ion chromatographic data that reveal relevant amounts of nitrates and nitrites on the specimens (see section 5.2), may be explained with the fact that the images at different ageing steps have not been acquired on the same area of the samples. Moreover, the actions of NOx on stone can take place in the

inner part of the rock, so that exposed stone surfaces may appear unchanged even if decay reactions occur.

Further investigations have been carried out by scanning laser µ-profilometry, a non-destructive technique which allows to obtain holographic reconstruction of the surfaces, as well as superficial profiles. Fig. 5.2 reports an example of the layout of the holographic reconstruction, compared with the same image acquired by optical microscopy (O.M.) at low magnification (2x).

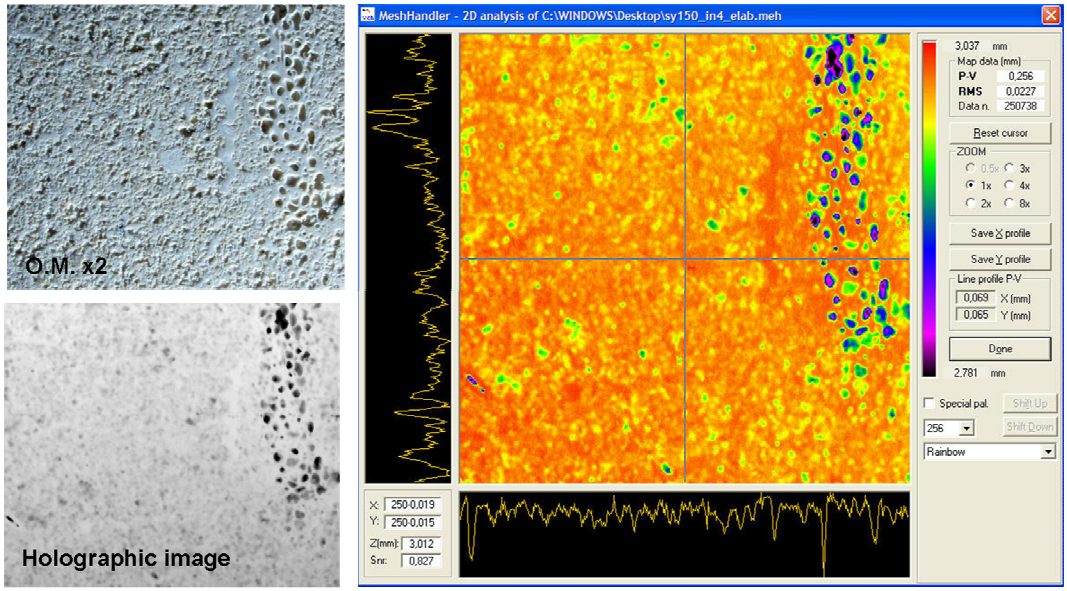

Fig. 5.2 – Comparison of optical microscopy and holographic images of Lecce stone surface

The same area of the same sample has been scanned before and after 700 h of ageing. The analysis consists in a series of vertical profiles with a sampling pitch of 20µm, so that the complete surface is reconstructed by interpolation.

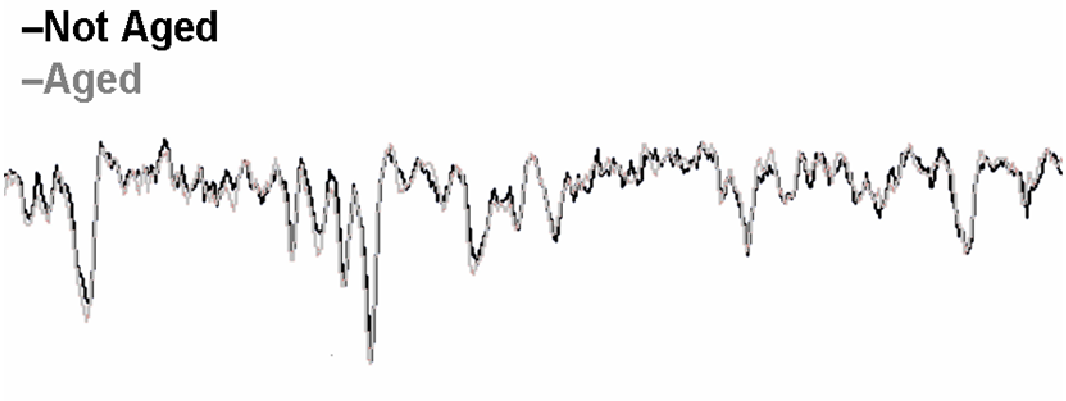

Fig. 5.3 - Comparison of the same profiles of the same sample before (black) and after 700h of ageing (grey)

At the resolution of 1 μm the two profiles are very close and the μ-profilometry data substantially confirm the results obtained by Environmental-SEM, where no corrosion evidences have been found.
At the same time, no significant colour variations of surfaces have been detected after 3000 h of ageing, thus the exposure of untreated and treated sample to NO_2 does not cause any chromatic changes, i.e. values of $\Delta E < 1$ has been observed for all samples.

5.2 Assessment of NOx impact on Lecce stone by ion chromatography

The results of the chromatographic analysis on the washing solutions of reference (untreated) and treated samples, at different stages of ageing, are reported in Tab 5.1.
After 96h of ageing, the amount of nitrates and nitrites detected on the reference sample is 18.3 ppm. All the treatments show a reduction of the NO_2 attack, especially Paraloid B72 applied by capillary absorption (1.8 ppm) and Hydrophase Superfici applied indifferently by brush or capillary absorption.
After 420 h of ageing, the amount of nitrites and nitrates detected on the untreated sample increases (36.9 ppm) and some of the treatments show a partial reduction of the NO_2 attack. PB 72-CA protect efficiently the material (18.9 ppm) and Sil shows the best performances, since the amount of salts on the sample treated with the silicon products is about one tenth in comparison with the untreated one.
Long term exposure of specimens to NOx highlights different behaviours of the conservation treatments. In fact, after 700 h of ageing, the amount of salts detected on the reference sample is 45.0 ppm and most of the treatments do not mitigate the stone weathering. Only Paraloid B72 applied by capillary absorption demonstrates to induce a slight reduction of the NO_2 attack (38.5 ppm).
Other treatments, such as NH-B and Ox-CA, show an amount of nitrates and nitrites higher than the reference sample. This behaviour may be explained by the fact that the distribution of the protective products occurs preferentially on the surface, without an efficient penetration inside the stone. This low penetration, even if it seems to reduce slightly the RP%, may trap the liquid water condensed inside the pores, accelerating the deterioration processes.

The same mechanism leads to the formation of a massive amount of nitrates and nitrites after 3000h of ageing. In fact, the quantity of salts found in the specimens treated with conservation products are around three times higher than in untreated samples (300 ppm vs. 100 ppm). On the other hand, comparable amounts of nitrates and nitrites have been also found in samples treated with Hydrophase Superfici, where the product should be well-distributed and a good penetration should be achieved.

		Aged 96h	Aged 420h	Aged 700h	Aged 3000h
		[N] (ppm)	[N] (ppm)	[N] (ppm)	[N] (ppm)
Treatments	**Not Treated**	18.3±0.1	36.9±0.1	45.0±0.1	98.1±0.1
	PB 72 - B	5.0±0.1	27.5±0.1	49.7±0.1	284.57±0.1
	PB 72 - CA	1.8±0.1	18.9±0.1	38.5±0.1	325.76±0.1
	NH - B	9.3±0.1	29.0±0.1	60.2±0.1	263.67±0.1
	NH - CA	10.2±0.1	30.0±0.1	47.4±0.1	317.85±0.1
	Sil - B	0.92±0.1	3.6±0.1	45.5±0.1	292.54±0.1
	Sil - CA	1.1±0.1	3.1±0.1	44.4±0.1	348.0±0.1
	Ox - CA	11.9±0.1	26.4±0.1	51.4±0.1	341.0±0.1

Tab. 5.1 – Ion Chromatography analyses on washing solutions of Lecce stone samples at different ageing times. [N] = [NO_2^- + NO_3^-] expressed as ppm of nitrogen. At every ageing step, one sample per treatment and a non treated sample have been washed. The standard deviations concern three repetitions of the IC analyses on the same samples.

The results in Tab. 5.1 also show that from the point of view of the application methods, capillary absorption is more effective at short time ageing, but brushing seems to be better at long term exposures.

For short ageing periods (96 h), all the treatments induce a decrease of the NO_2 attack on the calcareous stone. Nevertheless, this protective effect is quickly reduced increasing the ageing time (420h and 700h). At 3000h the changes caused by the conservation treatments, i.e. occlusion of the porosity, variation of wettability and transpirability, cause the acceleration of the decay reactions and processes.

The ion chromatography results demonstrate that NO_2 is very aggressive for Lecce stone, since the amounts of salts formed in the sample are remarkable. In spite of the considerable action of NOx, no corrosion signs have been detected on the surfaces (see section 5.1). These considerations lead to assume that NO_2 penetrates and diffuses inside the stone porosity and it reacts, degrading the rock from the inside. At the studied conditions, this process seems to be accelerated by the presence of conservation treatments which influence the water exchange (condensation and/or evaporation) phenomena, and they can alter the natural characteristics and behaviour of the material.

5.3 Assessment of the impact of NOx on Lecce stone by µ-CT

The ageing of Lecce stone samples of 3 x 3 x 10 mm^3 dimensions has been monitored by µ-CT: the specimens coming from Set 1 (samples 5 – 8, not treated), Set 2 (samples 12 – 15, treated with PB 72) and Set 3 (samples 19 – 22, treated with NH) have been exposed to NO_2 atmosphere, adopting the same temperature and relative humidity conditions, used for the larger samples (5 x 5 x 1 cm^3 dimensions).

The porosity of Set 1, Set 2 and Set 3 samples before and after ageing with NO_2 (700h) are presented in Tab. 5.2, Tab. 5.3 and Tab. 5.4, respectively.

	Set 1 - Samples not treated				
	5	6	7	8	Average
Porosity Before Ageing(%)	39.3	39.9	39.4	39.3	39.5±0.3
Porosity After Ageing (%)	31.2	32.6	31.8	34.1	32.4±1.25
Difference Before-After (%)	8.1	7.3	7.6	5.2	7.1±1.25

Tab. 5.2 - Porosity values (%) and standard deviations of Set 1 samples before and after ageing with NO_2

The untreated samples show the greatest variation in porosity. Unexpectedly, the action of NO_2 has caused a decrease of the empty spaces and not an increase as it is expected by the corrosion mechanism. On the other hand, the action of the nitrogen

oxides leads to the transformation of the calcite in nitrocalcite which remains in the rock structure. Moreover, the new formed salts (in particular calcium nitrate) crystallize with 4 molecules of water, giving crystals larger than calcite. On the contrary, the corrosive effects may be evident if the reaction between NOx and calcite occurs in monumental buildings exposed to rain. In this case, in fact, the reaction products (nitrates and nitrites) are washed out by the liquid water during precipitations, due to their high solubility in water. The accelerate ageing system used in these tests does not simulate exposed outdoor conditions, so that it seems reasonable that the porosity of the samples decreases. The same behaviour has been observed in samples of Set 2, treated with Paraloid B 72: the porosity decreases, though less in comparison with the untreated specimens (4.7% vs. 7.1%).

	Set 2 - Samples treated with PB 72				
	12	13	14	15	Average
Porosity Before Ageing(%)	33.9	36.3	36.7	38.9	36.4±2.0
Porosity After Ageing (%)	30.2	30.7	31.5	34.6	31.8±2.0
Difference Before-After (%)	3.7	5.6	5.2	4.3	4.7±0.9

Tab. 5.3 - Porosity values (%) and standard deviations of Set 2 samples treated with Paraloid B 72 before and after ageing with NO_2

	Set 3 - Samples treated with NH				
	19	20	21	22	Average
Porosity Before Ageing(%)	32.4	31.7	29.0	32.9	31.5±1.7
Porosity After Ageing (%)	33.4	32.6	30.1	33.7	32.5±1.6
Difference Before-After (%)	1.0	1.0	1.1	0.8	1.0±0.1

Tab. 5.4 - Porosity values (%) and standard deviations of Set 3 samples treated with Fluoroelastomer before and after ageing with NO_2

On the contrary, the samples treated with NH show a slight change of porosity of 1%, which has been considered to be due not to the NO_2 action, but to the instrumental uncertainty (see section 4.3.2).

The ageing has not caused changes in the pore size distribution, which remains substantially unvaried in all the samples. On the other hand, the wall thickness of Set 1 (Fig. 5.4) and Set 2 (Fig. 5.5) samples significantly changes: the amount of the thin walls decreases, while the amount of the thicker ones increases. This effect is certainly due to the action of NO_2, even if the mechanism which leads to these wall thickness distribution variations is still not completely clear. However, it is reasonable to suppose the growing of nitrocalcite crystals in small pores, where the water vapor condensation, and consequently the NO_2 absorption, is favoured. As a consequence, a pore occlusion may occur with a relevant contribution to the increase of the wall thickness.

The samples of Set 3, treated with Fluoroelastomer, do not show any relevant changes in the morphological parameters, thus this conservation treatment, in these experimental conditions, seems to protect Lecce stone from the weathering of NO_2. These results, not in accordance with those found by ion chromatography (see section 5.2), may be justified by a different distribution of the polymers in the stone, caused by the different dimensions of the investigated samples (50x50x10 mm^3 for the IC test vs. 3x3x10 mm^3 in this test).

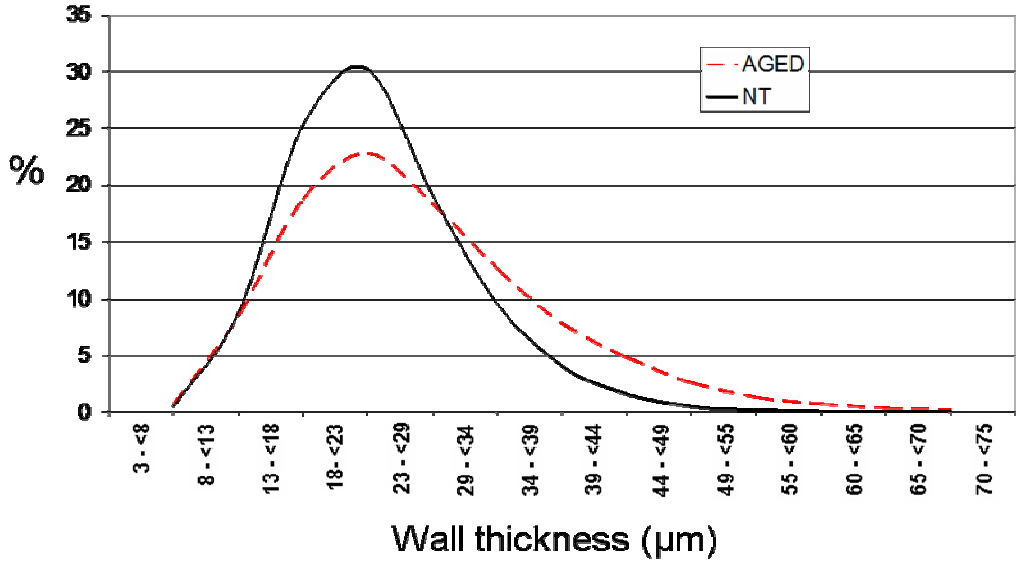

Fig. 5.4 – Wall thickness distribution of Set 1 samples not treated (in black) and aged (in red)

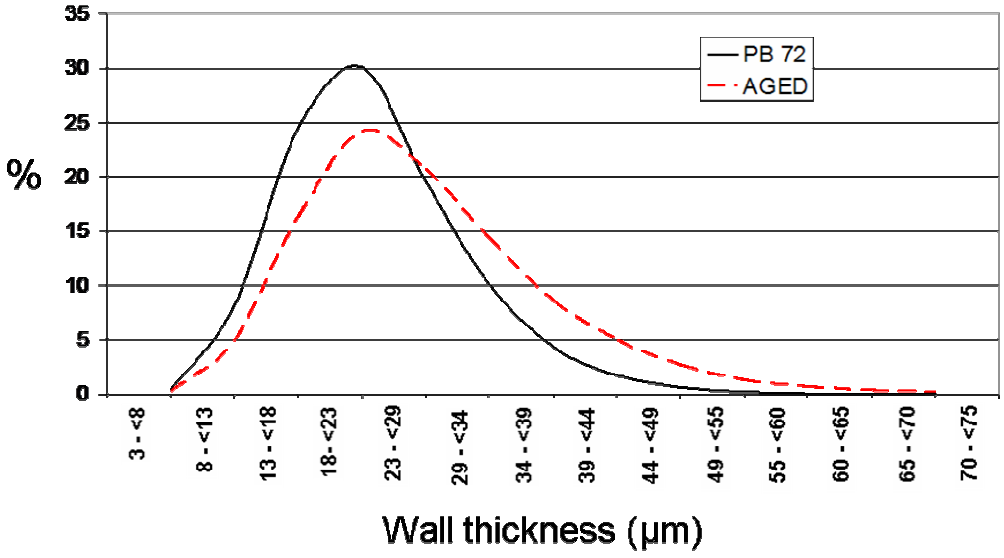

Fig. 5.5 – Wall thickness distribution of Set 2 samples treated with PB 72 (in black) and aged (in red)

5.4 Assessment of impact of NOx on Lecce stone by neutron imaging

Neutron experiments have been carried out with the aim of studying moisture uptake and evaluating the effects of NOx on stone samples. Since the action of these pollutants causes the formation of nitrates and nitrites in the limestone, samples of Lecce stone with dimension of 5 x 5 x 2 cm^3 have been treated with a known amount of calcium nitrate, in order to simulate the aged composition of the stone.

Lecce stone specimens have been treated with calcium nitrate by applying, on one side of the samples, a known amount of salt dissolved in water. After this treatment the stone has been dried first at room conditions, and then in calcium chloride dessiccator, until constant weight is reached. The list of these samples and the relative amounts of salt deposited are presented in Tab. 5.5.

Sample	A	B	C	D	E
Amount of Calcium Nitrate (g)	None	0.155	0.525	1.050	2.100

Tab. 5.5 – Amounts of calcium nitrate in Lecce stone samples of 5 x 5 x 2 cm^3 dimension.

A fundamental characteristic of nitrates and nitrites is to be deliquescent and then to absorb humidity from the environment. The graph presented in Fig. 5.6 shows the weight of water absorbed by Lecce stone samples with different amount of salt, put in a close box at 100% of RH%, but without liquid water.

The presence of deliquescent salts strongly influences the behaviour of the rock material, in fact, the natural sample A, where no salts have been added, absorbs about 1 g of moisture, while the sample with high amount of calcium nitrate, e.g. sample E, absorbs a higher amount of water, i.e. more than 12 g in 120 days. However, even if all the specimens have been exposed to moisture for four months, they do not result completely saturated yet.

The process of humidity uptake has been also followed by Magnetic Resonance Imaging (MRI), performing scans of the samples at different time points. MRI images with a voxel size resolution of 0.78 mm (Fig. 5.7) show the increasing amount of water vs. time in the sample E. However, this technique allows to visualize water in porous rock with limited resolution and sensitivity: water is visible when it is present in the order of grams.

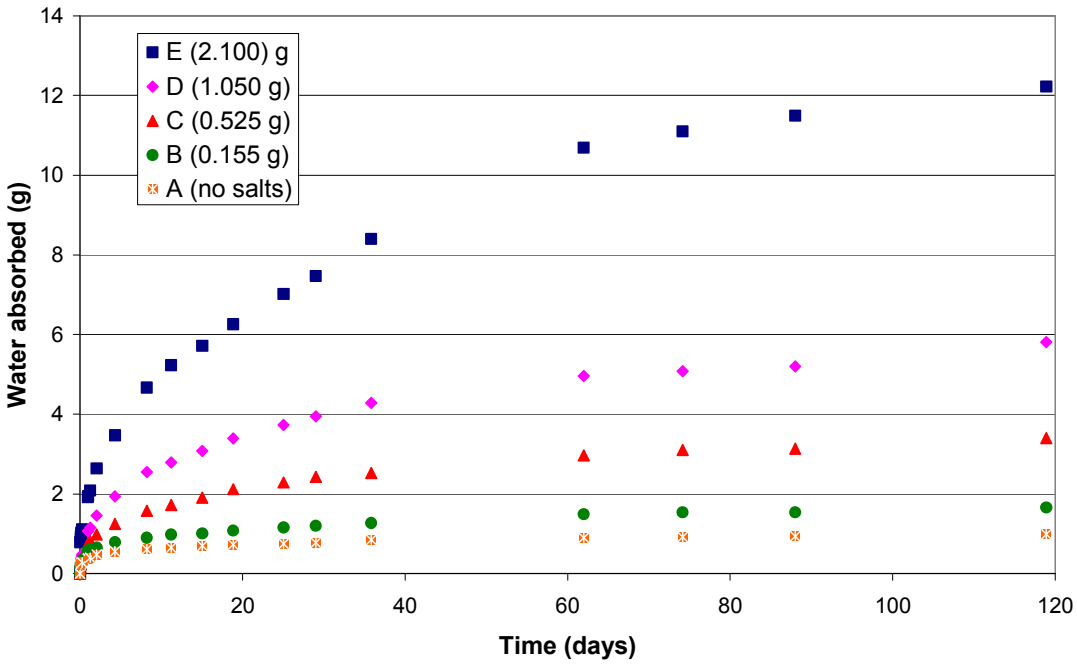

Fig. 5.6 – Moisture uptake by Lecce stone samples impregnated with different amounts of calcium nitrate.

The moisture absorption process can also be studied by neutrons radiography and tomography, with lower limit of detection and higher resolution in comparison with MRI. In fact, as explained in Chapter 3, neutrons are strongly attenuated by compounds containing hydrogen, so that even small amounts of water or organic material can be detected with a pixel size resolution of 115 μm.

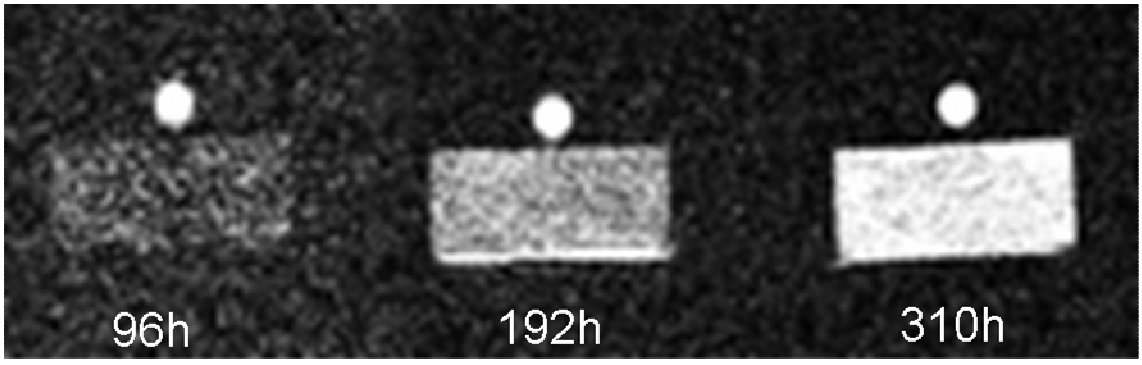

Fig. 5.7 – MRI images of a Lecce stone sample impregnated with 2.1 g of calcium nitrates after 96h, 192h and 310h

In order to study the moisture uptake, neutron radiography experiments have been performed as follows: the samples have been scanned in dry conditions, which are used as a reference, in order to determine the contribution of the stone to the neutron attenuation, and then in wet conditions, at different times of exposure to RH of 100%. Since it is difficult to reposition the sample in the beam, despite a dedicated sample holder, an IDL routine has been implemented with the aim of correcting the radiographs, to subtract the contribution of the rock and to estimate the amount of water present in the specimens.

The corrected radiographs of the samples treated with calcium nitrate at different time points are presented in Fig. 5.8.

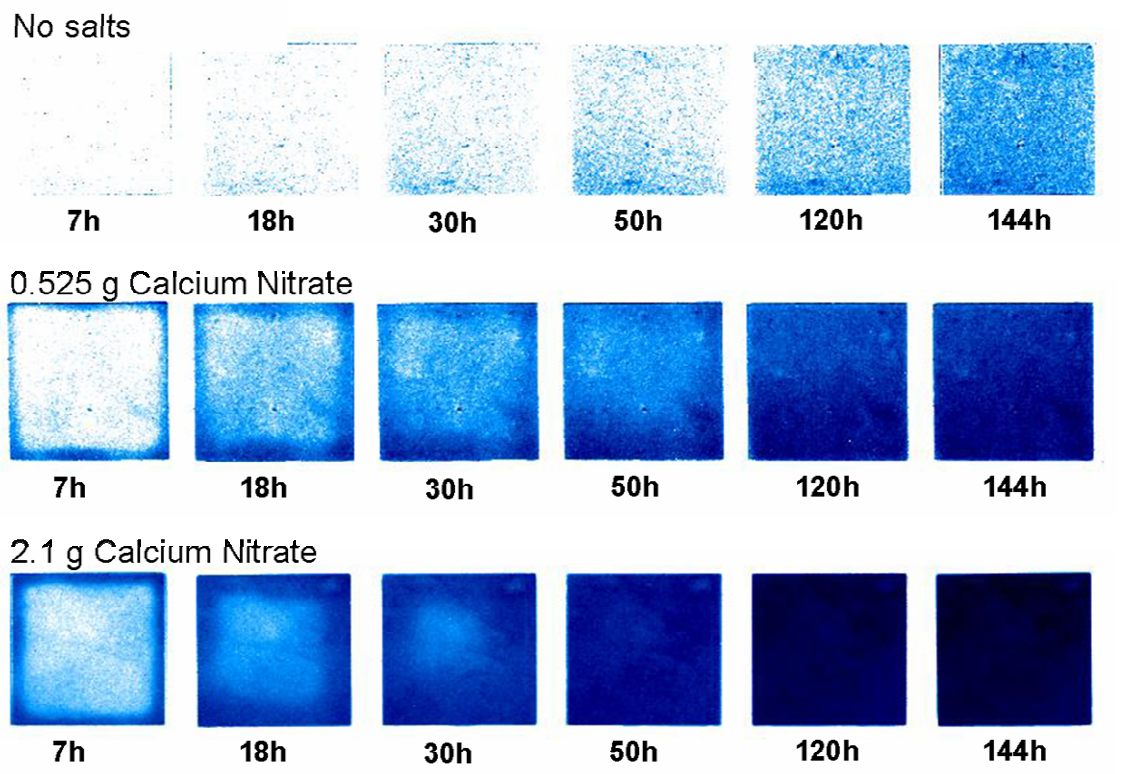

Fig. 5.8 – Time series of moisture uptake by Lecce stone samples treated with different amounts of calcium nitrate.

The amount of absorbed water can be calculated from the corrected radiograph, with the approximation that the neutrons are attenuated only by the water and that the neutron attenuation coefficient of water is 3.7 cm^{-1}. The comparison between neutron and weight methods to determine the moisture absorbed is presented in Fig. 5.9. The two methods produce different results: in relation to weight, neutron values are always underestimated. On the other hand, they show the same trend, so that the uptake process can be semi-quantitatively followed by NR.

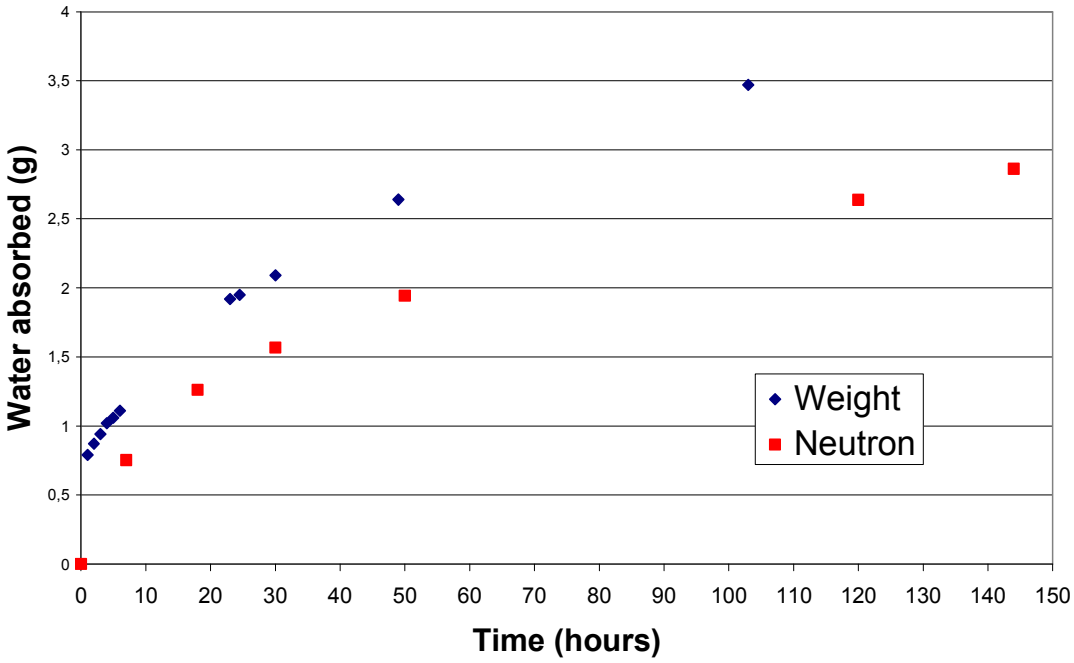

Fig. 5.9 – Comparison between neutron and weight method for the determination of the amount of moisture uptake in sample E

Neutron radiography appears to be a very sensitive technique, since absorbed water is already visible after a few hours of absorption. In stone artefacts, in which soluble and deliquescent salts are present, the moisture uptake is significantly faster; all the decay processes, in which water is involved, are therefore accelerated. Fig. 5.8 also shows that the humidity diffuses from the edges of the samples to the inner part and that in some areas the water seems to be locally more concentrated. These considerations are supported by the results obtained by neutron tomography analyses. The three dimensional rendering of sample E scanned after 60 hours of moisture uptake (Fig. 5.10), clearly shows that the humidity is absorbed preferentially from some sides, on which the solution of calcium nitrate have been distributed. This is the evidence that an increased moisture uptake by the stone material may be due to the presence of hygroscopic salts, such as nitrates.

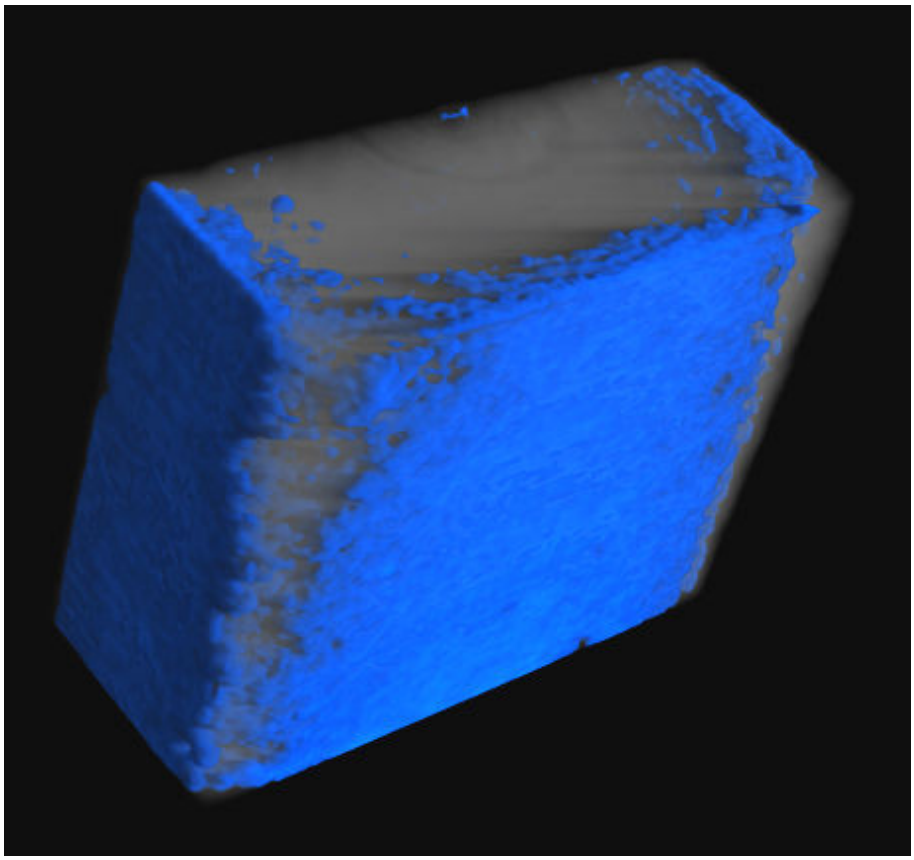

Fig. 5.10 – 3D rendering of the Lecce stone sample (5 x 5 x 2 cm^3) treated with 2.1 g of calcium nitrate after 60h of moisture uptake.

Other neutron experiments similar to those described previously have been performed directly on stone samples of 5 x 5 x 1 cm^3 dimensions, aged 3000h with NO_2. Neutron radiographies of aged specimens have been compared with those of samples prepared in the same way and treated with the same conservation treatment, but not aged. An example of the resulting images acquired at different time steps are given in Fig. 5.11, where two samples (aged and not aged) treated with PB 72-CA show different moisture absorption rate. This behaviour is due to the presence of deliquescent salts in the aged specimen, absent in the non-aged one. In general, all the aged samples show a higher neutron attenuation in comparison with the corresponding non-aged.

The time series of the mass of moisture uptake of Lecce stone samples treated with different conservation products and aged 3000h with NO_2 are presented in Fig. 5. 12. Treated and untreated samples show a very similar humidity absorption rate even if the untreated one shows higher vapour uptake. This behaviour confirms that the ageing caused a formation of nitrates and nitrites in all the samples, as found by ion chromatography analysis. With this gravimetric test, however, a more detailed quantitative evaluation of the performance of different conservation products could not

be performed. Probably it could be possible at longer times of moisture exposition, when the differences among the different treatments are more pronounced as suggested by Fig. 5.6.

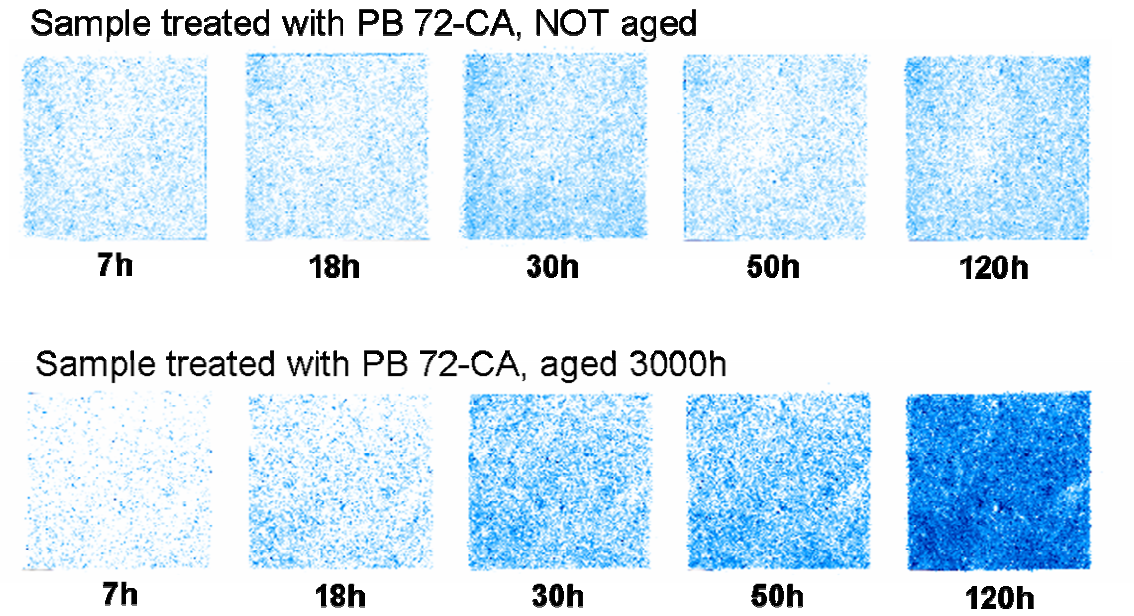

Fig. 5.11 – Time series of moisture uptake of samples treated with PB 72 by capillary absorption, not aged and aged 3000h with NO_2

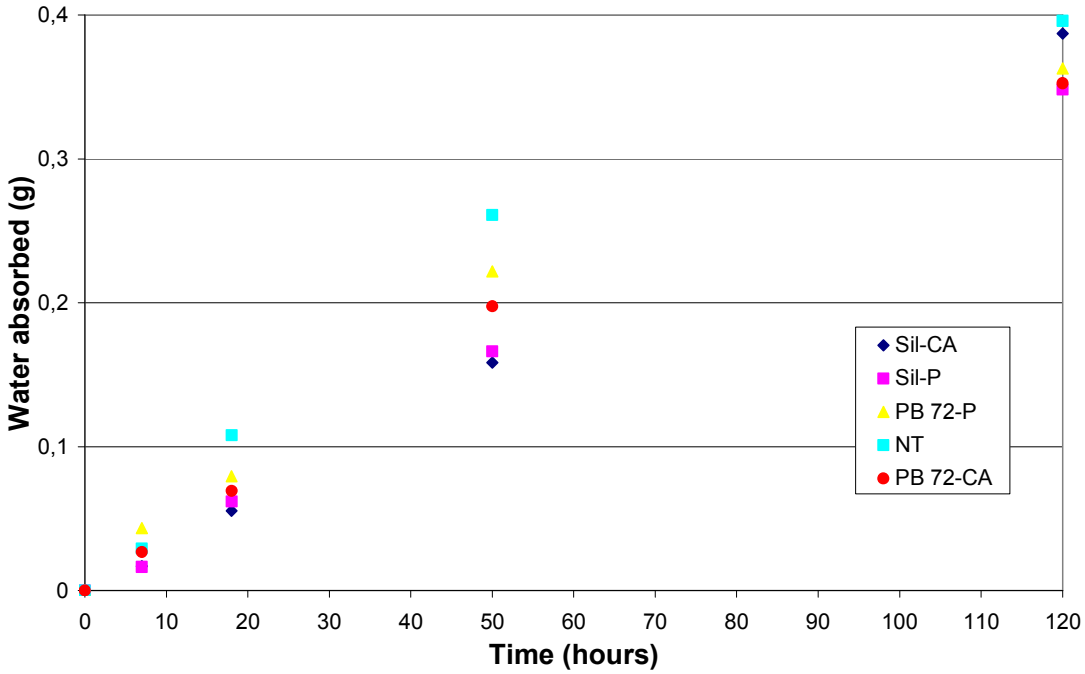

Fig. 5.12 – Time series of the mass of moisture uptake of Lecce stone samples treated with different conservation products and aged 3000h with NO_2

These results demonstrate that the formation of significant amount of nitrates and nitrites occurs in untreated as well as in treated Lecce stone samples and that the conservation treatments do not stop the moisture uptake and diffusion, successively accelerated by the presence of the hygroscopic salts produced in the rock structure as a consequence of the ageing.

Conclusions

In this PhD thesis the interaction between NOx and building stone materials has been studied though and accelerate ageing system which allows to expose laboratory samples at controlled temperature and humidity conditions.

The assembled ageing system is a powerful tool to obtain accelerated but not drastic ageing conditions, in presence of gaseous pollutants. It enables to accurately control the flow of the gases and other parameters reproducing daily thermo hygrometric variations, so it may be considered an efficient prototype in order to simulate the ageing induced also by atmospheric pollutants on objects and materials sheltered by rain and precipitations.

The results show that NO_2 is a very aggressive agent for Lecce stone, and calcareous stone in general, even if no liquid water (rain) is present. Despite the high amounts of nitrates and nitrites formed in the rock structure, no colour and morphological changes have been observed on the surfaces of the samples after the ageing. This may be justified by the reaction of NO_2 inside the pores of the stone, where the water condensation is more probable or the protective products are not well distributed or present. The tests performed on different protective products commonly used in stone conservation, show that they give high water repellence to the rock, but does not efficiently protect the material from the action of acidic pollutants, as NOx: for short ageing periods, all the treatments induce a decrease of the NO_2 attack on the calcareous stone. Nevertheless, this protective effect is quickly reduced increasing the ageing time. After 3000h the changes induced by the conservation treatments, i.e. occlusion of the porosity, variation of wettability and transpirability, cause the acceleration of the decay reactions and processes. These results lead to suppose that:

- NO_2 penetrates and diffuses inside the stone porosity and it reacts, degrading the rock from the inside. In fact, the decay process take place preferentially in the inner part of the stone, since the surface are intact and/or well protected by the conservation treatments
- The weathering process seems to be accelerated by the presence of conservation treatments which influence the water exchange (condensation and/or evaporation) phenomena, and they can alter the natural characteristics and behaviour of the material.

Depth penetration and homogeneous distribution are indeed key factor when stone is treated with conservation products.

X-ray μ-CT demonstrated to be a powerful tool for the investigation of the internal structure of building materials. The reconstructed cross sections and 3D rendering of the pores network, obtained by μ-CT, are able to show (qualitatively) and the dimensions (quantitatively) of the pores. Moreover, the data processing allows to calculate different parameters (surface-to-volume ratio, pores size distribution, SMI) useful to characterize the stone. Since μ-CT is a non-destructive technique and has a high reproducibility, the samples can be monitored during the conservation treatments or artificial ageing processes, following the changes in porosity of the specimens that may occur.

The performed statistical analysis makes the results more representative and provides an essential estimation of the changes the material undergoes because of the conservation treatments and allows to assess the errors connected with these changes. The polymer distribution in the internal structure of the rock is influenced by the physical and chemical properties of the products (molecular weight and chemical affinity with stone). In fact, NH, having high molecular weight and low affinity with calcarenites, causes a significant decrease in porosity with partial or complete blockage of some pores and non-homogeneous distribution inside the stone. On the other hand, PB 72, having lower molecular weight and a higher affinity for stone, causes small changes to the natural properties of Lecce stone with moderate variation of pore size and wall thickness distribution, suggesting a homogenous polymer distribution in the stone structure.

SR-CT and nano-CT can be useful to visualize and study the distribution of the products inside the pores, and analyzing samples taken from big treated specimens or real walls of historical buildings. The reconstructed images show that the conservation products coat the pore walls of the rock.

Neutron experiments help to study polymer distribution in stone samples and moisture uptake processes. The formation of significant amount of nitrates and nitrites occurs in untreated as well as in treated Lecce stone samples and the conservation treatments do not stop the moisture uptake and diffusion, successively accelerated by the presence of the hygroscopic salts produced in the rock structure as a consequence of the ageing.

These results allows to clarify the mechanism of decay, caused by NOx and to draw conclusions which may open new research to design new conservation products and technologies.

References

[1] EEA - European Environment Agency. http://www.eea.europa.eu/

[2] Blatt H and Tracy RJ, , Petrology: Igneous, Sedimentary and Metamorphic, Freeman W.H. and Co., 2nd Ed. 1994, ISBN 0-7167-2438-3

[3] Amoroso GG, Fassina V. Stone decay and Conservation. Elsevier, Amsterdam, 1983

[4] Sabbioni C. Contribution of atmospheric deposition to the formation of damage layers. Science of The Total Environment, 1995; 167(1-3): 49-55

[5] Turkington AV, Martin E, Viles HA Smith BJ. Surface change and decay of sandstone samples exposed to a polluted urban atmosphere over a six-year period: Belfast, Northern Ireland. Building and Environment. 2003; 38(9-10): 1205-1216

[6] Rijniers LA,Pel L, Huinink HP,Kopinga K. Salt crystallization as damage mechanism in porous building materials: a nuclear magnetic resonance study. Magnetic Resonance Imaging, 2005; 23(2): 273-276

[7] Cai H, Liu X. Freeze-thaw durability of concrete: ice formation process in pores. Cement and Concrete Research, 1998; 28(9): 1281-1287

[8] Beck K, Al-Mukhtar M, Rozenbaum O, Rautureau M. Characterization, water transfer properties and deterioration in tuffeau: building material in the Loire valley-France Building and Environment, 2003; 38(9-10): 1151-1162

[9] Lefevre RA. La pietra dei monumenti nel suo ambiente fisico. Ist. Poligr. e Zecca dello Stato, Roma, 1995, 195

[10] Piqué F, Dei L, Ferroni E. Physicochemical aspects of the deliquescence of calcium nitrate and its implications for wall painting conservation. Studies in Conservation, 1992; 37: 217-227

[11] Chambers LA. Classification an extent of air pollution problems. In: Stern AC. Air pollution problems, 3rd Ed., Vol. 1, Accedemic Press, New York 1976, pp. 3-22

[12] Morselli L. Deposizioni Acide, Maggioli Ed., Rimini, Italy, 1991

[13] Robinson AB, Robinson NE, Soon W,. Environmental effect of increased atmospheric carbon dioxide. Journal of the American Physicians and Surgeons, 2007; 12: 79–90.

[14] Charola AE. Acidic deposition on stone. US/ICOMOS Sci. J. III, 2001; 1: 19-58.

[15] Maravelaki-Kalaitzaki P. Black crusts and patinas on Pentelic marble from the Parthenon and Erechtheum (Acropolis, Athens): characterization and origin. Analytica Chimica Acta, 2005; 532(2): 187-198

[16] Manahan SE Environmental Chemistry 8th Edition. CRC Press, Boca Raton, FL, 2005

[17] Cotton, Wilkinson "Advanced inorganic chemistry" 4th ed., J. Wiley and Sons Inc., New York, 1984.

[18] Johannson L, Lindqvist O, Mangio R. Corrosion of calcareous stones in humid air containing SO_2 and NO_2. In: Rosvall J, Aleby S, editors. Air pollution and conservation. Safeguarding our architectural heritage. Elsevier, 1988.

[19] Bonazza A, Sabbioni C and Ghedini N. Quantitative data on carbon fractions in interpretation of black crusts and soiling on European built heritage Atmospheric Environment, 2005; 39(14): 2607-2618

[20] Potgieter-Vermaak SS, Godoi RHM, Van Grieken R, Potgieter JH, Oujja M and Castillejo M Micro-structural characterization of black crust and laser cleaning of building stones by micro-Raman and SEM

techniques. Spectrochimica Acta Part A: Molecular and Biomolecular Spectroscopy, 2005; 61(11-12): 2460-2467

[21] Massey SW. The effects of ozone and NOx on the deterioration of calcareous stones. Science of Total Environment, 1999; 227:109-121

[22] Judeikis HS, Stewart TB and Wren G. Laboratory studies of heterogeneous reactions of SO_2. Atmospheric Environment, 1978; 12(8): 1633-1641

[23] Peleg M, Burla E, Cohen I, Luria M. Deterioration of Jerusalem limestone from air pollutants: field observations and laboratory simulation. Environ Monitor Assess 1989; 12 (2): 191-201

[24] Ausset P, Crovisier J, Del Monte M, Furlan V, Girardet F, Hammecker D, Jeannette D, Lefevre R. Experimental study of limestone and sandstone sulphation in polluted realistic conditions: The Lausanne atmospheric simulation chamber LASC. Atmos Environ 1996; 30:3197-3207.

[25] Katsanos N, Vassilakos Ch. Theoretical analysis for measurement of building pollution parameters by gas chromotography. Journal of Chromatography A, 1991; 557(20): 469-479

[26] Vassilakos Ch, Katsanos N, Niotis A. Physiochemical damage parameters for the action of SO_2 and NO_2 on single pieces of marble. Atmospheric Environment A, 1992; 26(2): 219-223

[27] Vassilakos Ch, Salta A. Synergistic effects of SO_2 and NO_2 in their action on marbles studied by reverse flow gas chromatography. In: Theil M, editor. Conservation of stone and other materials. E&FN Spon, London, 1993.

[28] Gauri K, Gwinn J. Deterioration of marble in air containing 5-10 ppm SO_2 and NO_2. Durab Build Mater 1982/1983; 1:217-216.

[29] Judeikis H and Wren AG. Laboratory measurements of NO and NO_2 deposition onto soil and cement surfaces. Atmospheric Environment, 1978; 12: 2315-2319

[30] Kirkitsos P, Sikiotis D. Deterioration of Pentelic marble, Portland limestone and Baumberger sandstone in laboratory exposures to NO_2 : A comparison with exposures to gaseous HNO_3. Atmos Environ, 1996; 30(6): 941-950

[31] Martinez-Ramirez S, Puertas F, Blanco-Varela MT and Thompson GE. Studies on degradation of lime mortars in atmospheric simulation chamber. Cement and Concrete Research, 1997; 27(5): 777-784

[32] Camaiti M, Bugani S, Bernardi E, Morselli L, Matteini M. Effects of atmospheric NOx on biocalcarenite coated with different conservation products. Appl Geochem 2007; 22 (6):1248-1254

[33] Young ME, Cordiner P, Murray M. Chemical consolidants and water repellent for sandstone in Scotland. In: Historic Scotland Research Report 2003.

[34] Horie CV. Materials for conservation: organic consolidants, adhesives and coatings. Elsevier Butterworths-Heinemann, Burlington, MA, 1987.

[35] Lide DR (eds). Handbook of Chemistry and Physics. 83th Edition, CRS Press, Boca Raton, FL, 2002

[36] Borgioli L. Polimeri di sintesi per la conservazione della pietra. Il prato casa editrice, Padova (I), 2002. ISBN 88-87243-38-7

[37] Doherty B, Pamplona M, Selvaggi R, Miliani C, Matteini M, Sgamellotti A, Brunetti B. Efficiency and resistance of the artificial oxalate protection treatment on marble against chemical weathering. Applied Surface Science, 2007; 253(10): 4477-4484

[38] Casadio F, Toniolo L. Polymer treatments for stone conservation: methods for evaluating penetration depth. JAIC, 2004; **43**(1): 3-21

[39] Borgia GC, Camaiti M, Cerri F, Fantazzini P, Piacenti F. Hydrophobic treatments for stone conservation: influence of the application method on penetration, distribution and efficiency. Studies in Conservation, 2003; **48** (4): 217-226

[40] Masschaele B, Dierick M, Cnudde V, Van Hoorebeke L, Delputte S, Gildemeister A, Gaehler R, Hillenbach A. High-speed thermal neutron tomography for the visualization of water repellents, consolidants and water uptake in sand and lime stones. Radiation Physics and Chemistry, 2004; 71: 807-808

[41] Oddy A and Carroll S. Reversibility: does it exist? British Museum, London, UK, 1999

[42] Appelbaum B. Criteria for treatment: reversibility. Journal of the American Institute for Conservation, 1987; 26(2): 65-73

[43] Gomez-Heras M, Alvarez de Buergo M, Rebollar E, Oujja M, Castillejo M, Fort R. Laser removal of water repellent treatments on limestone. Applied Surface Science, 2003; 219(3-4): 290-299

[44] Favaro M, Mendichi R, Ossola F, Russo U, Simon S, Tomasin P and. Vigato PA. Evaluation of polymers for conservation treatments of outdoor exposed stone monuments. Part I: Photo-oxidative weathering. Polymer Degradation and Stability, 2006; 91(12): 3083-3096

[45] Fotakis C, Anglos D, Zafiropulos V, Georgiou S and Tornari V "Lasers in the Preservation of Cultural Heritage" CRC Press Taylor&Francis Group, Boca Raton, FL, 2007

[46] ISO 6783, Coarse aggregates for concrete - Determination of particle density and water absorption - Hydrostatic balance method. 1982

[47] UNI 10859, 2000. Norma Italiana Beni Culturali, Materiali lapidei naturali e artificiali, 'Determinazione dell'assorbimento d'acqua per capillarità'.

[48] DOC NORMAL 43/93, 1994. Materiali lapidei. Misure colorimetriche di superfici opache. Ed. CNR-ICR Comas Grafica, Roma.

[49] DOC NORMAL 20/85, Materiali lapidei, CNR-ICR, Roma, 1986

[50] The IUPAC Compendium of Chemical Terminology, 1997; 66: 583

[51] Chiantore O and Lazzari M. Photo-oxidative stability of paraloid acrylic protective polymers. Polymer 2001; 42(1): 17-27

[52] Matteini M, Moles A, Lanterna G, Nepoti MR. Preliminary monitoring on painted plasters and marble surfaces of a mineral protective treatment based on artificially formed calcium oxalate. Proceedings of II International Symposium "The oxalate films in the conservation of works of art" Milan, March 25-27 1996. Realini M and Toniolo L (eds)

[53] DOC NORMAL 21/85. Materiali lapidei. Permeabilità al vapor d'acqua. Ed. CNR-ICR Comas Grafica, 1982, Roma.

[54] Bugani S. Study of the interactions between nitrogen oxides (NOx) and stone materials treated with conservation products. Thesis. University of Bologna, Italy, 2004.

[55] Sirat GY, Psaltis D. Conoscopic holograms. Optics Communications, 1988; 65(4): 243-249

[56] Salvo L, Cloetens P, Maire E, Zabler S , Blandin JJ, Buffière JY, Ludwig W, Boller E, Bellet D, Josserond C. X-ray micro-tomography an attractive characterisation technique in materials science. Nuclear Instruments and Methods in Physics Research B, 2003; 200: 273–286

[57] Russ JC. The image processing handbook 5th edition. CRC Press, Boca Raton, 2007

[58] Hounsfield GN. Computerized transverse axial scanning (tomography). Part 1: description of system. British Journal of Radiology, 1973; 46: 1016-1022

[59] Mees F, Swennen R, Van Geet M, Jacobs P. (eds). Applications of x-ray computed tomography in the geosciences. Geological Society, London, Special Pubblication, 2003; 215:1-6

[60] Lyon RF. A Brief History of 'Pixel'. Digital Photography II, IS&T/SPIE Symposium on Electronic Imaging, 15–19 January 2006, San Jose, California, USA

[61] Sasov A and Van Dyck D. Desktop x-ray miscroscopy and microtomography. Journal of Microscopy (1998) 191: 151-158

[62] Agarwal BK. X-ray spectroscopy: an introduction, 2nd Ed. Springer-Verlag, New York, 1991.

[63] Jacobs P and Cnudde V. Can x-ray computed tomography contribute to cultural heritage and stone conservation though the non-destructive monitoring of deterioration and restoration processes? In: Van Grieken and Janssens (eds) Cultural Heritage and Environmental Impact Assessment by Non-destructive Testing and Micro-Analysis. 2005 Taylor&Francis Group, London

[64] Jacobs P, Sevens E, and Kunnen M. Priciple of computerised x-ray tomography and applications to building materials. The Science of total Environment (1995) 167: 161-170

[65] Jacobs P, Sevens E, Vossaert P and Kunnen. Non-destructive monitoring of interactive physical and biological deterioration of building stones by computerized x-ray tomography. In: Marinos P, Koukis G, Tsiambaos G and Stournaras g (eds). Engineering Geology and the Environment. Rotterdam, Balkema, 3163-3168

[66] Perret J, Prasher SO, Kantzas A, Langford C. Three-dimensional quantification of macro-pore network in undisturbed soil core. Soil Science Society of America Journal. (1999) 63: 1530-1543

[67] Van Geet M, Swennen R, Wevers M. Quantitative analysis of reservoir rocks by microfocus X-ray computerised tomography. Sedimentary Geology, 2000; 132: 25-36

[68] Van Geet M, Lagrou D, Swennen R. Porosity measurements of sedimentary rock by means of microfocus x-ray computed tomography (μCT). In: Mees F, Swennen R, Van Geet M, Jacobs P. (eds). Applications of x-ray computed tomography in the geosciences. Geological Society, London, Special Pubblication, 2003; 215: 51-60

[69] Appolonia CR, Fernandes CP, Rodrigues CRO. X-ray microtomography study of a sandstone reservoir rock. Nuclear Instruments and Methods in Physics Research A, 2007; 580: 629–632

[70] Gualda GAR, Rivers M. Quantitative 3D petrography using x-ray tomography: Application to Bishop Tuff pumice clasts. Journal of Volcanology and Geothermal Research, 2006; 154: 48–62

[71] Cnudde V, Cnudde JP, Dupuis C, Jacobs PJS. X-ray micro-CT used for the localization of water repellents and consolidants inside natural building stones. Materials Characterization 2004; 53: 259– 271

[72] Bugani S, Camaiti M, Morselli L, Van de Casteele E, Janssens K. Investigation on porosity changes of Lecce stone due to conservation treatments by means of x-ray nano- and improved micro-computed tomography: preliminary results. X-Ray Spectrom. 2007; 36: 316–320

[73] Brunetti A, Princi E, Vicini S, Pincin S, Bidali S, Mariani A. Nucl. Instrum. Meth. B 2004; 222: 235.

[74] Feldkamp LA, Davis LC, Kress JW. Practical cone-beam algorithm. J. Opt. Soc. Am. 1984; 1(6): 612-619

[75] Hildebrand T, Ruegsegger P. Quantification of Bone Microarchitecture with the Structure Model Index. Comp. Meth. Biomech. Biomed. Eng. 1997; 1: 15-23

[76] Miller JN and Miller JC. Statistics and Chemometrics for analytical Chemistry, 5th edition. Pearson Education New York, 2005.
[77] Winick H. Synchrotron Radiation Sources. World Scientific, Singapore, 1995
[78] A. Hofmann. The Physics of synchrotron Radiation. Cambrige University Press, 2004
[79] Röhlsberger R. Nuclear condensed matter physics with synchrotron radiation: basics, principles, methodology and applications. Springer-Verlag Berlin Heidelberg, 2004
[80] Watson RE and Perlman ML Seeing with a New Light: Synchrotron Radiation. *Science* 1978; 199: 1295-1302
[81] www.esrf.eu
[82] Withers PJ. X-ray nanotomogrphy. Materials today. 2007; 10(12): 26-34
[83] Olejniczak AJ, Tafforeau P, Smith TM, Temming H, Hublin JJ. Technical note: compatibility of microtomographic imaging systems for dental measurements. American Journal of Physical Anthropology, 2007; 134:130-134
[84] Koch A, Raven C, Spanne P, Snigirev A. X-ray imaging with submicrometer resolution employing transparent luminescent screens JOSA A, 1998; 15(7): 1940-1951
[85] Espeso JI, Cloetens P, Baruchel J, Härtwig J, Mairs T, Biasci JC, Marot G, Salomé-Pateyron M and Schlenker M. Conserving the Coherence and Uniformity of Third-Generation Synchrotron Radiation Beams: the Case of ID19, a `Long' Beamline at the ESRF. J. Synchrotron Rad. 1998;. 5(5): 1243-1249
[86] Raven C, Snigirev A, Snigireva I, Spanne P, Suvorov A. Phase-contrast computed microtomography with 50 keV synchrotron x-rays. Rev. Sci. Instrum. 1996; 67: 3359
[87] Snigirev A, Snigireva I, Kohn V, Kuznetsov S, Schelokov I. On the possibilities of x-ray phase contrast microimaging by coherent high-energy synchrotron radiation. Rev. Sci. Instrum. 1995; 66: 5486
[88] Cloetens P, Ludwig W, Baruchel J, Guigay JP, Rejmankova-Pernot P, Salome M, Schlenker M, Buffiere JY, Maire E, Peix G. Hard X-ray phase imaging using simple propagation of a coherent synchrotron radiation beam. J. Phys. D: Appl. Phys. 1999; 32:A145-A151
[89] Helfen L, Baumbach T, Mikulík P, Kiel D, Pernot P, Cloetens P, Baruchel J. High-resolution three-dimensional imaging of flat objects by synchrotron-radiation computed laminography. Appl. Phys. Lett. 2005; 86, 071915
[90] Berger H Advances in neutron radiographic techniques and applications: a method for nondestructive testing Applied Radiation and Isotopes, 2004; 61: 437-442
[91] Vontobel P, Lehmann EH, Hassanein R, Frei G. Neutron tomography: Method and applications. Physica B 2006; 385-386: 475-480
[92] A. Foderaro, “The elements of Neutron Interaction Theory”, The MIT press, ISBN 0-262-06033-7, 1971
[93] Lehmann EH, Vontobel P, Deschler-Erbb E, Soares M. Non-invasive studies of objects from cultural heritage. Nuclear Instruments and Methods in Physics Research A, 2005; 542: 68-75
[94] http://neutra.web.psi.ch/
[95] Lehmann EH, Vontobel P, Frei G, Brönnimann C. Neutron imaging-detector options and practical results. Nuclear Instruments and Methods in Physics Research A 2004; 531: 228-237
[96] Pel L, Ketelaars AAJ, Adan OCG, Van Well AA. Determination of moisture diffusivity in porous media using scanning neutron radiography. Int J Heat Mass Transfer, 1993; 36:1261–1267

[97] Prazak J, Tywoniak J, Peterka F, Slonc T. Description of transport of liquid in porous media: a study based on neutron radiography data. Int J Heat Mass Transfer 1990; 33:1105–1120

[98] Wilding M, Lesher CE, Shields K. Applications of neutron computed tomography in the geosciences. Nuclear Instruments and Methods in Physics Research A, 2005; 542: 290-295

[99] Milczareka JJ, Czachora A, El Abda A E-G, Wisniewskia Z. Dynamic neutron radiography observations of water migration in porous media. Nuclear Instruments and Methods in Physics Research A, 2005; 542: 232–236

[100] Hassanein R. Correction methods for the quantitative evaluation of thermal neutron tomography. PhD thesis. ETH - Swiss Federal Institute of Technology, Zurich (CH), 2006.

[101] Gonzalez RC, Wintz P. *Digital Image Processing*. Addison–Wesley. Reading, MA (USA), 1987

[102] Diamond S. Mercury porosimetry: An inappropriate method for the measurement of pore size distributions in cement-based materials. Cem. Concr. Res. 2000; 30: 1517-1525

[103] http://www.volumegraphics.com/

[104] Borgia GC, Camaiti M, Cerri F, Fantazzini P, Piacenti F. Study of water penetration in rock materials by Nuclear Magnetic Resonance Tomography: hydrophobic treatment effects. Journal of Cultural Heritage, 2000; 1: 127–132

[105] Borgia GC, Bortolotti V, Camaiti M, Cerri F, Fantazzini P, Piacenti F. Performance evolution of hydrophobic treatments for stone conservation investigated by MRI. Magnetic Resonance Imaging, 2001; 19: 513–516

List of abbreviations

SOx = Sulphur oxides

NOx = Nitrogen oxides

DeSOx = Systems for Sox removal

EU 15 = Area of European Union with fifteen countries

RH% = Relative humidity

RH_{eq}% = Equilibrium relative humidity

UV = Ultra violet

MRI = Magnetic resonance imaging

WP% = porosity accessible to water

CT = Computed tomography

μ-CT = Micro computed tomography

SR = Synchrotron radiation

SR-CT = Synchrotron radiation computed tomography

PB 72 = Paroild B72

NH = Fluoroelastomer or Fluororubber

Sil = Hydrophase superfici

Ox = Ammonium Oxalate

Tg = Glass transition temperature

M_W = Average molecular weight

PE% = Protective efficacy

RP% = Residual Permeability

AISI = American Iron Steel Institute

ESEM = Environmental Scanning Electron Microscopy

INOA = National Institute of Applied Optics

CCD = Charge coupled device

ROI = Region of interest

VOI = volume of interest

BW = Band width

ESRF = European Synchrotron Radiation Facility

SLS = Swiss Light Source

APS = Advanced Photon Source

SPring-8 = Super Photon ring-8GeV

NT = Neutron tomography

NR = Neutron radiography

FRELON = Fast reading low noise

NEUTRA = Neutron Transmission Radiography

IDL (Interactive Data Language

QNI = Quantitative Neutron Imaging

MIP = Mercury intrusion porosimetry

SMI = Structure model index

OM = Optical microscope

Acknowledgements

Come nella tesi di Laurea, la pagina dei ringraziamenti è stata la prima che ho scritto nel tentativo di non dimenticare nessuna delle persone, delle avventure e dei sogni che mi hanno permesso di arrivare a questo traguardo che oggi, in effetti, mi sembra sempre meno tale e sempre di più una nuova partenza.
La prima persona che vorrei ringraziare è il mio relatore e mentore Prof. Luciano Morselli, che ha seminato stimoli, aiuti e cazziatoni nella dose perfetta per estrarre da me il massimo. Oltre a questa sua empatia considerevole, mi ha aiutato a maturare molti aspetti fondamentali del mio carattere e a guardarmi fuori oltre che banalmente dentro. Lo stesso posso dire, anche se in modo diverso, della Dr. ssa Camaiti. Mara in più di 5 anni non ha mai dato un solo segno di cedimento, a tratti mi ha letteralmente trascinato, trasmettendomi tutta la passione ed entusiasmo possibili, dimostrandomi che le lunghe giornate in laboratorio, o a casa nel weekend, alla fine, pagano e ti lasciano la soddisfazione e leggerezza di una giornata primaverile di sole. Ringrazio sinceramente il Prof. Koen Janssens dell'Università di Anversa, che accogliendomi nel suo gruppo (progetto ATHENA MEST-CT 2004-504067, Marie Curie Actions) ha dato una svolta a tutto il mio lavoro, introducendomi a nuovi campi, idee e prospettive, oltre che a sostenere economicamente il mio progetto. Un ulteriore ringraziamento va al Prof. Castellucci del LENS per il suo indispensabile supporto e al Prof. Fotakis del FORTH-IESL di Heraklion per avermi dato la possibilità di lavorare nel gruppo di olografia con Kostas e Jannis a fianco di Vivi Tornari eccellente ricercatrice.
Tra le persone che hanno partecipato attivamente al mio lavoro di tesi e che hanno dedicato molti dei loro sforzi, tempo ed energie non posso dimenticare la Dr. Elke Van de Casteele e tutto lo staff di SkyScan davvero insuperabili per dedizione e disponibilità, Dr. Peter Cloetens beamline scientist di ID19 a ESRF, Ing. Peter Vontobel e Dr. Eberhard Lehmann del NIAG al PSI, Prof. Fantazzini e Dr. Gombia per analisi MRI.
Un ringraziamento speciale lo vorrei riservare alle tantissime persone che ho incontrato in questi 3 anni, con cui ho condiviso scuole, corsi, esperienze, dentro e fuori i laboratori, che hanno contribuito alla mia crescita personale e professionale con i loro consigli e confronti sempre fruttuosi. Hanno sicuramente fatto sì che il mio cervello continuasse a funzionare anche quando la stanchezza, la frustrazione, la delusione e l'abbattimento mi avevano vinto (e vi assicuro che ce ne sono stati di quei momenti!). In particolare Bart, per avermi fatto apprezzare quanto di bello e buono ci sia in Belgio, Wout "the IDL master" per la sua amicizia e il suo aiuto, Jana compagna di (dis)avventure e progetti, il Dr. Fabri, Elena, tutti i ragazzi "Gruppo Ambiente&Beni Culturali" @ UNIBO, lo staff del Dipatimento di Chimica Industriale, Cristina, i ragazzi di Anversa (Roel, Peter, Bart, Koen, Gert, Veerle), Giulia&Mattia @ UNIFE ma più in generale tutto il gruppo di ARG, Andrea Carminati & Paolo Montagna ottimi esempi, Veerle Cnudde (ha avuto un maschio!), Bert e Jelle dell'Università di Gent, Laszlo, Matthias, Jacub "Cuba" Jarozewich, Viviana, Sara Kaps, Polina, Alex da Rostov, Austin, Daniela, Simone Cagno, lo staff ICVBC (precari in testa).
La lista è davvero lunga, ma ognuno loro mi ha lasciato ricordi ed eredità preziosissime.
A seguire per molto di più di un dovere di riconoscenza, tutti quelli che mi hanno accompagnato nel mio percorso, regalandomi la loro energia ed entusiasmo. Alex nelle Pleiadi inesplorato arcipelago greco dove fanno un olio spettacolare (remember: I WANT YOU!), Pitü, Bea& Giulio porto sicuro, Chiara, Vale in voli pindarici sulle scale, Milton, Maaike (ora so come fare il sushi!), Cristina la jesolina (ciabatte alla mano), Becuz (ora so cosa vuol dire pulire!), Pippo&Robi coppia del secolo, Lore+Jared+Sere+Luca+Lidia, Carlo&Lafrà, Silvia (la logistica non ha più segreti per

me), i Molesti tra montagna e vacanze last minute (oddio ho riperso l'aereo!), Marza (mai avuto denti così bianchi!), Dr. Floros e Fidel (mai sentito un cane nero con questo nome!), Lety (lingua fatta persona), Juliette (non hai visto Parigi senza aver visto la finale 2006 Italia-Francia a St. Michel!), Sabri, Jack such a strong man, il BRRR vecchio compagno di banco e di sbronze, Andre e i ragazzi di via della colonna 35, PunkyB&Malish, Noel, Eli (te lo affido, trattamelo bene!), France e ultima ma spesso prima ed unica, Giorgia.

Riservo uno spazio particolare per i miei affetti più intimi e il mio SE. Ringrazio i miei genitori, Alba e Renato, da sempre i miei più grandi tifosi con cieca e infinita fiducia, mio fratello Matteo con cui condivido la poesia della chimica, mia cugina Barbara senza la quale non potrei pensare di stare, i miei zii Luciano ed Albertina che mi sono stati vicinissimi in ogni mia esperienza e i miei cugini Davide e Lorenzo. In ogni mio giorno per quanto mi trovassi lontano da casa mi hanno trasmesso il loro calore e appoggio.
In ultimo, ringrazio tutti gli ostacoli, difficoltà, ingiustizie e dimostrazioni di ignoranza, stupidità e approssimazione che ho dovuto affrontare. Sono stati il vero monito su come non volevo essere e la vera motivazione a guardarmi dentro, a superarmi per essere migliore e, a mia volta, cercare di migliorare questo mondo.

If you can dream it, you can do it

Bologna, 21 Gennaio 2008